Winter 2012

Geochemistry and Release of Contaminants from Cohesive Sediments of the Great Bay Estuary, New Hampshire

Vincent Percuoco
University of New Hampshire, Durham

GEOCHEMISTRY AND RELEASE OF CONTAMINANTS FROM COHESIVE SEDIMENTS OF THE GREAT BAY ESTUARY, NEW HAMPSHIRE

BY

VINCENT PERCUOCO

Bachelor of Science, Iowa State University, 2010

THESIS

Submitted to the University of New Hampshire
in partial fulfillment of
the requirements for the Degree of

Master of Science

in

Earth Sciences : Oceanography

December 2012

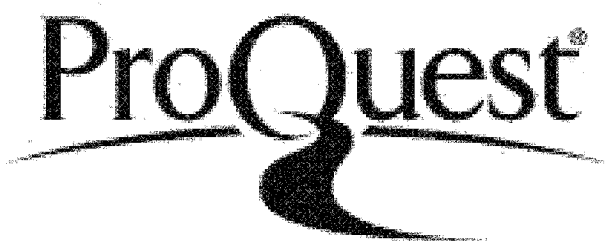

ProQuest LLC
789 East Eisenhower Parkway
P.O. Box 1346
Ann Arbor, MI 48106-1346

This thesis has been examined and approved.

Linda Kalnejais

Thesis Advisor: Linda Kalnejais

Assistant Professor

Department of Earth Sciences

J. H. Pennock

Jonathan Pennock

Associate Professor

Department of Natural Resources

and the Environment

Diane L. Foster

Diane Foster

Associate Professor

Department of Mechanical Engineering

12/9/2012

Date

ACKNOWLEDGMENTS

Scientific investigation is a rigorous and arduous process that can rarely be accomplished alone. This study was no exception, as it would not have been possible without the help of numerous others–all who deserve recognition for their contributions.

First, I thank my graduate advisor Professor Linda Kalnejais. My progress as a researcher and scientist over the past two years is a result of her abilities as a teacher, and the extraordinary quality (and quantity) of mentoring I received through her. I also thank Professors Jon Pennock and Diane Foster for serving on my thesis committee and providing the helpful comments which transformed this work into the finished product.

I also thank Tom Gregory, Sean Shellito and Jon Hunt for their assistance in core collection. I thank Laurent Officer, Cathleen Turner, Meagan Wengrove, Rebecca Demers, Sophie Burke and Taylor Langkau for their superb help in both field work and further sample processing in the laboratory.

My trace metal results would not have been possible without the help of Florencia Prado, who spent numerous hours preparing the ICP-MS and troubleshooting the issues that developed, her insight was invaluable. Furthermore, thanks to Steve Phillips for showing me the inner workings of the CHN analyzer.

Finally, I thank Olivia de Meo for introducing me to the wonderful world of Latex, and Shivanesh Rao and David Filipovic for their important insights into issues I had with MatLab and JMP. This work was funded by New Hampshire SeaGrant, a UNH Earth Science Teaching Assistantship, The Great Bay Stewards Program, and the UNH Earth Science Department.

TABLE OF CONTENTS

List of Tables

List of Figures

ABSTRACT

GEOCHEMISTRY AND RELEASE OF CONTAMINANTS FROM COHESIVE SEDIMENTS OF THE GREAT BAY ESTUARY, NEW HAMPSHIRE

by

Vincent Percuoco

University of New Hampshire, December, 2012

The role of cohesive sediments as a source of nutrients and metals to the Great Bay Estuary, NH was investigated by analyzing the porewater of several sediment cores obtained from three fields sites. Contaminant fluxes were compared between several release mechanisms including: molecular diffusion calculated from porewater profiles, bioturbation during core incubations, and sediment resuspension under simulated erosion. Ammonium, phosphate, silica, and nitrate accumulation in porewater lead to diffusive fluxes of 0.3-2, 0-0.5, 0.3-2, and -0.1-0.1 mmol m^{-2} day^{-1} respectively. Fluxes from bioturbation were on the same order of magnitude. Under simulated erosion, nutrient fluxes were over an order of magnitude greater than predicted from advection of eroded porewater. In several cases the first particles to be eroded were enriched in trace metals over bulk sediment concentrations. Total sediment fluxes from these processes are comparable to riverine inputs, thus must be accounted for when quantifying contaminant budgets to the Great Bay.

CHAPTER 1

Accumulation of Nutrients and Metals in Cohesive Sediment of the Great Bay Estuary, NH

The geochemistry of cohesive sediments of the Great Bay Estuary, NH was investigated in the spring, summer and fall in order to quantify nutrient regeneration rates, diffusive fluxes to the overlying water, and metal concentrations in sediment particulates. Pore water and sediment were extracted from duplicate sediment cores at three field sites. Concentrations of particulate-phase iron, manganese, copper, chromium, cadmium and lead were relatively constant in the upper 20 cm of sediment although slightly lower concentrations were observed at the sediment-water interface, suggesting possible removal or less enrichment of metals in recently deposited sediment. However, particulate phase trace metals at the field sites were well below screening values (ten Brink et al., 2002). Pore water accumulation of ammonium, phosphate, silica, and to a lesser extent nitrate, in the upper 20 cm of sediment were observed at each site. Pore water profiles indicated that several diagenetic reactions occur in the upper 0-4 cm of sediment and beneath 4 cm nutrients are regenerated through organic remineralization coupled with sulfate-reduction–which drives the accumulation of nutrients. Ammonium and phosphate regeneration rates were determined by application of an organic remineralization, sulfate-reduction model and found to range from 0.003-0.33 and 7.4 x 10^{-4}-0.51 μmol cm_s^{-3} day^{-1}, respectively. Nutrient diffusive fluxes were on the order of 0.3-2, 0-0.5, 0.3-2, and -0.1-0.1 mmol m^{-2} day^{-1}

for ammonium, phosphate, silica and nitrate, respectively. The comparability between previous studies indicate benthic fluxes have not changed significantly over the past 30 years. The rates of nutrient input to the Great Bay due to sediment diffusive fluxes were found to be less than riverine inputs in the spring but higher than riverine inputs during the fall. These results indicate that it is necessary to consider cohesive sediments as a source of nutrients when quantifying nutrient budgets to the Great Bay.

1.1 Introduction

Interactions between biological and chemical cycles in sediment are crucial in determining the ecological health in estuarine and shallow coastal environments (Smith et al., 1999). The inorganic nutrients ammonium (NH_4^+), phosphate (PO_4^{3-}), and nitrate (NO_3^-) have been implicated in several studies (Arrigo (2005); Tyrrell (1999) and references therein) as dominant factors controlling coastal and oceanic primary productivity–the basis of marine ecosystems. In significant contrast to the open ocean, estuarine nutrient availability is high due to land-runoff and remineralization of terrestrial organic matter, leading to higher production. Human land-use practices (fertilizer application) and point-sources increase nutrient input to the coastal ocean (Nixon, 1995). When nutrient availability causes excessive productivity, eutrophication may occur and drive a regime shift in the estuarine ecosystem. Deleterious effects to the environment and ecosystem such as hypoxia, decreased biodiversity, and emergence of invasive species are prominent in eutrophicated ecosystems (Smith et al., 1999).

Similarly, metals have a profound impact on biological health, both animal and human. At high concentrations, many dissolved metals are acutely toxic and can inhibit fundamental biochemical and reproductive processes (ATSDR, 2012). Metals

may also accumulate in marine organisms subjected to prolonged exposure, causing adverse health effects to consumers. This is important to the health of Great Bay's indigenous fish and invertebrate populations as previous research has shown increased amounts of certain trace metals in winter flounder, Atlantic tomcod, and lobster in several areas of the estuary (Trowbridge and Jones, 2009). Furthermore, with the current emphasis on oyster restoration and farming (PREP, 2009) the issue of metal contamination will continue to be important. Thus knowledge of both nutrient and metal (contaminant) cycling are essential for moderating anthropogenic effects on contaminant release.

Nutrients and metals are supplied to the estuaries through numerous pathways; utilizing all interfaces between air, water, and sediment. Like all systems, contaminant accumulation depends upon inputs and outputs as well as contaminant generation within the estuary. Primarily, nutrient regeneration and metal regeneration occurs in sediment. At the sediment-water interface, contaminant release to the overlying water occurs by diffusive flux through sediment. This process may be enhanced by activity of bioturbating organisms, turbulence in the overlying water (Vanderborght et al., 1977), resuspension (Kalnejais et al., 2007, 2010) or similar sediment disturbances such as trawling or dredging (Eggleton and Thomas, 2004).

The balance between oxic and anoxic conditions in sediment and bottom waters creates a unique chemical interplay between organic matter, nutrients, metals, and sulfide. Microbes regenerate nutrients within sediments through a series of redox reactions coupled with remineralization of organic matter (Froelich et al., 1979). These chemical pathways proceed in a stepwise fashion from surficial sediments to depth, from the highest energy yielding reactions to the lowest per mole of organic matter. Microbes performing aerobic respiration utilize dissolved oxygen (DO) as a terminal electron acceptor, causing a shift from oxic to suboxic conditions in upper sediment layers. Unlike aerobic bacteria, the enzymes of most anaerobes are unable to break

complex organics, resulting in a series of redox reactions coupled with anaerobic respiration in the suboxic and anoxic zone (Kristensen, 2000). These processes affecting metal and nutrient chemistries can occur on the scale of millimeters to centimeters and require high resolution sediment and pore water data to fully understand geochemical processes at work.

This study was aimed towards understanding nutrient and metal cycles occuring in the Great Bay Estuary, NH. Previous work has shown that nutrients are regenerated in the upper sediment layers due to organic remineralization coupled with sulfate reduction (Hines, 1981; Orem, 1982). Furthermore, these sediments may release nutrients, as in the case of ammonium and silica, or have little to no fluxes or even uptake, as in the case of phosphate and nitrate (Lyons et al., 1982). Increased runoff (GBSC, 2010) and primary production (PREP, 2009) in the Great Bay has the potential to increase organic input to the sediment, thereby increasing nutrient regeneration and nutrient efflux. Thus, continuous monitoring of sediment fluxes are required to maintain sediment budgets over longer times scales.

Chromium pollution is of notable concern in Great Bay sediment due to historical dichromate input from a tanning facility on the Cocheco River (Capuzzo and Anderson, 1973), but sediment enriched in lead and silver have also been observed at several sites (Trowbridge and Jones, 2009). Information regarding temporal trends of solid-phase metals in the Great Bay Estuary is limited. The National Coastal Assessment (NCA) which gathered large spatial and temporal metal data in the early 2000's only analyzed metals from homogenized sediment samples near the sediment water interface. Depth-profiles of particulate phase metals are necessary in order to determine trends on metals over longer times scales.

The purpose of this study was two-fold. First, to explore how seasonal and spatial variability alters contaminant accumulation through changes in sediment biogeochemistry of Great Bay, and second, to quantify and compare contaminant effluxes from

sediment to other sources of contaminants to the Great Bay Estuary. Sediment cores were obtained between the spring, summer and fall from several sites with varying sediment characteristics, biological activity and hydrodynamics. High resolution pore water and particulate data are presented relating seasonal effects on contaminant accumulation and release. A sulfate-reduction model is employed to account for the kinetics of nutrient regeneration in sediment pore water. Contaminant fluxes from molecular diffusion are compared to past estimates of other nutrient input to assess if conditions within the Great Bay are changing.

1.1.1 Field Site

The Great Bay Estuary, shown in Figure 1-1, is a mesotidal estuary consisting of the Great Bay, Little (Upper and Lower) Bay, and seven tidal rivers located in New Hampshire and Maine, U.S. The average tidal range varies between 2.5 m at the mouth of the estuary to 2.1 m at mouth of the Squamscott River (NOAA, 2012). Maximum tidal currents may reach up to 2.0 m/s (Bilgili et al., 2005). Main channel depths for the Great Bay and Little Bay are approximately 10 m and 3 m respectively (Bilgili et al., 2005). However, the average depth for Great Bay is approximately 2 m (Armstrong et al., 1976), so up to 50% of the Little and Great Bay can be exposed as mudfats at low tide (Bilgili et al., 2005).

The bedrock, made up of the Kittery and Eliot formations, consists primarily of metamorphic dark-gray slates (NOAA, 2012), with igneous intrusions of diorite and monzonite present in some areas (Oczkowski, 2002). Fringing salt marshes consisting of *Spartina alterniflora* and *Spartina martens* are present in numerous areas in the estuary. The estuary supports a number of commercial and recreational fisheries including winter flounder, herring, smelt, Atlantic tomcod, Coho salmon, and striped bass (NOAA, 2012). Near the seafloor, benthic invertebrates include American lobster, *Gemma gemma* and *Macoma balthica* molluscs, several species of polychaete

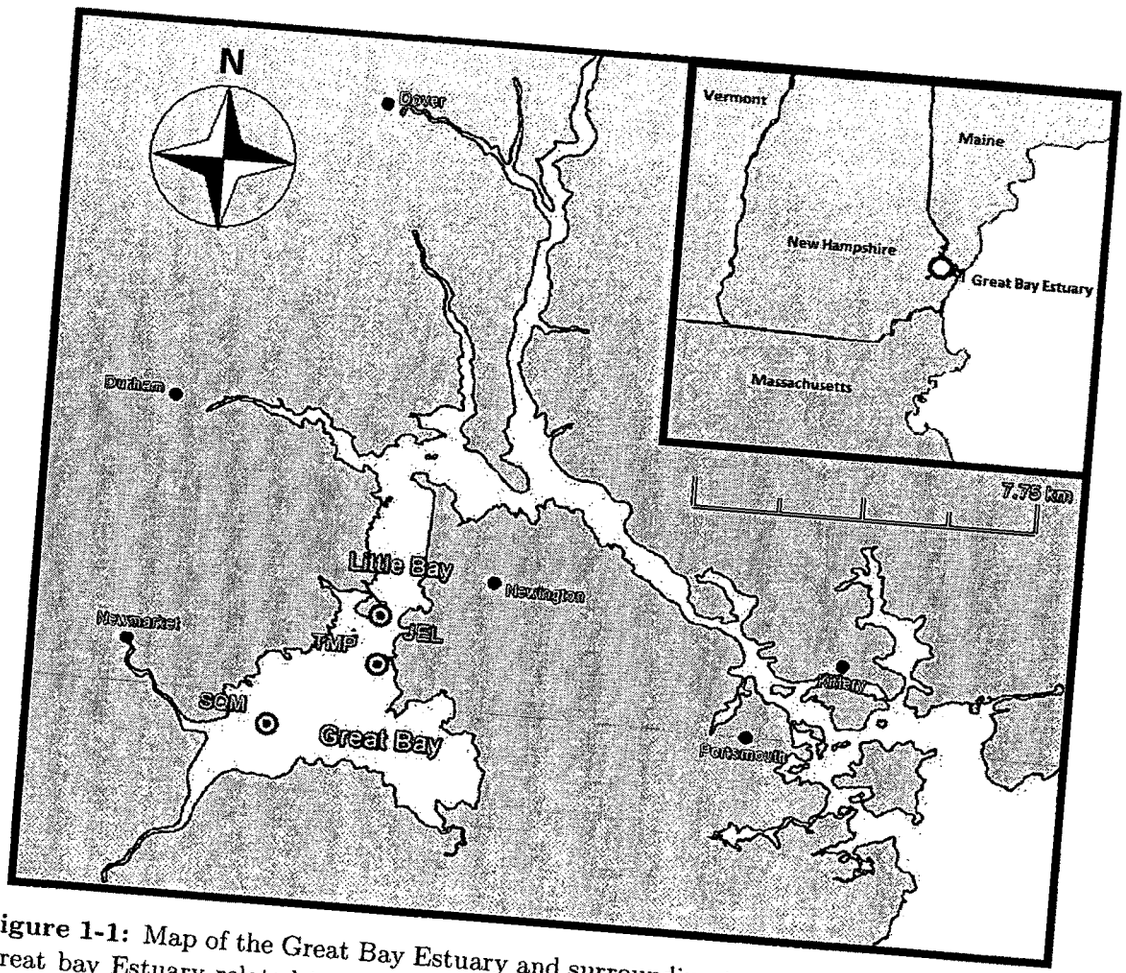

Figure 1-1: Map of the Great Bay Estuary and surrounding towns. A regional map of the Great bay Estuary related to other New England states is shown in the the inset. Study sites are marked with bullet symbols.

(*Nereis sp.*) and acorn worms, sand shrimp (*Crango septemspinosus*), Atlantic horseshoe crab (*Limulus polyphemus*), and several species of snails (Winston and Anderson, 1971).

In recent years, urbanization of the surrounding watershed has lead to several problems with physical and biological implications to the estuary. Increases in impervious surfaces in the surrounding watershed have increased siltation in several areas of the Little Bay and tidal rivers (GBSC, 2010). Total nitrogen export to the estuary has increased by 42%, which has increased chlorophyll-A and lowered dissolved oxygen concentrations in several parts of the estuary (PREP, 2009). Furthermore, toxic contaminants (chromium, copper, and lead) in sediment have exceeded screening values in several areas, though the bioaccumulation in tested organisms has not been as severe (PREP, 2009).

1.2 Methodology

1.2.1 Field Work

Four sites were chosen as representative of sediment chemistry in the Great Bay. Undisturbed sediment cores were obtained in quadruplicate using 10.8 cm (internal diameter) acid-cleaned polycarbonate barrels. Divers using SCUBA were employed to gather cores from the Thomas Point (TMP) and Squamscott (SQM) sites, while cores near the cove of Jackson Estuarine Lab (JEL) were gathered by-hand. Cores from JEL were collected during falling tide while while sediment was still inundated. Excess overlying water was stored in a 30 L acid-cleaned carboy.

All plasticware used in the extraction, storage, and analysis of metals from sediment pore water were pre-cleaned with trace-metal grade 20% HCl. Plasticware used for nutrients samples were pre-rinsed with copious amounts of 2 MΩ water. All steps of pore water extraction were performed under a nitrogen atmosphere to prevent oxi-

Table 1.1: Description of field site characteristics. Water depths at TMP and JEL are from Wengrove (2012).

	TMP	Spring JEL	Fall JEL	SQM
Lat(decimal)	N 43.08152	N 43.09174	N 43.09174	N 43.06743
Long (decimal)	W 70.86461	W 70.86474	W 70.86474	W 70.89423
Date	9-24-2010	6-3-2011	8-4-11	8-16-2011
Collection Method	Diver	Hand	Hand	Diver
Water Depth (m)	2-4 m	1.5-4 m	1.5-4 m	4 m
Temperature (°C)	18.4	18.7	22.6	21.5

dation artifacts. A glove-bag was purged with N_2 gas 2-3 times before enveloping the sectioning apparatus. Nitrogen was allowed to flow continually through the glove-bag during sectioning. Sediment cores were held by vice while a piston inserted into the base allowed the sediment to be incrementally raised past the upper edge of the core barrel. Layers of sectioned sediment cake were inserted into either 25 mL (screw-cap) or 50 mL (snap-cap) test tubes, and centrifuged for approximately 10-20 minutes in either an IEC International Centrifuge (model HT) or (need JEL centrifuge name, 8000 rpm, 10°C)) centrifuge. Supernatant pore water was carefully extracted using 15 mL acid-cleaned syringes and filtered through 0.45 μm polysulfone syringe filters. The resulting solution was pipetted into 4 mL sampling vials containing 400 μL of Optima trace metal grade nitric acid.

1.2.2 Porosity Measurements

Separate sediment cores were analyzed in sections to derive changes in sediment total porosity with core depth. After sectioning the sediment was weighed and allowed to dry in a VWR International (model 1305U) oven at 60°C. Water content was determined by mass difference. Porosity was calculated volumetrically assuming densities of 2.65 g cm^{-3} and 1.02 g cm^{-3} for bulk sediment and seawater, respectively.

1.2.3 Nutrient Analysis

All nutrient analyses were performed using standard spectrophotometric methods with either a Milton Roy Spectronic 601 or a Perkin Elmer Model SIMAA 6000 atomic adsorption spectrophotometer. Table 1.2 lists each analysis, the slope of the calibration curves, the squared Pearson product moment correlation coefficient (r^2) and the limit of detection (LOD). The limit of detection (LOD) was calculated as the average plus five times the standard deviation of the test blank (Appendix A).

Table 1.2: Standard spectrophotometric analyses to test for nutrients and sulfide, average squared Pearson product moment correlation coefficients (r^2) and limits of detection (LOD)

Species	Method	Source	Average r^2	LOD (μM)
Ammonium	Phenol Blue	Strickland and Parsons (1968) Gieskes et al. (1991)	0.992	2±2
Nitrate-Nitrite	Resorcinol	Zhang and Fischer (2006)	0.996	2.5±2
Phosphate	Molybdate Blue	Strickland and Parsons (1968) Gieskes et al. (1991)	0.998	0.5±0.3
Silica	Molybdate Blue	Strickland and Parsons (1968)	0.999	0.5±0.5
Sulfide	Methylene Blue	Cline (1969)	0.997	-

The resorcinol test was a method developed for spectrophotometric determination of dissolved nitrate-nitrite in seawater, and its application to pore water samples was introductory in this study. The process involves addition of sulfuric acid, hydrochloric acid, and resorcinol to a pore water sample. The sulfuric acid leads to a protonation of a hydroxl group on the nitrate (in the form of nitric acid due to the lower pH) and converts it to the nitronium ion (NO_2^+), which in turn nitrifies resorcinol (Zhang and Fischer, 2006). The reaction is catalyzed by chloride. The nitrified resorcinol reflects a pinkish hue and absorbs maximally at 505 nm.

1.2.4 Metal Analysis

Trace metals in the erosion chamber water and sediment samples were measured with a Nu Instruments (Attom) mass spectrometer (MS). In an ICP-MS aqueous

solutes are turned into an aerosol by nebulization with an inert gas (argon) and ionized by passing through a plasma field. A series of capacitors and magnets direct the sample stream into a detector. For any given element, the spectrometer detects based on the mass-to-charge ratio of the incoming ions and returns counts per second (cps) of ions hitting the detector. Sediment pore water only had to be diluted to be analyzed by the MS whereas particulate-phase metals required first to be put in aqueous solution by a strong acid digestion.

Digestion Procedure

Particulate phase metals were digested using a combination of concentrated nitric acid, hydrogen peroxide, and hydrochloric acid. A total digestion was not undertaken as the undigested phases (silicates) do not represent the portion of sediment that usually leads to metal release (Forstner, 1980). The method was a combination of a USGS total digestion methodology (Briggs and Meier, 1999) and an EPA partial digestion methodology (3050B, 1996) for analysis of sediment, soils and sludges with ICP-MS. In addition to sediment samples collected from the Great Bay, the digestion procedure was perfomed on sediment reference materials (MESS-3, PACS-2), on Nuclepore filter membranes (see Chapter 2) and blank vials to determine background metal concentrations. The digestion procedure was as follows:

1. Homogenize sediment sample
2. Weigh 0.2 g (to nearest 4 decimal places) of sample into a Teflon vial.
3. Rinse sediment sample from side walls with a minimum of MQ water
4. Addition of 2 mL of 50% HNO_3 (1 mL MQ H_2O, then 1 mL conc HNO_3)
5. Heat samples on hot plate to 95°C for 10-15 minutes, remaining moist
6. Add 1 ml of concentrated HNO_3
7. Heat samples at 95°C for 30 minutes
8. Repeat steps 6 and 7 if the oxidation hasn't gone to completion, indicated by brown fumes. Keep the sample moist.

9. After cooling, add 400 μL MQ water, and 600 μL 30% H_2O_2
10. Warm the sample vial
11. Add 200 μL 30% H_2O_2
12. Repeat steps 10 and 11 until effervescence subsides, but not more than 10 steps (2 mLs of 30% H_2O_2)
13. Add 2 mL concentrated HCl
14. Heat the samples to 95°C for 15 minutes
15. Repeat if the reaction has not gone to completion

Sample Preparation and Dilution Scheme

Sample and standard solutions were prepared in 10 ppb Indium (In) with 2% nitric acid. The calibration standards were prepared using AccuStandard ICP-MS analytical standards, and covered the range of concentrations expected in the samples. The In internal standard was used to compensate for changes in cps intensities during sampling. Standards were run at the beginning and end of each session and mid-way during long days. When flucuations in running conditions occured that compromised the data, such as plasma de-ignition or clogging of the uptake capillaries, standard curves were verified again. Bracketing standards were run approximately every 7-10 samples to also monitor machine drift.

Erosion chamber and pore water samples used for the detection of dissolved Mn and Fe were diluted 1:20 and 1:100, respectively. Sediment digests were diluted 1:35 in order to keep silver and cadmium above the detection limits. The large concentration ranges between elements proved to be problematic in developing dilution schemes for samples. In addition to accounting for the concentrations within the sediment itself, the dilution scheme had to compensate for varying amounts of sediment on filter papers. The low dilution factor used to maintain silver and cadmium above the LOD also meant that the solutions were concentrated in major ions, which have the tendency to disrupt the plasma source and precipitate in machine orifices. How these

matrix effects were accounted for during data interpretation is discussed in the next section.

Instrumentation

ICP-MS machine settings are listed in Table 1.3. Measured isotopes were ^{52}Cr for Cr, ^{55}Mn for Mn, ^{56}Fe and ^{57}Fe for Fe, ^{63}Cu and ^{65}Cu for Cu, ^{66}Zn and ^{68}Zn for Zn, ^{107}Ag for Ag, ^{111}Cd for Cd, and ^{208}Pb for Pb. Each sample scan consists of three cycles with each cycle consisting of 500 sweeps over a precise mass range. The cps spectrum is then integrated and given as a final output in counts per second

Table 1.3: Typical operating settings of the ICP-MS for trace metal analysis. Data acquisition time differed depending on the number of elements run, and was less on days in which Fe/Mn were analyzed.

Instrumental Parameter	Set Point
Resolution	3000
Forward Power	1200 W
Nebulizer Ar gas flow	26-30 psi
Auxiliary Ar gas flow	1 L/min
Coolant flow	13 L/min
Cones	Ni sampler and skimmer
Acquisition method	Magnetic jump with electric scan over small mass range
Channels per mass	20
Number of cycles	3-5
Number of sweeps	500
Dwell time	1000 μs
Data acquisition time	$<$ 390 sec

The slopes of the calibration curves were determined by the following formula:

$$S = \frac{STD_{cps}}{In_{cps}} \frac{[In]}{[STD]} \tag{1.1}$$

where STD is the analyte in concentration ([ ]) and cps output units. All calibration curves were forced through the origin, however sample concentrations fell well above

the origin and were unaffected by any possible increases in relative error.

A decrease in In counts was most pronouced when running the concentrated sediment digests. This resulted in changes between the slope of Eqn. 1.1 at the beginning and the end of each run. In this situation, the rate of change in slope was assumed linear and approximated according to the following equation:

$$Z = \frac{S_f - S_i}{N_f - N_i} \tag{1.2}$$

where N is the sample number, and the subscripts f, i refer to final and intial. The sample numbers were used as a proxy for time because roughly the same amount of time passed between subsequent samples. The individual metal (Me) concentration of a sample solution was then:

$$[Me] = \frac{Me_{cps}}{In_{cps}} ZN[In]_x \tag{1.3}$$

Concentrations were then corrected for the amount of metals added during digestion using concentrations obtained from acid blanks. Metal content of digested filter papers were subtracted from the erosion cores samples. Metal contamination in the acid and filter papers was essentially neglible after dilution, and for the most part were statistically similar to standard blanks.

Measurements of standard reference materials (SRM) were used to validate this digestion and detection scheme. It was discovered after running multiple sessions of sediment digests that some metals from the SRMs were greatly different from previously determined values (see next section). A matrix calibration was run to determine if sediment matrix effects had an influence on the slopes of the calibration curves. Known amounts of metals were pipetted into a sample digestion of unknown metal concentration. The resulting slope (Eqn. 1.1) of this new set of 'standards' should have matched the slope of the dilute clean standards that were previously used

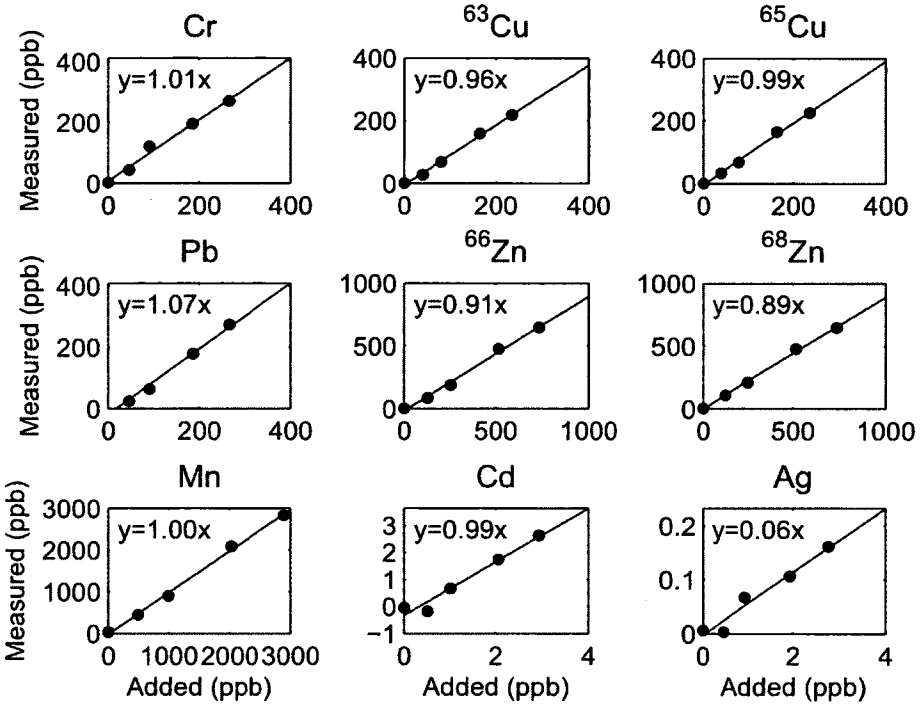

Figure 1-2: Plots of actual measured concentrations versus added concentrations for individual solutes for the ICP-MS matrix calibration. Linearity was observed in all species, however a matrix effect was observed for silver and zinc due to the lesser amounts detected than what was added

to determine concentrations if no matrix effects occured. This was found to not be the case for zinc and silver as the slopes were variable by up to 10% for Zn and 95% for Ag. Ag data was disregarded in result analysis because of the significant matrix effect. For Zn, the difference between the matrix slopes (which are representative of these digestions) and the slopes obtained from the dilute standard solutions was taken into account by multiplying the concentrations by the percent difference of the two slopes.

Calibration curve slopes and the lower limits of detection are shown in Tables 1.4 and 1.5. There was good comparability between different days of analysis for all elements except Cr on 16-Jun. The lower output of Cr relative to the other days of analysis was anomalous, but might have been a result of the calibration. Cr data from this day was disregarded. The LOD (ppb) were orders of magnitude below the range of metal concentrations in sediment digestates (Table 1.5). Detection limits of Fe and Mn on days in which only pore water or erosion chamber samples were run were 1.5 and 0.2 ppb respectively.

Table 1.4: Slopes of calibration curves at the beginning of each run according to Eqn. 1.1. Dissolved pore water and erosion core samples were run on the two days in September, the following days were digested sediment samples.

	Element						
Date	Cr	Mn	Fe	Cu	Zn	Cd	Pb
14-Sep	-	0.84	44	-	-	-	-
16-Sep	-	1.4	69	-	-	-	-
14-Feb	1.4	1.2	54	5.6	15	-	1.4
24-Apr	2.0	2.0	56	5.4	17	12	2.1
16-Jun	0.1	1.4	57	5.4	15	9.7	1.5
18-Jun	1.5	1.7	63	5.5	15	10	1.3
22-Jun	-	1.4	56	-	-	-	-

Table 1.5: Lower limit of detection (LOD, ppb) for each trace metal and session of ICP-MS analysis. Calculated according to Eqn A.3 in Appendix A. Dissolved pore water and erosion core samples were run on the two days in September, the following days were digested sediment samples.

	Element						
Date	Cr	Mn	Fe	Cu	Zn	Cd	Pb
14-Sep	-	0.06	2	-	-	-	-
16-Sep	-	0.2	1	-	-	-	-
14-Feb	0.1	0.1	2	0.3	0.9	-	0.05
24-Apr	0.2	0.4	2	0.2	1	0.02	0.1
16-Jun	0.03	0.3	16	0.4	1	0.01	0.1
18-Jun	0.4	1	2	0.2	2	0.02	0.04
22-Jun	-	0.2	2	-	-	-	-

Accuracy and Precision

Within each run, the analytical precision (%RSD) of prepared acid standards were all below 10%, generally falling below 5% RSD for most elements (Table 1.6). Cd was the exception, however Cd was orders of magnitude lower in concentration than the other elements, and the magnitude of the precision reflects the difficulty for producing precise data close to the lower limit of detection. The elemental accuracies were generally within 10%.

Although the precision was good for any given day of running, the precision was slightly lower between different sessions of analysis (Table 1.6, "'Sediment Digestate'"). The concentration variation between different analyses should be within the analytical precision for each element. This was not the case for Cr, Pb and perhaps Fe as concentrations for these elements changed between subsequent runs (Table 1.6). One reason for the poor precision between runs may have been due to changing concentrations in the stored digestate solutions. The solution pH's were determined post-analysis and found to be well below a pH of 1–making removal by precipitation unlikely. Because concentrations increased in the stored digestate it is possisble that leaching of metals from non-dissolved silicates may have occured during the several months over which these analyses took place.

Table 1.6: Accuracy (first columns, calculated as the % difference between detected and actual concentrations) and Precision (% RSD) from each day of analysis using daily-prepared acid standards. Digested sediment extracts were run on multiple days to check the variability in precision between sessions (Sediment Digestate)

	Elemental Accuracy (% difference) and Precision (% RSD)													
Date	Cr		Mn		Fe		Cu		Zn		Cd		Pb	
14-Feb	-1.6	4.6	1.3	1.3	-1.0	3.1	-1.0	3.1	-1.9	5.2	-	-	-1.0	4.8
24-Apr	1.0	3.2	0.54	1.6	0.29	2.0	-0.33	2.0	0.10	1.2	-0.30	1.0	2.6	6.0
16-Jun	1.8	6.4	-1.5	5.7	-1.3	5.5	-1.1	2.9	-1.2	4.0	-1.2	2.6	0.14	5.0
18-Jun	-5.8	2.3	-1.9	1.7	-3.3	2.0	-4.0	1.7	-4.7	2.6	4.4	6.2	-4.5	1.8
22-Jun	-	-	-7.6	1.8	-7.1	2.4	-	-	-	-	-	-	-	-
Sediment Digestate	-	24	-	7.0	-	12	-	1.9	-	1.3	-	-	-	24

Table 1.7: Concentrations (ppm) and % recovery of metals analyzed from digestions of standard reference material from each day of analysis. The trace metal concentrations and error for each SRM is listed in the headings.

		Element (Detected concentration (ppm), % Recovered)													
	Date	Cr		Mn		Fe		Cu		Zn		Cd		Pb	
Certified MESS-3 (ppm)		105±4		324±12		43400±1100		33.9±1.6		159±8		0.24±0.01		21±0.07	
	14-Feb	30	28	258	80	28900	67	26	76	116	73	-	-	12	55
	24-Apr	42	40	281	87	29900	69	30	88	117	74	0.18	75	17	80
	18-Jun	34	32	298	92	30400	70	29	86	126	79	0.20	83	15	71
	22-Jun	-	-	319	98	32700	75	-	-	-	-	-	-	-	-
Certified PACS-2 (ppm)		90.7±4.6		440±19		40900±600		310±12		364±23		2.11±0.15		183±8	
	14-Feb	34	37	218	50	23500	58	206	66	249	68	-	-	100	55
	24-Apr	49	54	242	55	25200	62	215	69	254	70	1.6	76	90	49
	18-Jun	45	50	237	54	24500	60	247	80	253	70	1.4	66	106	58
	22-Jun	-	-	200	45	23000	56	-	-	-	-	-	-	-	-

Analytical accuracy was good for standards prepared daily, but the case was different for standard reference material. Certified SRM trace metal concentrations are listed in Table 1.7 alongside the detected concentrations and % recovery determined for each analytical session. The lower recoveries of metals from SRMs are due to the digestion procedure employed. SRM certified values are reported for total digestion of sediment, therefore the partial digestion used in this study to quantify the most labile contaminants resulted in less than 100% metal recovery. The validity of the procedure is supported by the fact that metals extracted between subsequent SRM digestions were consistent (Table 1.7), suggesting that the target mineral phases (Fe/Mn oxides, carbonates, sulfides, and organics) were fully digested.

Less than 100% metal recovery has been reported in other studies using partial digestions. Townsend et al. (2007) compiled a list from several studies using partial digestions with 1 M HCl and compared the % recoveries to metals extracted from total digestions for MESS-3 and PACS-2 reference materials. Metals recovered from totally digested sediment were within 5% of the certified values, however metals extracted from sediment digested with 1 M HCl was significantly less (generally less than 50% recovery for MESS-3 sediment and 75% for PACS-2). For example, recovery of Cr was only 3% from MESS-3 sediment and 13% from PACS-2, whereas only 55% of Mn was recovered from MESS-3 and 12% from PACS-2. Likewise, only 20% of Fe was recovered from both SRMs. The % metal recovery was higher in this study for all metals compared to Townsend et al. (2007), suggesting more metal is digested based on the strength of the acid digestion and the use of the hydrogen peroxide and nitric acid to oxidize the sample. These lower % recoveries in SRMs (Table 1.7) do not disparage the reliability of the digestion procedure, instead they indicate that like Great Bay sediment several trace metals are locked in highly refractory mineral phases existing in reference materials. In the future more SRM samples should be digested according to Section 1.2.4 to establish metal recoveries over a

greater sample population. Furthermore, non-digested sediment may be compared to digestates using x-ray diffraction (XRD) to verify that the target mineral phases are indeed fully solubilized.

1.2.5 CHN Analysis

Total carbon (TC), total organic carbon (TOC), and total nitrogen (TN) analyses where performed using a Perkin Elmer Series II 2400 CHN Elemental Analyzer on samples from one core at each of SQM and Fall JEL sites. Sediment samples (20 mg) were initially analyzed for total carbon (TC) and total nitrogen (TN). Sample splits (20 mg) were digested using sulfurous acid according to the method of Phillips et al. (2011) to determine weight percent of TOC. Inorganic carbon was calculated as the difference in percent weights of TC and TOC. Quality control was insured with an acetanilide internal standard and Soil Standard Silty OAS B2182 prepared by Elemental Microanalysis with weight percents of 1.89 TOC, 0.30 inorganic carbon (IC) and 0.18 TN.

1.2.6 Determination of Molecular Diffusive Fluxes

The nutrient and metal fluxes from pore water due to molecular diffusion were calculated by modifying Fick's First Law to account for temperature, sediment tortuosity, and salinity. Modifications were similar to Wijsman et al. (2002) as referenced in Boudreau (1997). It was assumed that the advection due to sediment compaction was negligible (Orem, 1982). Fick's First Law relates the flux rate of a diffusing species to a solute-specific diffusivity constant (D_o, units $cm^2\ s^{-1}$), and the concentration gradient according to Equation 1.4

$$F = -D_o \frac{\partial C}{\partial z} \tag{1.4}$$

where F is flux rate (μmol s^{-1} cm^{-2}), C is concentration (μmol cm^{-3}) and z is depth (cm). For all species except $Si(OH)_4$, diffusivity was temperature corrected using diffusivity constants at infinite dilution and empirical parameters from Boudreau (1997) as listed in Table 1.8. Equation 1.5 shows the linear relationship between a diffusivity constant and temperature.

$$D_o = m_o + m_1 T \tag{1.5}$$

where T is temperature (^{o}C), m_o is diffusivity (cm^2 s^{-1}) at T = 0^{o}C, and m_1 is an ion-specific empirical parameter (cm^2 s^{-1} $^oC^{-1}$). In the case of dissolved silica, a molecular diffusivity constant according to Wollast and Garrels (1971) was used. In situ water temperatures were approximated using temperature data gathered by the Great Bay buoy. Temperatures were averaged over a weekly interval centered on each sampling date.

Table 1.8: Empirical parameters for calculating molecular diffusivity constants (Boudreau, 1997), and silica diffusivity coefficient according to Wollast and Garrels (1971).

Nutrient	m_o	m_1	D_o 10^6 cm^2 s^{-1} at T = 25^{o}C
NH_4^+	9.5	0.413	19.8
HPO_4^{2-}	3.26	0.177	7.69
NO_3^-	9.5	0.388	19.2
$Si(OH)_4$	-	-	5

The salt matrix of seawater alters diffusing species due to coulombic interactions between solutes and major ions. The effect on diffusivity can be expressed using the ratio of water and seawater viscosities at T = 25^{o}C (Boudreau, 1997):

$$\frac{D_{sw}}{D_o} = \frac{\mu_o}{\mu_{sw}} \tag{1.6}$$

where D_{sw} is diffusivity ($cm^2\ s^{-1}$) in seawater, u_o and u_{sw} are the viscosities (centipoise) of water and seawater respectively. Diffusion of a solute through interstitial pore water is also governed by the path of the solute takes along a concentration gradient. Tortuosity (ϕ) is a dimensionless proportion which accounts for the convoluted or constricted pathways traversed by diffusing species. Several empirical correlations relate sediment tortuosity to sediment porosity (θ). In this experiment, a modified Weissberg relationship was employed to describe the tortuosity (Boudreau, 1997).

$$\phi^2 = 1 - ln(\theta^2) \tag{1.7}$$

and then modify the Fickian Diffusion equation

$$F = -\frac{D_{sw}}{\phi^2}\frac{dC}{dy} \tag{1.8}$$

D_{sw} denotes the diffusivity of a nutrient in seawater. Nutrient fluxes resulting from molecular diffusion were calculated using linear regressions of the concentration profiles from the oxic zone (approximately first 6 pore water data points). Fluxes of nitrate-nitrite were calculated using the concentration gradient between the first pore water data point and the overlying water (explained in Sec: 1.3.5).

1.3 Results and Discussion

1.3.1 Sediment Characteristics

Organics

Cores of approximately 20 to 30 cm length were collected from each site. The difference between oxic and anoxic sediment was apparent by a color change from brownish/gray to black in the upper 2 cm of sediment at each site. The black color was most likely due to precipitated iron sulfides, as sulfide odor was experienced

during sectioning. Total carbon (TC) determined by CHN analysis ranged 1.8-3.9 % and 1.8-3.1 % (g C g^{-1} sediment) at JEL and SQM, respectively. Total nitrogen (TN) ranged 0.20-0.28 % at JEL and 0.19-0.34 % at SQM. Organic carbon at both sites made up 90 % of the TC (Fig. 1-3). The inorganic portion was most likely from shell debris and does not represent bulk sediment composition.

Profiles of OC, and C:N did not yield trends with sediment depth (Fig. 1-3). Average particulate C:N (mol/mol) in JEL Core 2 was 10.2 (σ_D = 1.45), whereas at SQM Core 2 C:N was 10.6 (σ_D = 1.47). Both are similar though slightly larger than the Redfield ratio of 6.63 C:N for marine phytoplankton (Redfield, 1958). The difference is most likely from organic material of terrestrial origins as vascular plants tend to have higher C:N ratios due to cellulose production (Meyers, 1994). Sparse eelgrass was encountered in cores from JEL while leafy material was observed at SQM. Orem (1982) found average organic C:N at SQM to be 9.5, however the JEL site was 12.6 in the upper 30 cm of sediment. The difference at JEL suggests that sediment variability may occur over relatively small spatial scales, or over longer temporal periods.

Porosity

Porosity in the upper 3 cm of sediment at JEL increased between June and August (Fig. 1-4). In some cases high porosity at the sediment-water interface is the result of sediment deposited quicker than the time required for sediment consolidation (Boudreau, 1997). However, sediment porosity has also been correlated with active bioturbation (Mulsow et al., 1998). Previous studies in the Great Bay have found that that bioturbation decreases concomitant with the decrease in salinity gradient from the mouth of the Estuary (Winston and Anderson, 1971), which may explain why sediment reworking is higher at JEL than at SQM (Hines and Jones, 1985). In this study, polychaete worms, snails, clams and small crabs were all observed at JEL

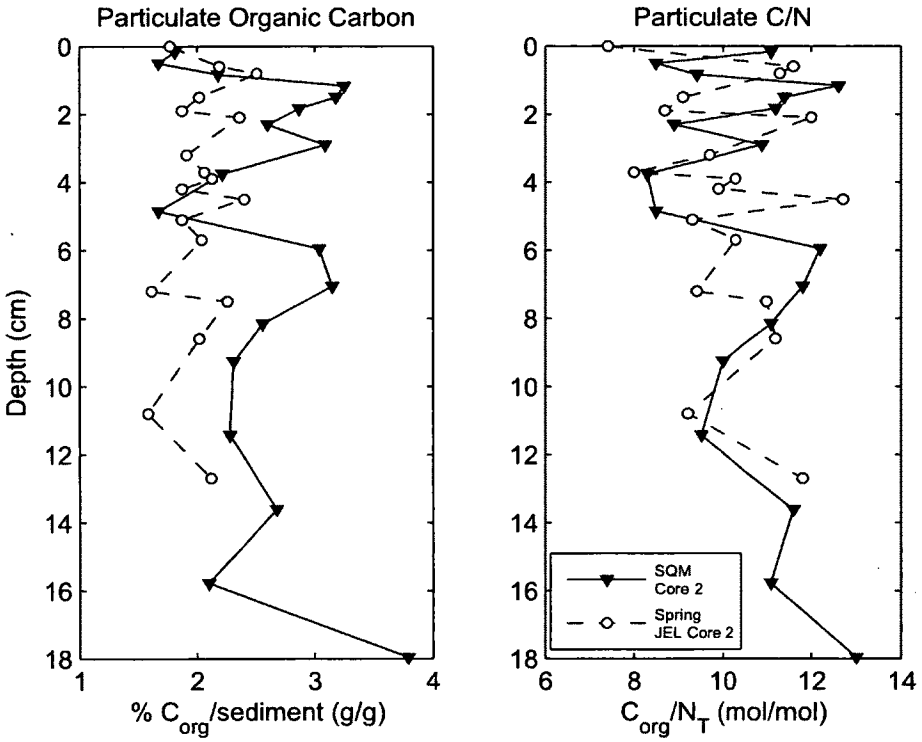

Figure 1-3: Particulate organic carbon, and organic carbon to nitrogen ratio of two sediment cores.

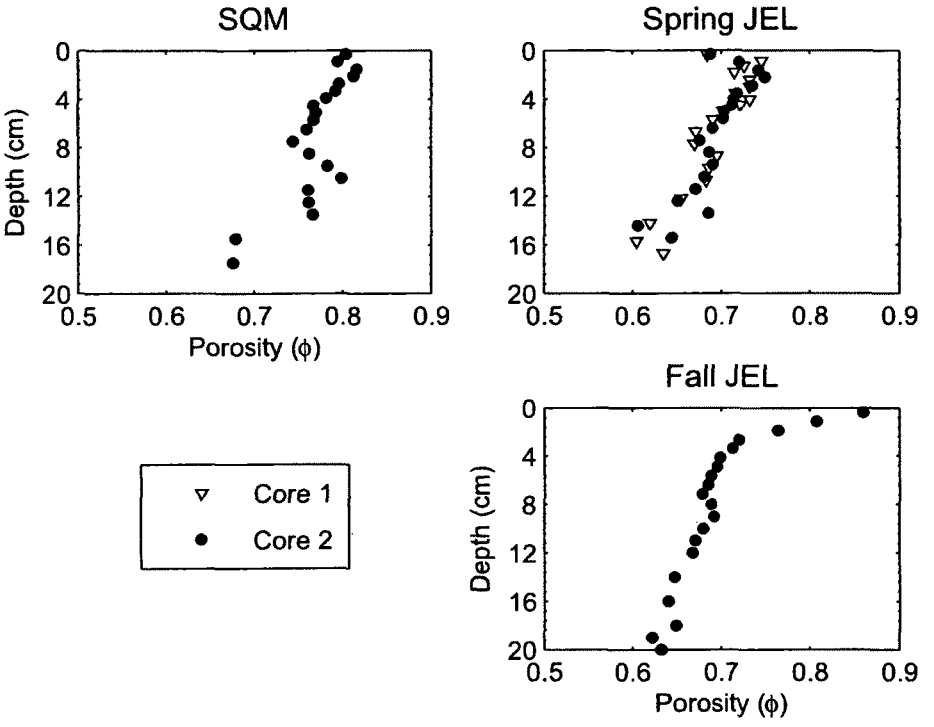

Figure 1-4: Porosity for cores obtained from three field sites. Note: Due to the destructive sampling associated with porosity these cores are different than the cores presented for nutrient and metal profiles.

sediment. Futhermore, the polychaete *Nereis* sp. and lugworm *Arenicola marina* were discovered in Spring JEL Core 1 and Fall JEL Core 1, respectively. Sediment around the burrows was similar in color (brownish-gray) to the oxic sediment at the interface, and sharply contrasted the bulk anoxic sediment. Burrowing organisms cycle water through sediment, allowing oxidation of anoxic sediment inducing a color change in the sediment (see NH_4^+ and PO_4^{3-} results). Beneath the top few centimeters porosity was higher at SQM (0.8) than at Spring and Fall JEL (0.7) even though less bioturbation occurs near this site (Hines and Jones, 1985). Porosity at each site approached 0.6-0.7 beneath 16 cm.

1.3.2 Porewater nutrients

Ammonium and Phosphate

Dissimilatory organic matter remineralization releases nitrogen (N), phosphorus (P), inorganic carbon and organic moieties into the dissolved phase. N and P in the forms of ammonium (NH_4^+) and ortho-phosphate (PO_4^{3-}) accumulate in anoxic sediments but are relatively depleted in oxic sediment. Although minor excursions and microgradients were present, NH_4^+ increased from the sediment-water interface to depth in all cores (Fig. 1-5). Concentrations in the first pore water samples (0.15-0.20 cm depth) from TMP, Spring JEL and Fall JEL cores ranged 10-20 μM, but were four times greater in samples from SQM (40-80 μM). NH_4^+ at depth was greatest at SQM (1000-1300 μM), and least at JEL during the spring, reaching 130-170 μM. Spatial variation was evident between sites but remarkably similar within core duplicates (Fig. 1-5). The variability was most pronouced between cores gathered at JEL during August–likely due to the activity of bioturbating organisms.

In comparison to NH_4^+, there was significant variability in dissolved phosphate between duplicate cores at sites other than at SQM (Fig. 1-6). Phosphate is intimately tied with the presence of metal oxides, and depletion of dissolved phosphate in oxic sediment may result from adsorption to or co-precipitation with oxide minerals (Ruttenberg, 1992). Like NH_4^+, phosphate is generated by organic remineralization. However phosphate attached to metal oxides may re-dissolve if the host minerals are reduced, creating an additional source to pore water (Lehtoranta et al., 2009). Phosphate ranged from 0-11 μM at the sediment-water interface in all cores. Phosphate approaches an asymptotic concentration at depth, which was greatest at SQM (450 μM) and least at JEL. Surprisingly, pore water phosphate at JEL did not appear to increase between the spring and fall. This was unexpected given that microbial metabolism would have increased from higher temperatures as suggested by the in-

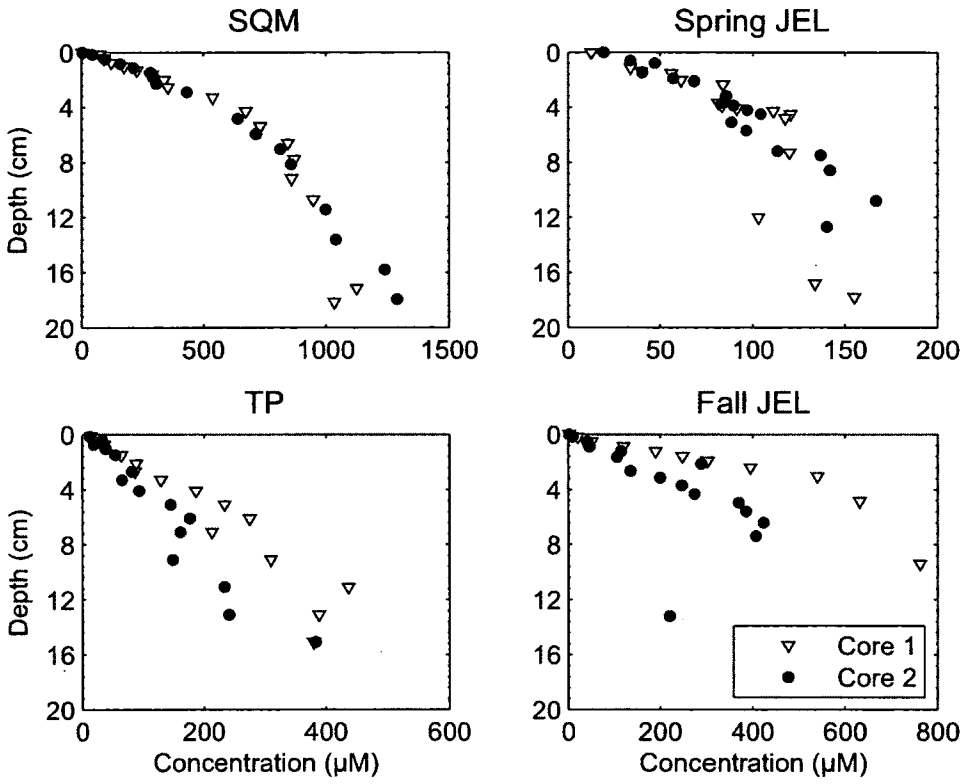

Figure 1-5: NH_4^+ pore water profiles of duplicate cores from each field site.

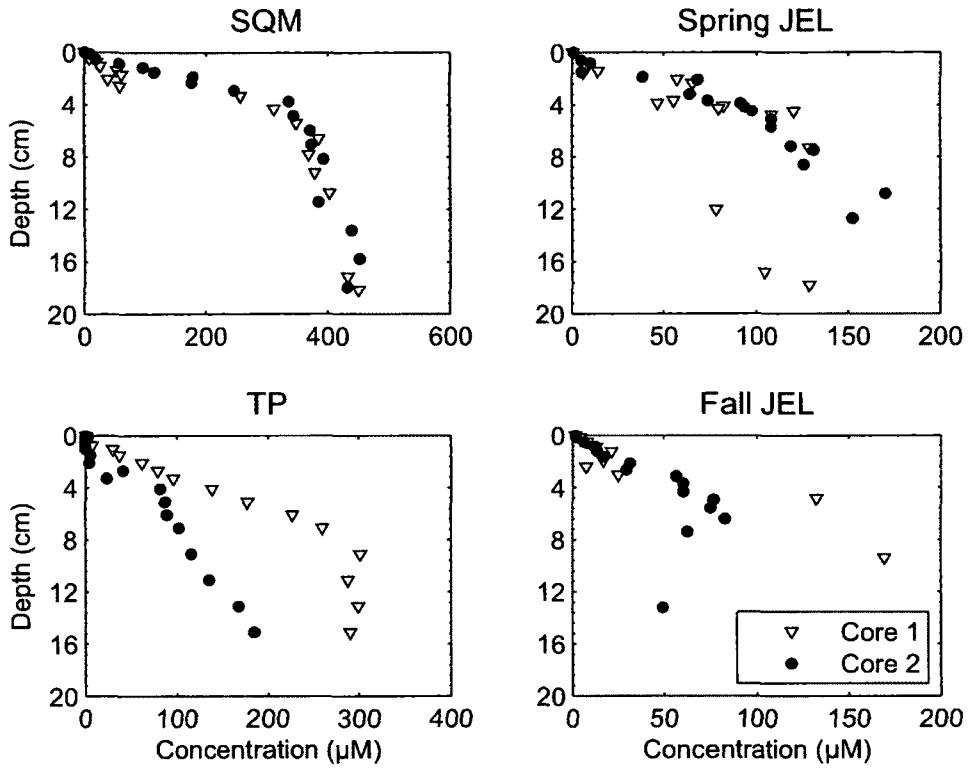

Figure 1-6: Phosphate pore water profiles of duplicate cores from each field site.

crease in NH_4^+ between seasons (Fig. 1-5). Table 1.9 lists the ratio of dissolved NH_4^+ to PO_4^{3-} in Great Bay pore waters, and kinetically corrected N:P ratios (see Section 1.3.4). Values are reported based on an average N:P ratio taken from all samples below 4 cm from the sediment-water interface, as N:P ratios fluctuated above 3-4 cm–likely an adsorption effect. Error is the standard deviation of the mean.

Oxidizing sediment is not only at the sediment-water interface. Bioirrigating organisms which pump overlying water into burrows may create an oxic environment extending radially from the burrow (Kristensen, 2000). This was apparent in several of the Spring JEL Core 1 and Fall JEL Core 1. Hines and Jones (1985) found that sulfate reduction in JEL sediments tended to be higher nearer to the sediment-water interface. However, dissolved sulfide did not accumulate in pore water because of

Table 1.9: Molar N:P ratios of dissolved NH_4^+ to PO_4^{3-} ($\pm$ 1 σ_D) and corrected molar N:P ratios using the diagenetic modeling approach of Orem (1982). N:P for Fall JEL Core 1 was approximated by substituting the k_N rate constant for k_P and solving for C_{Po} in Equation 1.17.

	Dissolved N:P		Corrected N:P	
Site	**Core 1**	**Core 2**	**Core 1**	**Core 2**
TMP	1.2 $\pm$ 0.2	1.6 $\pm$ 0.3	3.0	4.2
Spring JEL	1.2 $\pm$ 0.2	1.0 $\pm$ 0.1	2.9	2.3
Fall JEL	4.6 $\pm$ 0.2	5.1 $\pm$ 0.7	17.1	14.1
SQM	2.3 $\pm$ 0.2	2.4 $\pm$ 0.4	6.9	3.7

reduction of iron oxides that were redistributed during sediment reworking (Hines and Jones, 1985). The activity of organisms at JEL in essence introduces O_2 at depth allowing phosphate to be adsorbed to iron oxides. The depletion of phosphate is indicated by the higher N:P ratio at Fall JEL in comparison to SQM (Table 1.9).

Interestingly, the N:P of dissolved NH_4^+ and phosphate in anoxic sediment of the Great Bay is much less than the standard Redfield ratio (106C:16N:1P) for marine organic matter (Redfield, 1958). As stated previously, the organic origins at JEL and SQM are most likely marine with small but significant contribution from land. In the absence of removal mechanisms organics undergoing microbial remineralization would distribute the same stoichiometric N:P to the dissolved phase as in the original material (Berner, 1977; Martens et al., 1978). However, differential removal processes such as diffusion and adsorption alter the input from microbial remineralization, thereby masking the actual N:P ratio of decaying organics (Berner, 1977). Thus the effect of diffusion and adsorption must be taken into account to determine organic N:P ratios and model nutrient regeneration rates (see Section 1.3.4).

Silica

Release of silica to the dissolved phase is dependent primarily on the dissolution of biogenic opal and siliceous clays (Aller et al., 1985). Dissolved silica primarily takes the form of silicic acid ($Si(OH)_4$), but can also form polymers of $Si(OH)_4$ within

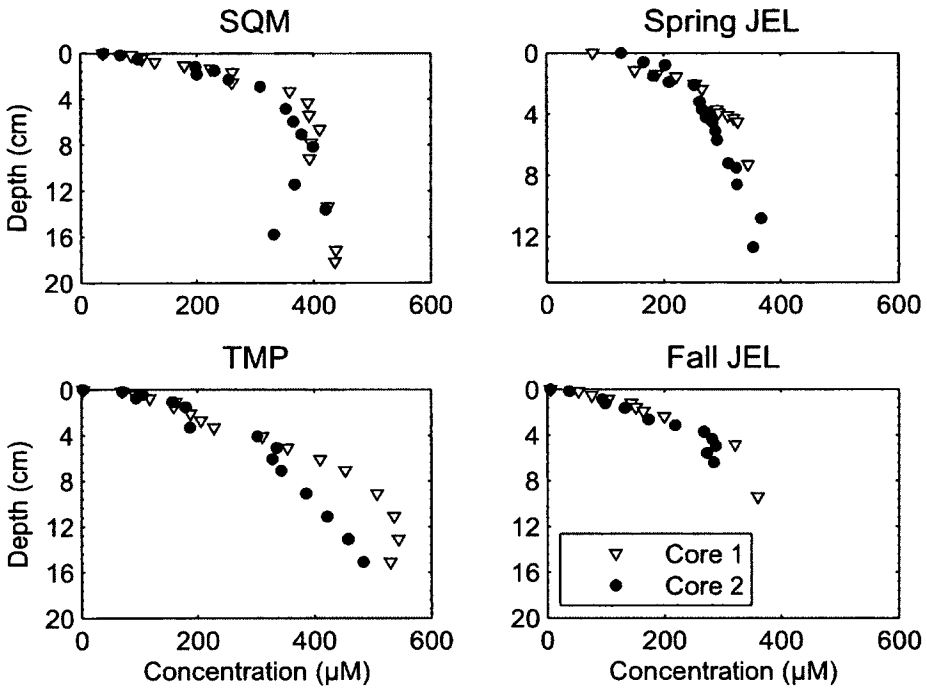

Figure 1-7: Concentration profiles of dissolved $Si(OH)_4$ from duplicate cores at each site

typical pH ranges of seawater (Wollast, 1974). The rate of dissolution is a function of temperature, pressure, solid surface area, and impurities in the dissolving opal (Sarmiento and Gruber, 2006). In the Great Bay, silica concentrations (Fig. 1-7) increased from the sediment-water interface to depth in all cores, but the gradient decreases with depth, Similar to profiles obtained by Gehlen et al. (1995) in the North Sea. Concentrations at depth were approximately 300-600 μM. At the interface, the highest concentrations were observed during the spring at JEL (80-130 μM). An exponential decay equation may be fit to silica profiles (Gehlen et al., 1995), however, the relationship would be less accurate at depths away from the sediment-water interface. A linear correlation sufficed for flux calculations at the interface.

Vanderborght et al. (1977) attributed water turbulence to elevated silica exchange in the upper layer (0-5 cm) of sediments from the North Sea. This layer was characterized by lower, relatively constant silica concentrations–analogous to a well-mixed layer. Beneath this zone silica profiles are similar to those obtained from Great Bay.

The absence of any type of well-mixed layer in pore waters indicates that fluid turbulence does not greatly influence dissolved silica near the interface. This is because the sediment porosity in the Great Bay (0.65-0.85) is less than North Sea sediments of Vanderborght et al. (1977)(greater than 0.9). Between Spring and Fall JEL the concentration gradient in the oxic-suboxic zone increased (between 0-4 cm depth, Fig. 1-7) indicating enhanced removal rates, most likely from bioturbation.

The contribution of dissolved silica from opal dissolution becomes minimal as pore water becomes saturated. The solubility of amorphous silica (1 atm pressure) as a function of temperature can be shown with the following relation (Wollast, 1974):

$$\log c = -0.309 - 0.723\frac{10^3}{T} \tag{1.9}$$

where c is solubility (moles/L) and T is temperature (K). Based on water temperatures during sampling periods silica solubility would be approximately 1600 and 1800 μM in the spring and fall respectively. The detected concentrations were 3-4 times less at depth. Numerous studies have also found $Si(OH)_4$ to be undersaturated with respect to opal in sediment pore water, by up to 40% (Sarmiento and Gruber, 2006). Two explanations may account for the silica undersaturation. First, either dissolution is kinetically slow due to low surface area, the presence of organic coatings on opal surfaces, and impurities in the opal matrix, or second, authigenic mineral formation occurs (Sarmiento and Gruber, 2006). Because $Si(OH)_4$ becomes asymtotic at depth, for example at SQM between 4-20 cm depth (Fig. 1-7), it seems more likely that silica concentrations are becoming saturated to the point where authigenic mineral formation becomes thermodynamically favorable. Amorphous silica is known to co-precipitate with magnesium in the form of sepiolite according to the following reaction (Wollast, 1974):

$$2Mg^{2+} + 3SiO_2(aq) + 4OH^- \rightarrow Mg_2Si_3O_8(s) \tag{1.10}$$

The equilibrium constant for the reaction is $10^{-37.2}$. Using the magnesium concentration of standard seawater (54 mM Mg^{2+}) and the pH range during sampling times (7.7-7.9) supersaturation of SiO_2 would occur between 380-700 μM. This concentration range matches well with the observed silica concentrations. Thus, authigenic mineral formation provides a likely explanation for the consistent range of seasonal silica concentrations at depth.

1.3.3 Dissolved and Particulate Metals

Dissolved Phase Iron and Manganese, and Sulfide

Iron and manganese concentrations in pore water were measured in one sediment core from the August sampling at JEL. Pore water profiles of these two species are given in Figure 1-8. As expected, the peak of both species occured near the sediment-water interface and rapidly decreased with depth. At the peaks, dissolved Mn and Fe concentrations were appromately 20 and 55 μM, respectively. In a temporal study at JEL, Hines et al. (1984) measured dissolved Fe concentrations during winter, spring, and summer for the years 1978-1980. The range of summer (measured in July) values they obtained was approximately 0-270 μM. The values for Fe from this study fall on the low end of this range. The range of yearly values for dissolved Mn obtained by Hines et al. (1984) from the upper 2 cm of at JEL was 15-52 μM. Likewise, Mn concentrations fall within this range.

Generation of Mn and Fe in pore water comes from dissimilatory reduction of manganese and iron hydroxides (MnO_2, FeOOH) during microbial oxidation of organic matter (Froelich et al., 1979). These reactions occur sequentially after aerobic respiration and denitrification have occured. The reduction of mineral Mn and Fe oxides reduces their oxidative states, from Mn(IV) to Mn(II) and Fe(III) to Fe(II) and form soluble species that accumulate in pore waters. At the sediment-water interface concentrations are low due to re-oxidation with dissolved O_2, and subsequent mineral

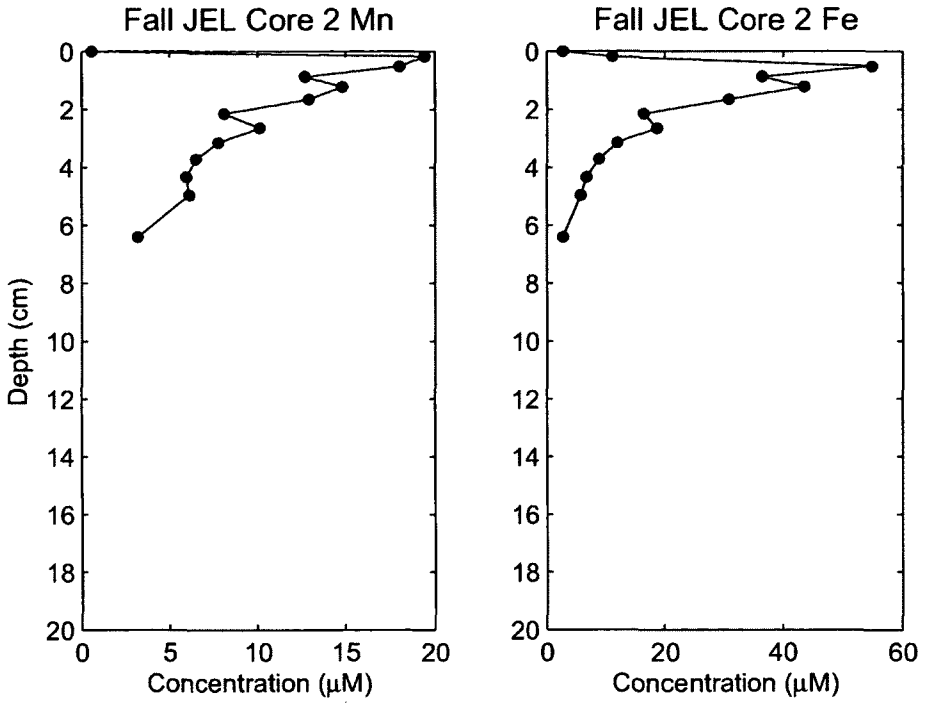

Figure 1-8: Pore water concentrations of iron and manganese at JEL in August 2011. The mean standard error of iron and manganese are 0.25 and 1.0 μM respectively. Detection limits were 0.3 and 2 μM for Mn and Fe respectively.

formation and/or adsorption. Mn reduction occurs shallower than Fe reduction due to the relative standard free energy (ΔG) output from each reaction (approximately -3000 kJ/mol for Mn reduction, -1500 kJ/mol for Fe reduction)(Froelich et al., 1979). The proximity of the peak in Mn to the sediment-water interface in comparison to Fe reflects this.

Dissolved Fe and Mn oxides produced near the surface diffuse to deeper sediments where they may react with dissolved sulfide produced through sulfate-reduction (Fig. 1-9). In the absence of oxygen, metal sulfides remain in reduced form and may be permanently buried (Cantwell et al., 2002). These pore water profiles show the same trend of decreasing metal concentration with depth. Sulfide was not detected in JEL sediments during August, but this does not indicate sulfate-reduction to sulfide did not occur, as titration of Fe with sulfide would remove sulfide from solution (Hines and Jones, 1985). Sulfide from TMP cores was depleted near the sediment-water interface

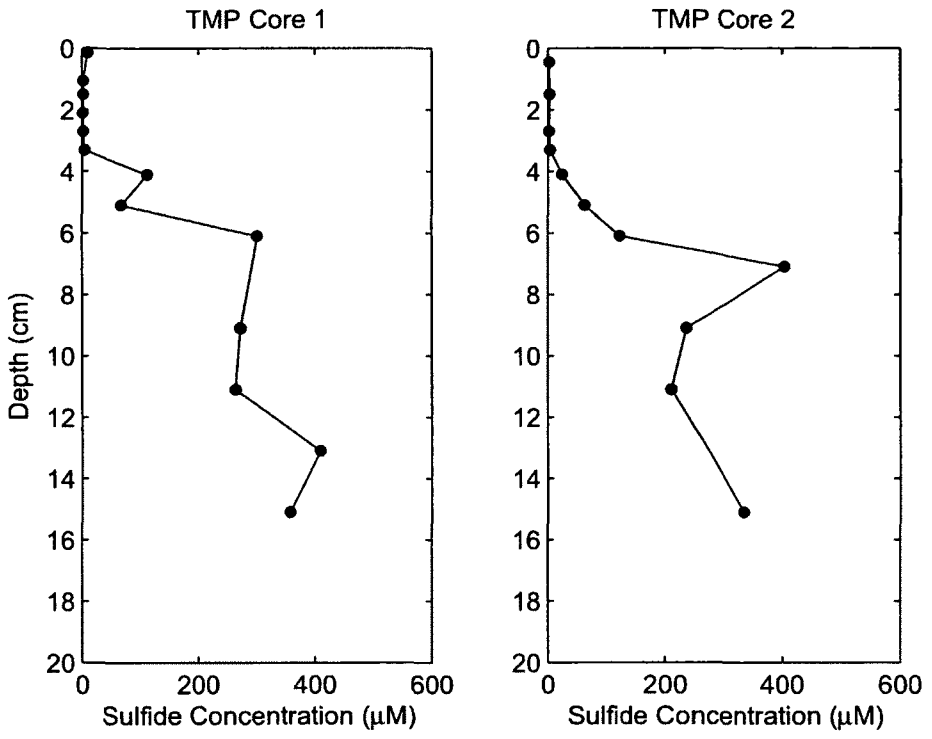

Figure 1-9: Pore water concentrations of dissolved sulfide at TMP in August 2010

where it would be easily oxidized back into sulfate. Concentrations began to increase beneath 3 cm (Fig. 1-9) and approached 400 μM at 16 cm depth. The instances of Fe(II) depletion after 3-4 cm at Fall JEL and accumulation of sulfide beneath 3 cm at TMP suggest that iron-reduction in the Great Bay is only significant in the top 3 cm of the sediment, below which sulfate-reduction reactions dominate.

Although Fe and Mn are important as micronutrients for primary production, their chief biogeochemical significance is their role in the cycling of adsorbed contaminants, both nutrients and metals. The Great Bay overlying water and surface sediments are oxic. As a result, molecular diffusion of Fe(II) and Mn(II) into the overlying water may be less significant than oxidation and precipitation/adsorption of these metals at the sediment-water interface. Similarly, mixing of reduced particulate trace metals from lower in the sediment due to sediment distubances or bioturbation may allow these metals to oxidize and concentrate at the sediment-water interface due to adsorption

to iron and manganese oxides or particulate organic matter. Results that exemplify this are presented in Chapter 2.

Nitrate

There are several processes controlling nitrate in Great Bay pore waters. Primarily NO_3^- is generated by aerobic respiration (Froelich et al., 1979), and nitrification of ammonium in oxic and suboxic sediment (Santschi et al., 1990), and depleted by denitrification in anoxic sediment. NO_3^- generation did not affect the concentration profiles of NH_4^+, as NH_4^+ concentrations were generally 1-2 orders of magnitude larger. A NO_3^- peak was apparent in most cores (Fig. 1-10), although the depth over which these processes occured was significantly different between sites. Generally NO_3^- concentrations increased from 0-5 μM to 10-45 μM at the peak. Core 2 from SQM was an exception, as NO_3^- increased to 460 μM at 1.2 cm depth.

As indicated by the presence of reduced Fe in the dissolved phase within 1 cm depth (Section 1.3.3), the pore water becomes suboxic within a couple of centimeters depth allowing of the potential of denitrification. Thermodynamically, denitrification is higher energy-producing reaction and therefore should complete before the reduction of Fe(III) (Froelich et al., 1979). Only in the SQM cores was the peak in nitrate observed within the top cm of sediment. The decrease in nitrate after the peak is due to the intitiation of denitrification–which acts as a sink for N by conversion of NO_3^- to dinitrogen gas (Froelich et al., 1979).

These nitrate-nitrite results are contradictory to the notion that microbial reactions proceed based on reduction of the highest energy-yielding reductant first (Froelich et al., 1979), as nitrate maxima were observed in anoxic sediment below the zone of iron reduction (see Section 1.3.3). Furthermore, a few samples turned a dark maroon/black color, and gave high absorbances above the range constrained by the calibration curve. These large erroneous values may have been due to high

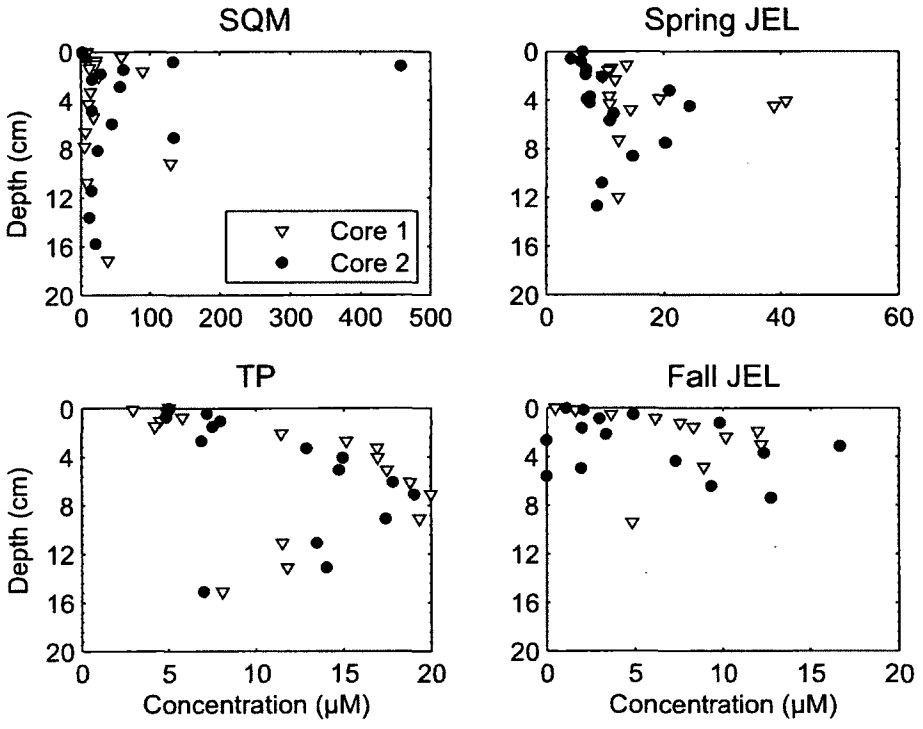

Figure 1-10: Nitrate-Nitrite porewater profiles of duplicate cores from each field site. Concentrations below the detection limits were plotted as zero.

organic content from fecal material that was centrifuged and subsequently filtered. This problem was only observed in samples from Spring and Fall JEL. In Spring and Fall JEL pore waters nitrate concentrations also changed significantly on the scale of millimeters (Fig. 1-10). It is difficult to say with confidence what caused the flucuation between these pore water samples as they do not appear to follow a trend, but it may be due to localized microenvironments high in organics excreted by benthic organisms.

Orem (1982) also found that NO_3^- in anoxic pore water of the Great Bay did not neccessarily follow the trend predicted by thermodynamics, as he observed nitrate in the zone of sulfate reduction. He also observed concentrations upwards of 500 μM sporadically in samples up to 100 cm depth. Microbial nitrification in stored samples is not a likely culprit in either study because pore waters were filtered through 0.45 μm filter membranes (this study) or filtered and treated with sodium azide (Orem, 1982). Furthermore, if purely chemical oxidation of ammonium to nitrate occured in the stored samples then higher concentrations of nitrate would have been observed in deeper sediments, which was not the case. One possibility is that NH_4^+ is oxidized to NO_3^- in the anoxic zone, leading to a peak in NO_3^-.

After denitrification the peaks in the anoxic zones (SQM cores at 6-8 cm, TMP cores at 8 cm, Fall JEL at 3 cm Fig. 1-10) suggest a process that causes anaerobic oxidation of NH_4^+ to NO_3^-. Above these peaks all nitrate is depleted in pore water, indicating that denitrification has removed all available NO_3^- produced through nitrification and aerobic respiration at the sediment-water interface. Similarly below these zones NO_3^- is removed. Previous work has revealed anaerobic oxidation of ammonium using manganese oxides as electron acceptors (Bartlett et al., 2008), and other authors have speculated microbially-mediated NH_4^+ oxidation through sulfate-reduction in anoxic sediment (Schrum et al., 2009). Peaks in sulfide (Fig. 1-9) can also be seen at 7 cm depth in both TMP cores, supporting the possibility of anaerobic

oxidation of NH_4^+ through sulfate reduction, though it is difficult to distinguish this as an underlying process with this data. Extraction and analysis of bacteria below the zone of Fe reduction, or incubation of sediment from the 7-8 cm horizon may provide valuable insight and explanation of these observations.

Particulate Phase Metals

Great Bay sediment was analyzed for trace metals to quantify metal content and compare it to particulate phase metals that are released during sediment resuspension (Chapter 2). One sediment core from each Spring JEL and SQM were analyzed. Depth profiles of particulate Cr, Mn, Fe, Cu, Zn, Cd, and Pb are shown in Figs. 1-11 and 1-12. Average values at each site are listed in Table 1.11. At SQM, the greatest difference in metal profiles was above 4 cm, below which all metals followed the same trend. The profile of Pb is skewed towards higher concentrations at depth however, probably a result of lower Pb input from leaded gasolines in recent decades (Calender and Metre, 1997). Trace metals at SQM correlate significantly with Fe, Mn and % organics (Table 1.10). Although several of these metals are strong organic chelators (e.g. Cu) and are usually associated with organic matter, Fe and Mn tend to be present as oxy-hydroxides or sulfides, and the similarity between profiles of Mn/Fe and % organics below 4 cm (Fig. 1-11) indicate that the small flucuations in metal concentrations may have been due to dilution by silicates (sands, silts) at each depth. However, it is also possible that seasonal flucuations in the redox boundary between oxic and anoxic sediment causes reduced Mn or Fe to precipitate out at different depths (Burdige, 1993).

Metals profiles from JEL were more different from each other relative to those from SQM. From the sediment-water interface to approximately 4 cm depth, concentrations

Table 1.10: Pearson correlation coefficients (r) for each trace metal correlated with Mn, Fe or C_{org} for $p < 0.05$. Cells marked with a '*' were not significant. Values of Cr at JEL were not analyzed.

	SQM			JEL		
	Mn	Fe	C_{org}	Mn	Fe	C_{org}
Cr	0.71	0.63	*	-	-	-
Mn	1	0.57	*	1	0.83	*
Fe	0.57	1	0.54	0.83	1	*
Cu	0.76	0.72	0.63	0.69	0.82	*
Zn	0.75	0.66	0.63	0.79	0.81	*
Cd	*	*	0.62	*	*	*
Pb	0.80	*	0.57	*	*	*

slightly decrease. Between 4-5 cm there was a peak in concentrations, and below 5 cm concentrations increased with depth. Again the Pb profile was skewed towards higher concentrations in deeper sediment. Unlike the SQM site, metals at JEL did not significantly track the changes in % organics. Instead, Cu, Zn, and Mn all correlated significantly with Fe ($p < 0.05$, $r = 0.82, 0.81, 0.83$ respectively, Table 1.10). The absence of any trace metal correlation with organics at JEL suggests that the bulk of labile trace metals in the solid phase associate with Fe and Mn, and the correlations between particulate metals and organics observed at SQM are likely due to dilution of fine-grained sediment by sand and silt at each depth.

At both sites levels of trace metals were comparable to natural background levels of sediment (Table 1.11). Furthermore, all metals were well below particulate-phase screening levels. This is important because Cr pollution is of notable concern in Great Bay sediment due to dichromate input from a tanning facility on the Cocheco River (Capuzzo and Anderson, 1973). Average sediment values of Cr (Table 1.11) are slightly above the typical concentration (62 ppm) for clayey sediment (Richard and Bourg, 1991). Cr is usually present as trivalent Cr (Cr(III)) in natural settings, and precipitates as a mixed hydroxide with Fe (Richard and Bourg, 1991). This was apparent at SQM as Cr correlated with particulate Fe (Table 1.10). Cr concentrations are lower at the sediment-water interface which may be a result of lower

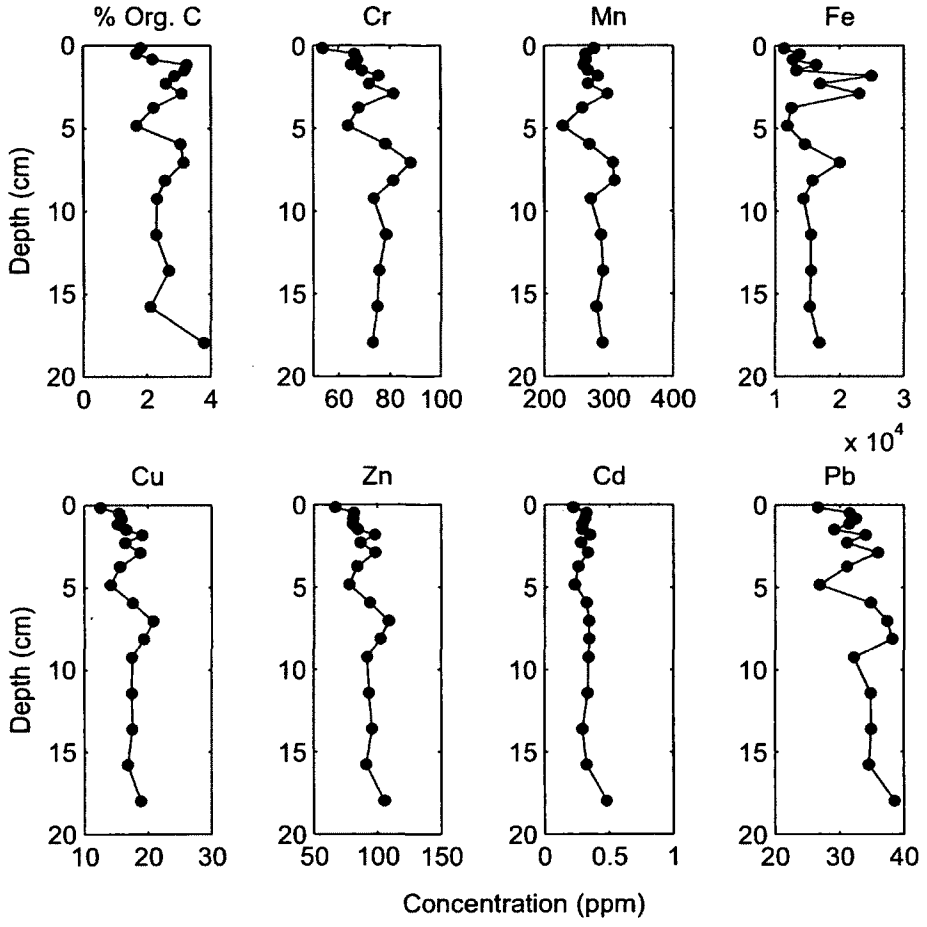

Figure 1-11: Organic content and concentrations of trace metals in sediments at SQM. All concentrations are plotted as ppm sediment except for organic carbon which is plotted as a weight percentage. Errors are 3, 6, 380, 0.6, 3.5, 0.02 and 0.8 ppm for Cr, Mn, Fe, Cu, Zn, Cd, and Pb respectively

input from deposition. However, Cr might not have caused noticible changes at the JEL and SQM sites due to their distances from the Cocheco River. The relatively lower concentrations at the sediment-water interface at both sites suggests a removal mechanism or that metal enrichment has decreased in recently deposited sediment.

To determine if the metal content of the JEL and SQM sites are representative of the Great Bay Estuary as a whole, sediment metal concentrations were compiled from the National Coastal Assessment (EPA, 2000). The NCA was a study conducted by the EPA to monitor environmental conditions of U.S. coasts and estuaries during the

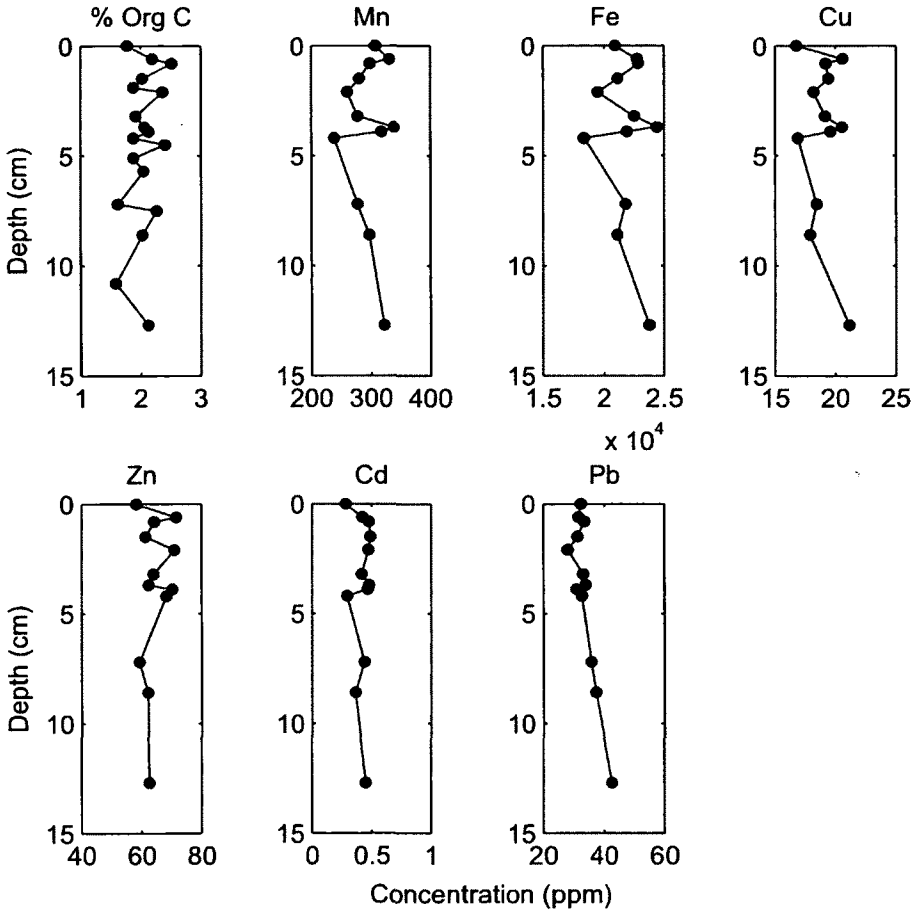

Figure 1-12: Organic content and concentrations of trace metals in sediments near the Jackson Estuarine Lab. All concentrations are plotted as ppm sediment except for organic carbon which is plotted as a weight percentage. Cr data was disregarded due to poor calibration (Table 1.4). Errors are 30, 2400, 1.8, 4.5, 0.02, and 4.6 ppm for Mn, Fe, Cu, Zn, Cd, and Pb respectively

early to mid 2000s. Average concentrations of trace metals in the upper 20 cm of sediment from JEL and SQM are listed in Table 1.11 alongside metal concentrations from the NCA. NCA data are digestions of homogenized sediment obtained by a grab sampler from the top 2 cm layer of sediment (EPA, 2000). The sediments were totally digested using a combination of nitric/hydrofluoric acid, and analyzed using graphite furnace atomic analysis for Ag, Cd, and Pb; and optical-emission inductively coupled plasma analysis (ICP-OES) for the remaining metals (EPA, 2000). Values from the present analysis all are within the range of values determined by the NCA, and are relatively close to estuarine-wide metal concentrations, indicating that JEL and SQM sites are representative of Great Bay Estuary sediment, and that sediment resuspension phenomena at these sites is applicable to the Great Bay as a whole (see Chapter 2).

Table 1.11: Average ($\pm\sigma_E$) particulate metal concentrations at JEL and SQM, and average ($\pm\sigma_D$) particulate metal concentrations from the National Coastal Assessment (EPA, 2000). Background levels are from uncontaminated estuarine soil (ten Brink et al., 2002). Sediment quality guidelines from Long et al. (1998) as cited in ten Brink et al. (2002) are screening levels (Level-Low,Medium) of bulk sediment composition which have been shown to affect benthic organisms. All concentrations in ppm.

	JEL	SQM	NCA	Background	Level-Low	Level-Medium
Chromium	-	73±2	90±60	70	81	370
Manganese	295±9	277±4	400±100	-	-	-
Iron	21800±500	16000±700	20000±10000	-	-	-
Copper	19.0±0.4	17.4±0.4	20±10	30	34	270
Zinc	65±1	92±2	80±40	90	150	410
Cadmium	0.42±0.02	0.34±0.02	0.6±0.5	0.35	1.2	9.6
Lead	33±1	34±1	40±20	35	47	220

1.3.4 Diagenetic Model

To determine rates of N and P regeneration within Great Bay sediment a diagenetic model of sulfate-reduction was applied to data from anoxic porewater. Chemical kinetics govern remineralization rates and reaction rates change depending on the dominant diagenetic reaction. Sulfate reduction reactions oxidize organic matter by

using sulfate as the terminal electron acceptor, thereby reducting sulfate to sulfide. A generalized reaction is shown in Equation 1.11 where x, y, and z are stoichiometric constants depending on the makeup of the organic material (Berner, 1979).

$$(CH_2O)_x(NH_3)_y(H_3PO_4)_z + \frac{x}{2}SO_4^{2-} \rightharpoonup xCO_2 + yNH_3 + zH_3PO_4 + \frac{x}{2}S^{2-} + xH_20 \tag{1.11}$$

In the top 20 cm sediments from JEL and SQM, Hines (1981) determined using a ^{35}S radiotracer technique that sulfate-reduction reactions were significant causes of organic remineralization. Berner (1980) applied the steady-state diagenetic equations for solid phase metabolizable organic decomposition ($\bar{C}_i$, μmol g^{-1}, Eqn. 1.12), and derived a model describing the generation of dissolved N, P from sulfate-reduction (Eqn. 1.13). This model assumes that adsorption and diffusion are the only processes removing N and P from the dissolved phase, equilibrium adsorption follows a linear isotherm, there is no authigenic mineral precipitation, there is no oxidation of NH_4^+, and diffusion is by molecular processes only (Berner, 1980). Westrich and Berner (1984) tested the model of Berner (1980) by incubating known amounts of planktonic organic carbon in homogenized anoxic sediment. In addition to proving the reaction was first-order, they found that rates of sulfate-reduction were determined by the lability of the decomposing organic material and that organics may be separated into two metabolizable fractions with decay rate constants varying by a factor of 10 (Westrich and Berner, 1984). From Figures 1-10 and 1-8, it is apparent that nitrate reduction and iron and manganese oxide reduction both occur in the upper 0-4 cm of sediment. Beneath the top 3-4 cm dissolved N:P ratios are relatively constant with depth, and Mn and Fe are no longer reduced, indicating that sulfate-reduction becomes dominant. The diagenetic equations for N, and P remineralization by sulfate-reduction are as follows:

$$\frac{\partial \bar{C}_i}{\partial t} = -w\frac{\partial \bar{C}_i}{\partial z} - k_i \bar{C}_i \tag{1.12}$$

$$\underbrace{\frac{\partial C_i}{\partial t}}_{\text{Accumulation}} = \underbrace{\frac{D_i}{1+K_N}\frac{\partial^2 C_i}{\partial z^2}}_{\text{Diffusion}} - \underbrace{w\frac{\partial C_i}{\partial z}}_{\text{Advection}} + \underbrace{\frac{F k_i \bar{C}_i}{1+K_N}}_{\text{Generation}} \tag{1.13}$$

where C_i is the dissolved pore water concentration of i (μmol cm^{-3}), $\bar{C}_i$ is the solid-phase concentration of i in the decaying organics (μmol g^{-1}), z is depth from the sediment-water interface (cm), w is sedimentation rate (cm s^{-1}), D_i is diffusivity (cm^2 s^{-1}), t is time (s), and k_i (s^{-1}) is the rate constant for decomposition. An adsorption constant (K') is used to describe the ratio of solute adsorbed to sediment (μmol g^{-1}) to the dissolved concentration. K' is converted to a dimensionless adsorption constant (K) which is the ratio of the total pools of adsorbed to dissolved solute represented by Equation 1.14:

$$K = K'\frac{\rho_s(1-\phi)}{\phi} = K'F \tag{1.14}$$

where ρ_s is sediment density (g L^{-1}) and ϕ is porosity. The term F is a constant used to convert between the dissolved and particulate phase and defined as mass particulate per volume of pore water.

N and P diagenesis were postulated to be at steady-state after performing a scale analysis on Equation 1.13. For example, using values for NH_4^+ in Table 1.12 and Eqn.1.15, the magnitude of the accumulation term (10^{-8}) in comparison to the diffusion (10^{-7}), advection (10^{-9}), and generation (10^{-6}) terms indicate temporal changes in the accumulation of NH_4^+ in porewater is 1-2 orders of magnitude less than diffusion and generation. The magnitude of this accumulation term, however, reflects the maximum value expected from the spring-summer seasonal difference, and thereby overstimates yearly porewater accumulation budgets. In reality, the comparability

between nutrient profiles from previous work in the Great Bay (Orem, 1982), and as well as similar nutrient fluxes over the past three decades (see Sec.1.3.5) indicate that there is neglible accumulation over the course of years. Performing a scale analysis on a larger temporal dataset, preferably spanning several years, would more accurately describe yearly nutrient accumulation in porewater. The results from the scale analysis, however, indicate the steady-state assumption is reasonable.

$$\underbrace{\frac{\Delta C_T}{T}}_{\text{Accumulation}} \approx \underbrace{\frac{D}{1+K}\frac{\Delta C_Z}{Z^2}}_{\text{Diffusion}} - \underbrace{w\frac{\Delta C_Z}{Z}}_{\text{Advection}} + \underbrace{\frac{Fk\bar{C}}{1+K}}_{\text{Generation}} \tag{1.15}$$

Table 1.12: Variables used for scale analysis on Eqn 1.13 to support the steady-state hypothesis. ΔC_T was calculated as the difference in porewater nutrient concentrations beneath 4 cm at JEL between the spring and fall, whereas ΔC_Z was calculated from the porewater concentration gradients at JEL.

Parameter	NH_4^+	PO_4^{3-}	Source
w (cm s^{-1})	10^{-8}	10^{-8}	Hines and Jones (1985)
T (s)	10^{7}	10^{7}	Time between samplings at JEL
k (s^{-1})	10^{-8}	10^{-8}	Westrich and Berner (1984)
F (g_{sed} cm^{-3})	10^{0}	10^{0}	Current Study
D (cm^2 s^{-1})	10^{-5}	10^{-6}	Current Study
ΔC_T (μmol cm^{-3})	10^{-1}	10^{-2}	Current Study
ΔC_Z (μmol cm^{-3})	10^{0}	10^{0}	Current Study
Z (cm)	10^{1}	10^{1}	Current Study
$\bar{C}$ (μmol g_{sed}^{-1})	10^{2}	10^{0}	Orem (1982)
K	10^{0}	10^{0}	Rosenfeld (1979), Krom and Berner (1980)

Solutions to these diagenetic equations are then as follows:

$$\bar{C}_i(z) = \bar{C}_{io} exp^{\frac{-k_i}{w}z} \tag{1.16}$$

$$C_i(z) = \frac{w^2 F \bar{C}_{io}}{D_i k_i + (1+K_i)w^2}\left[1 - \exp\left[\frac{-k_i}{w}z\right]\right] + C_i(0) \tag{1.17}$$

where $\bar{C}_{io}$ is the fraction of metabolizable organic i (μmol g^{-1} sediment) at the

sediment-water interface. Values for K in anoxic sediment fall within the range of (0.2-1.6) for NH_4^+ (Rosenfeld, 1979), and (1.7-1.9) for PO_4^{3-} (Krom and Berner, 1980). Accurate values for K were unnecessary because the term $D_i k_i$ was orders of magnitude larger than term $(1+K_i)w^2$ assuming K_i falls within two orders of magnitude of previously determined values.

$$Rate = Fk_i\bar{C}_i = Fk_i\bar{C}_{io}exp\left[\frac{-k_i}{w}z\right] \tag{1.18}$$

Sulfate-reduction is considered to be a first-order reaction following simple stoichiometric decomposition (i.e. $k_N = k_P = k_S$, Eqn. 1.18) (Berner, 1977, 1980). Consequently, Eqn. 1.17 should yield comparable values of k_N and k_P when fitted to NH_4^+ and PO_4^{3-} profiles. The rates of sulfate-reduction can vary up to eight orders of magnitude, and are primarily dependent on the metabolizability of the organic material being degraded (Westrich and Berner, 1984). In areas with higher deposition rates, organic material can quickly transfer below the zone of aerobic remineralization causing sulfate-reduction rates to increase (Berner, 1979). In fact, k_S has been shown to vary linearly with the square of sedimentation rate for numerous sites, and can be approximated according to the following equation (Berner, 1979):

$$k_i = Aw^2 \tag{1.19}$$

where A is a proportionality constant (0.04 yr cm^{-2}). In the Great Bay, Orem (1982) determined k_N, k_P, and k_S at several sites using this diagenetic modeling approach. Rate constants for these three species differed by orders of magnitude ($k_N = 3 \times 10^{-5}$ to 6×10^{-3} yr^{-1}, $k_P = 2 \times 10^{-5}$ to 1×10^{-2} yr^{-1}) likely due to the poor resolution of the data. To determine Great Bay sulfate-reduction rate constants using data from this study, Equation 1.17 was fitted to the above NH_4^+ and PO_4^{3-} profiles (Figs. 1-5, 1-6) beneath 3-4 cm using JMP 9 statistical software. Examples of model fits to

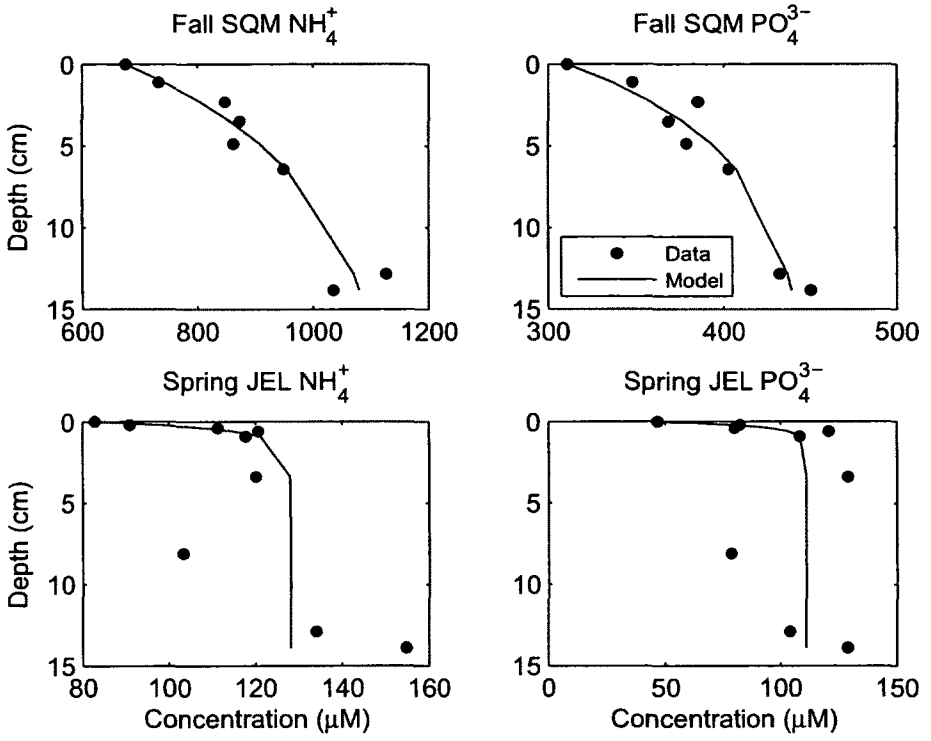

Figure 1-13: Four fits of Eqn. 1.17 to pore water NH_4^+ and PO_4^{3-} concentration profiles from SQM and Spring JEL showing one good fit (SQM) and one poor fit (Spring JEL) for both NH_4^+ and PO_4^{3-}. Only data below 3-4 cm were considered. The depths of these data were shifted upwards by subtracting the depth of the shallowest pore water sample used in the model so the sediment-water interface would be represented by 3-4 cm.

field data are shown in Fig. 1-13 in the best case and worst case scenarios; primarily model fits were similar to the SQM core regressions.

Table 1.13: First order rate constants (yr^{-1}) for generation of N and P in the Great Bay.

	Core 1		**Core 2**	
	k_N	k_P	k_N	k_P
Spring JEL	0.42	0.70	0.027	0.019
Fall JEL	0.036	0.15	0.12	0.26
SQM	0.028	0.036	.0082	.025
TMP	0.045	0.070	-	-

First-order rate constants are listed in Table 1.13. In contrast to the results obtained by Orem (1982), there is good agreement between k_N and k_P in individual

cores as well as between sites. The site variability may be a result of the influence of benthic organisms, as sulfate-reduction would increase in bioturbated sediments due to transfer of fresh organic material to depth (Hines and Jones, 1985). Similarly, bioturbation may explain the differences beween cores at Spring JEL (Core 1 had a polychaete worm) and also may be responsible for the poor fit for Spring JEL Core 1 (Fig. 1-13). Using the sedimentation rate of 0.2 cm yr^{-1} (Hines and Jones, 1985) the value of k_i predicted from Eqn. 1.19 was 1.6 x 10^{-3} yr^{-1}. The difference between k_N, k_P from this study and that calculated by Eqn. 1.19 indicate that sulfate-reduction in the Great Bay is significantly greater than environments with similar deposition rates. It is likely that transfer of fresh/labile organics to Great Bay anoxic sediment due to bioturbation is significant and that the high rate constants (Table. 1.13) reflect this.

Table 1.14: Values for particulate organic N and P concentrations (% of sediment) of decaying organics beneath the top 3-4 cm of sediment. Values of N from CHN analysis were from Core 2 at each site (Section 1.3.1

	Core 1		**Core 2**		
	N_o	P_o	N_o	P_o	N (CHN Analysis)
Spring JEL	0.15	0.31	0.021	0.016	0.20-28
Fall JEL	0.14	0.21	0.28	0.03	-
SQM	0.25	0.069	0.24	0.049	0.19-0.34
TMP	0.097	0.11	-	-	-

Values for metabolizable organic N (N_o) obtained from the diagenetic model match average values of particulate organic N obtained from CHN analysis (Section 1.3.1), further supporting the diagenetic modeling approach (Table 1.14). Particulate organic P was not measured, but model values were about an order of magnitude greater than values measured directed by Orem (1982) for similar Great Bay sediments. This suggests there may be additional sources of P to pore water in anoxic sediment, such as P released from reduction of Fe oxides (Lehtoranta et al., 2009).

Using Eqn. 1.18, N and P remineralization rates were translated into sulfate-reduction rates by multiplying by a stoichiometric constant of 5 SO_4^{2-} per NH_4^+ (using Eqn. 1.11 and the ratio 10 C:N from CHN analysis). Maximum model sulfate reduction rates (nmol mL^{-1} day^{-1}) ranged 8-820 at Spring JEL (June), 64-430 at Fall JEL (August), and 16-56 at SQM (August). These calculated values fall within the range of values obtained by Hines (1981) using the S^{35} radiotracer technique on sediment incubations, which ranged 66-96 at JEL (May), 59-330 at JEL (late July), and 3-35 SQM (late October).

Table 1.15: Maximum nutrient regeneration rates (μmol cm_s^3 day^{-1} of NH_4^+ and PO_4^{3-} calculated from the diagenetic model for each sampled core.

	Core 1		**Core 2**	
	NH_4^+	PO_4^{3-}	NH_4^+	PO_4^{3-}
Spring JEL	0.33	0.51	0.0030	0.00074
Fall JEL	0.026	0.022	0.17	0.095
SQM	0.023	0.020	0.0062	0.0064
TMP	0.018	0.018	-	-

Nutrient regeneration rates calculated from this model gives quantitative insight into whether cohesive sediment acts as a potential source of nutrients to the overlying water of the Great Bay. The range of maximum N and P regeneration rates (Table 1.15) obtained from all cores between the spring and fall was 0.003 - 0.33 and 0.0007 - 0.51 μmol cm_s^3 day^{-1} respectively. Differences in the nature of organics and temperatures between the Great Bay make it hard to compare regeneration rates to other studies. However, these values are on par with regeneration rates obtained by Klump and Martens (1989) from incubations of anoxic sediment (3-5 % organic carbon) from Cape Lookout Bight. Regeneration rates in that study ranged 0.03 - 0.51 and 0.005 - 0.032 μmol cm_s^3 day^{-1} for NH_4^+ and PO_4^{3-} respectively. The comparability between k_N and k_P, between N_o from the model and from CHN analysis, the match between

model sulfate-reduction rates and previously determined sulfate reduction rates in the Great Bay, and the similarities between N and P regeneration rates with other studies suggest this model is applicable in the Great Bay. This model allows measurement of the rate of nutrient regeneration below 3-4 cm, which drives the accumulation of pore water nutrients and determines the magnitude of molecular diffusive flux.

1.3.5 Nutrient Flux Rates

Nutrient Diffusive Fluxes

It is evident from the previous sections that nutrients regenerate and accumulate in Great Bay pore water, however concern lies in whether or not nutrients can be released to the overlying water where they then may support primary production. Potential nutrient fluxes due to molecular diffusion as calculated by Fick's First Law (Section 1.2.6) are shown in Table 1.16. The flux errors were calculated from the uncertainty of linear fits to concentration profiles (See Appendix A). Pearson correlation coefficients (R) are included in Table 1.16 to show the goodness of fit. Nitrate fluxes were calculated based on the gradient between the overlying water and the first pore water point, as linearity was not observed in most profiles.

Table 1.16: Fluxes of nutrients due to molecular diffusion (mmol m^{-2} day^{-1}) and Pearson correlation coefficients (R) for fluxes that were calculated using linear regression of pore water profiles. Fluxes that were calculated by using concentration difference of the overlying water and first pore water data point have '-' listed for r^2.

Site	SQM		Spring JEL		Fall JEL		TMP	
Core	1	2	1	2	1	2	1	2
Ammonium	1.7±0.1	1.8±0.1	0.2±0.0	0.2±0.0	2.0±0.0	1.5±0.1	0.3±0.0	0.2±0.0
r^2	0.97	0.98	0.72	0.87	0.99	0.83	1.00	0.78
Phosphate	0.2±0.0	0.5±0.0	0.1±0.0	0.1±0.01	0.0±0.0	0.1±0.0	0.1±0.0	0
r^2	0.93	0.96	0.55	0.73	0.68	0.92	0.95	-
Nitrate	-0.1	0	0.1	0.1±0.0	0.1±0.00	0.1	0	0
r^2	-	-	-	0.82	0.97	-	-	-
Silica	1.7±0.1	1.3±0.1	0.4±0.1	0.3±0.0	1.0±0.0	0.9±0.1	0.5±0.0	0.7±0.1
r^2	0.98	0.86	0.79	0.74	0.96	0.97	0.90	0.89

Potential NH_4^+ fluxes calculated from Fick's First Law revealed a positive efflux of NH_4^+ from the sediment to the overlying water in all cores. Fluxes of ammonium are greatest during the fall at JEL and SQM. The same goes for dissolved silica and phosphate. Lyons et al. (1982) investigated benthic fluxes during July from JEL (9 runs) and SQM (6 runs) using in situ flux chambers. They calculated the contribution of molecular diffusion to total flux and concluded that it significantly understimated actual in situ fluxes. However, diffusive fluxes of NH_4^+ calculated from the current study are comparable to the fluxes they observed in situ (Table 1.17), whereas phosphate and silica fluxes from this study were greater at SQM and lesser at JEL compared to their in situ flux measuremnts. Lyons et al. (1982) attributed the negative flux of silica at SQM to a benthic diatom uptake. This may be the cause of their phosphate depletion also. The higher in situ fluxes of phosphate and silica at JEL was attributed to bioturbation (Lyons et al., 1982). Silica and phosphate fluxes at JEL in this study may also be underestimates of actual fluxes as effects from bioturbation were not included in the estimates in Table 1.16. Officer (2012) measured benthic nutrient fluxes using incubations of multiple sediment cores during July 2011. Those cores were obtained one to two weeks before the fall sampling at JEL, and as evident between Tables 1.17 and 1.16, are comparable with nutrient fluxes calculated from this study.

Table 1.17: Nutrient benthic fluxes determined during the month of July by [1]Lyons et al. (1982), [2]Officer (2012), units of mmol m^{-2} day^{-1}. Negative values indicate flux into the sediment

Site	JEL[1]	JEL[2]	SQM[1]
Ammonium	1.20 - 3.36	0.34 - 1.67	0.29 - 2.35
Phosphate	0.23 - 0.34	0	(-0.38) - 0.03
Nitrate	0.06 - 0.16	0 - 0.06	(-0.72) - 0.20
Silica	1.73 - 4.49	2.02-2.17	(-0.41) - 0.36

In comparison to other sites in the U.S., nutrient fluxes from sediment of the Great Bay Estuary does not seem to be extremely released or limited (Table 1.18). Fluxes from Great Bay cohesive sediment fall within approximately an order of magnitude of other studies. NH_4^+ release from diffusion falls generally middle range for oxic sediment. Nitrate and silica fall at the lower end of these spectrum of values. Phosphate on the other hand was generally higher than other sites, however the difference in phosphate concentrations of the top pore water and the overlying water was generally minimal and there are some sites where no phosphate is released (TMP site especially). The relatively lower values for nutrient release as a result of sediment flux indicates that relative to other estuaries, other inputs may dominate the nutrient budget.

Table 1.18: Sediment-water fluxes from previous studies. All units in mmol m^{-2} day^{-1}. Data from Malecki et al. (2004) and Lerat et al. (1985) are compilations of fluxes from multiple studies using benthic chambers, sediment incubations or pore water profiles. Negative values indicate flux into the sediment. Data from Banta et al. (1995) is total DIN (NH_4^+ + NO_3^-).

Study Area	Sediment Type	Redox	NH_4^+	NO_3^-	PO_4^{3-}	$Si(OH)_4$	Reference
Chesapeake Bay	sand, clay	oxic	1.4 - 12	-	-	-	Malecki et al. (2004)
Indian River Lagoon	sand, mud		1.3 - 2.6	-	0.0051 - 0.050	-	" "
Neuse River Esuary	subtidal, sand	oxic	.0093 - 0.68	-	-	-	" "
St. Johns River	mud	oxic	-	-	-.0042 - 0.019	-	" "
		anoxic	0.15 - 2.03	-	0.076 - 0.38	-	" "
Long Island Sound	sand, mud	oxic	0.0002 - 0.0007	-	-	-	" "
			-1 - 5	0 - 16	-	-	Lerat et al. (1985)
Buzzards Bay	-	-	1.6	-	-	-	" "
Narragansett Bay	-	-	2.4	-	-	12	" "
Georgia Bight	-	-	4.0	0.25	-	-	" "
San Franscisco Bay	mud	-	0.41-5.0	-	-	2.1-7.0	" "
Cape Lookout Bight	-	-	0.67-25	-	-	-	" "
Buzzards Bay	mud	oxic	0 - 4.1		-	-	Banta et al. (1995)
Great Bay Estuary	mud, silty sand	oxic	0.2-2.0	-0.1-0.1	0-0.5	0.4-1.7	Present Study

Comparison to Riverine Inputs

Oczkowski (2002) determined seasonal inputs of ammonium, nitrate, phosphate, and silica from seven tidal rivers (Bellamy, Cocheco, Lamprey, Oyster, Salmon Falls, Squamscott, and the Winnicut) flowing into the Great Bay Estuary. Water samples were collected from each river twice a month, and nutrients were analyzed colorimetrically using a Lachat 8000 QuikChem Analyzer. Water discharge was estimated using USGS discharge gauges located near the sampling locations. The effluents of waste-water treatment facilities beneath the sampling stations were also accounted for in discharge estimates. In Figure 1-14, seasonal estimates of riverine inputs are compared to sediment fluxes for the spring and fall.

Oczkowski (2002) calculated fluxes (kg nutrient/day) by multiplying nutrient concentrations in each river by respective river discharges measured on each collection day. Seasonal fluxes from each river were determined through statistical analysis of fluxes for three month periods (Spring: March, April, May; Fall: September, October, November). The range of riverine inputs varied depending on river with both the Cocheco, Lamprey and Salmon Falls rivers exhibiting the highest nutrient input (similar to the recent work of Wood and Trowbridge (2012)) and the largest range of concentrations. Riverine inputs were variable up to 50-100%. In this study, nutrient fluxes from Oczkowski (2002) were taken as the median input from all seven river effluents (See Oczkowski (2002) pgs 35-37) to approximate the most consistent riverine fluxes. Sediment fluxes were calculated in the spring using nutrient fluxes from Spring JEL and in the fall using using the maximum fluxes from either the Fall JEL or SQM sites (Table 1.16). An estimate of 5334 acres representing areas of mud and sandy mud (Wengrove, 2012) for the Great Bay was used to scale up sediment diffusive fluxes. This estimate was obtained through an ARC-GIS mapping of areas with fine-grained sediments in the Little and Great Bay using a compilation of previous recorded sediment data (Wengrove, 2012). It does not take into account surface

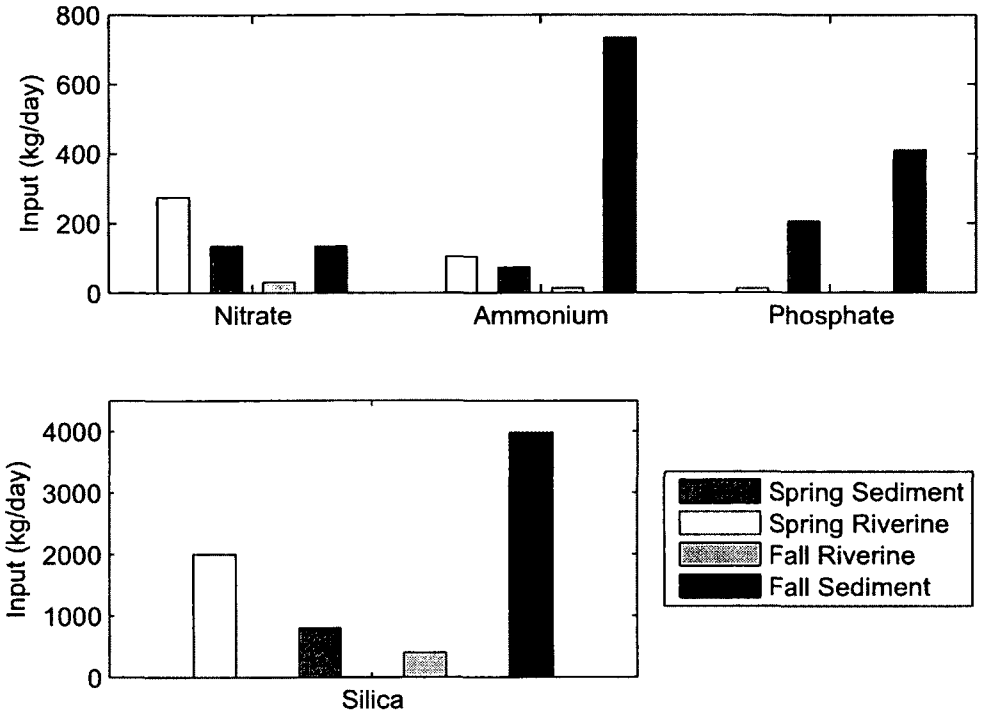

Figure 1-14: Riverine (Oczkowski, 2002) and sediment nutrient fluxes to the Great Bay during the spring and fall. Input due to sediment may be variable up to 20% due to variability of diffusive fluxes between sites. It is likely that the estimate of cohesive sediment area in the Great Bay contributes more error (see text).

topography and likely underestimates actual sediment distribution.

Between the spring and fall there is a change in the dominant mechanism of nutrient release to the Bay. In the spring, riverine inputs are dominant largely due to the spring melt–which contributes to increased runoff and subsequent discharge. Furthermore, lower microbial activity through the winter and spring have not yet led to significant accumulation of pore water nutrients, which diminishes sediment fluxes. In the fall, river discharge subsides and nutrient regeneration in sediment increases from organic remineralization and biogenic opal dissolution, causing sediment inputs to dominate. Phosphate from rivers during both seasons was lower than from sediment, likely due to association with suspended particulate matter. This also indicates

that the input of PO_4^{3-} from sediment may not be so large, as adsorption to SPM occurs over time in the overlying water. Likewise oxidation of NH_4^+ to NO_3^- may increase the amount of NO_3^- over time.

This comparison between riverine and sediment nutrient input only takes into account species in the dissolved phase. The fact that suspended particulate matter (ranging 1-10.9 mg/L, (Wood and Trowbridge, 2012)) is also transported by rivers means that nutrients associated with the solid phase must also be taken into account. Such an endeavor is rigorous in nature and beyond the scope of this work. It should be noted, however, that while nutrients associated with SPM may be significant to consider, nutrients in the dissolved phase are the more bioavailable.

1.4 Conclusion

Duplicate sediment cores were gathered from multiple sites within the Great Bay and analyzed for nutrients and metals in dissolved pore water as well as a suite of trace metals in the sediment particulate phase. The results from this investigation revealed that the biogeochemistry of the Great Bay Estuary leads to an accumulation of nutrients and metals in cohesive sediment pore water between the spring, summer, and fall. Dissolved ammonium and phosphate are generated by microbial remineralization of terrestrial and marine organic matter. The diagenetic reactions: aerobic remineralization, nitrate, manganese and iron reduction contribute to organic remineralization (nutrient regeneration) in the top 2 cm of sediment, below which sulfate-reduction determines nutrient regeneration rates. Ammonium and phosphate flux to the sediment-water interface, but are lessened in concentration due to adsorption reactions and nitrification of ammonium to nitrate. However, concentrations of nitrate are 1-2 orders of magnitude less than ammonium and do not significantly affect the concentrations of ammonium. Silica accumulation is fairly constant through

each season in the top 20 cm, though less than the saturation concentration for dissolved silica. Precipitation and removal of silica from solution by formation of solid sepiolite provides an explanation for the constant seasonality of silica.

Molecular diffusive fluxes determined by Fick's First Law are comparable to Great Bay benthic fluxes determined by other authors using sediment incubations and in situ benthic chambers. The magnitude of the fluxes for ammonium, nitrate, and silica fall in the middle to lower end of the range estuaries in the continental United States, though phosphate fluxes were slightly higher. In the spring, riverine inputs to the Great Bay are higher than from sediment fluxes. In the fall, on the other hand, sediment fluxes from mud and sandy mud are up to an order of magnitude higher than riverine inputs.

Particulate-phase metals at two field sites were relatively constant with depth in the upper 20 cm of sediment. There are slightly lower concentrations at the sediment-water interface that may be a result of winnowing of fine-grained material. Particulate metals correlate with organic matter, manganese and iron concentrations in the sediment, but variability with depth for both organic matter and metals is most likely due to the relative silicate mineral concentrations at each depth. The sites chosen in this study are comparable to areas of the Great Bay which most likely have not been subjected to direct discharge of metal pollution. Data more pertinent to metal contamination might come from sediment of the tidal rivers, as these are likely to be closer to point sources.

Some important points can be made from this work. First, seasonal changes in sediment biogeochemistry determines the distribution of contaminants in pore water which may be released, as shown in this work and multiple analogous studies (Hines and Jones, 1985; Hines et al., 1984; Hines, 1981; Orem, 1982; Lyons et al., 1982). Second, the range of diffusive fluxes from cohesive sediment in the Great Bay has been nearly the same for the past 30 years and can be easily estimated using pore water

concentration profiles. Finally, contributions of nutrients from cohesive sediment to the Great Bay can exceed riverine inputs under typical weather conditions. The impact of extreme weather or tidal conditions, specifically ones that cause sediment erosion, upon contaminant fluxes are explored in the next chapter.

CHAPTER 2

Release of Nutrients and Metals from Cohesive Sediment due to Resuspension

The impact of sediment resuspension of cohesive sediments on nutrient and metal release was investigated by simulating resupension using a laboratory erosion chamber on eight sediment cores collected from the Great Bay Estuary, NH. Erosion of sediment initiated when the bed-applied shear stress exceeded 0.14 N/m^2. Both the depth of erosion and erosion rate increased with higher shear stress. Erosion rates exponentially decreased with time when the shear stress was held constant. Between 0.14-0.27 N/m^2 net erosion ceased within minutes and was similar to a pulse of sediment to the overlying water, whereas at shear stresses above 0.27 N/m^2 steady-state was not attained even after an hour. In most cases the first particles to be eroded were enriched in trace metals even though bulk sediment concentrations were at background levels. Surficial particles in one case were enriched in chromium, lead, copper, and zinc by 300-500%. The fluxes of ammonium, nitrate, silica and phosphate during erosion were over an order of magnitude greater than what was predicted from advection of eroded porewater. In situ data collected during Tropical Storm Irene indicated that areas of sediment that do not experience high shear stresses during the Great Bay's regular tidal cycle can be subjected to stresses up to 0.35 N/m^2 during weather events, increasing the potential for contaminant release. Large contaminant releases over short time scales means that knowledge of the physical and chemical processes underlying resuspension is essential in order to quantify contaminant input to Great Bay waters.

2.1 Introduction

From data presented in Chapter 1, it is apparent that nutrients and metals accumulate in Great Bay sediment and pore waters. The rate of release of these contaminants depends upon the physical mechanisms of diffusion, advection, and sediment transport. In Chapter 1, diffusive nutrient fluxes were quantified and found to be released in appreciable amounts (mmol m^{-2}) over the course of a day. Like diffusion, sediment disturbances can remobilize contaminants, but through physical displacement of particulate and dissolved species from sediment to the water column (Couceiro et al., 2009; Kalnejais et al., 2007, 2010). Furthermore, differing biogeochemical characteristics of sediment, pore water and overlying water such as pH, redox potential (Eh), temperature, salinity and microbial distribution influence the chemical reactions that occur in the sediment (Zoumis et al., 2001; Cantwell et al., 2002). Thus, sediment disturbances not only cause physical transport, but also alter the physical and chemical setting of nutrients and metals, thereby altering ensuing chemical reactions and influencing the release and bioavailability of these contaminants (Eggleton and Thomas, 2004). The chemistry and erosion of fine-grained sediments are the focus of this study because of their ability to adsorb relatively higher amounts of metals due to large surface area compared to sand (Cantwell et al., 2002), and their nature when undergoing erosion.

Erosion is caused naturally by bioturbation, wave and currents from tidal and wind activity, or from human activities such as dredging, trawling, and fishing (Eggleton and Thomas, 2004). The difference between most fine-grained muddy sediments in comparison to sandy sediments is that mud particles exhibit a cohesive force of attraction upon each other. Mud cohesion results from the negative electrochemical surface charge of mud particles interacting with surrounding positively charged ions and organic matter–which act as a bridge between individual particles (Taki, 2001). This cohesive force acts in addition to the forces of friction and gravity to prevent

sediment resuspension. When an outside force is applied to a mud bed that exceeds the cohesive, gravitational and frictional forces, sediment is eroded and resuspended into the overlying water. The mimimal force (per unit area) required to resuspend sediment is termed the 'critical shear stress' (τ_c). At stresses lower than τ_c, deformation of the bed may occur due to the rheology of mud (Babatope et al., 2006), but sediment does not leave the bed.

Through the interaction between the physical mechanism of erosion, and the chemistry of the overlying water, contaminants may be released. Previous work has shown that sediment undergoing simulated resuspension can release dissolved nutrients and metals in greater quantities that what is advected from eroded pore water (Kalnejais et al., 2010). Furthermore, in some cases eroded particles may also be enriched in metals in comparison to bulk sediment (Kalnejais et al., 2007; Cantwell et al., 2002). Metal content in fine-grained sediment tends to be higher because of the larger surface area (per unit mass) available for adsorption (Cantwell et al., 2002). Collisions between particles during resuspension can increase metal scavenging by breaking up aggregates and increasing surface area (Cantwell et al., 2002). Over time in the overlying water, further chemical desorption (Morin and Morse, 1999), as well as scavenging (Cantwell et al., 2002) by suspended particulate matter may cause contaminant release into the dissolved phase or enrichment of the particulate phase. Finally, dissolved oxygen in the overlying water has the potential to cause aerobic remineralization (Froelich et al., 1979) of resuspended organic matter as well as oxidizing reduced minerals such as metal sulfides (Eggleton and Thomas, 2004), providing yet another pathway for release.

The siltation in the Great Bay has been a result of urbanization of the surrounding watershed, and the increases in impervious surfaces has contributed to runoff and reduced water clarity (PREP, 2009). Waters higher in suspended solids have the potential to shoal waterways by transport and deposition of large amounts of sediment

to areas with lower flow velocities. Traditionally, higher turbidity has caused problems for the life cycles of filter feeders and eelgrass in several subtidal zones of the estuary (Great Bay Siltation Committee (GBSC), 2010). Erosion and resuspension of deposited sediment may have the same physical implications, thus study of erosion in Great Bay sediments is a necessity. Furthermore, policy decisions on remediation of areas with higher siltation are exploring the option of large-scale dredging projects to remove sediment(GBSC, 2010). Although this study is geared more towards sediment erosion occuring in natural settings, it also provides insight into contaminant release that may occur from dredging.

The objective of this study was to determine the critical shear stress required for fine-grained sediment erosion and to quantify the release of nutrient and metal contaminants from resuspension of fine-grained sediment of the Great Bay Estuary. Sediment erodibility is determined for eight cores within the Great Bay. Contaminant releases from simulated erosion using an EROMES erosion chamber are presented for both the dissolved and particulate phase. Seasonal pore water concentrations and geochemistry from Chapter 1 are drawn upon to explain differing contaminant releases between seasons. Characteristics of the overlying water measured using a Hydrolab Datasonde are employed to explain chemical reactions occuring in the overlying water. Through analysis of the above results, a clearer picture of potential contaminant releases to the Great Bay Estuary is made apparent.

2.2 Methodology

2.2.1 Erosion Experiments

The erosion apparatus employed to simulate in-situ shear stress is an EROMES erosion chamber modified for trace metal analysis (Kalnejais et al., 2007). For each erosion experiment, cores were collected and stored as mentioned in Chapter 1 1.2.1.

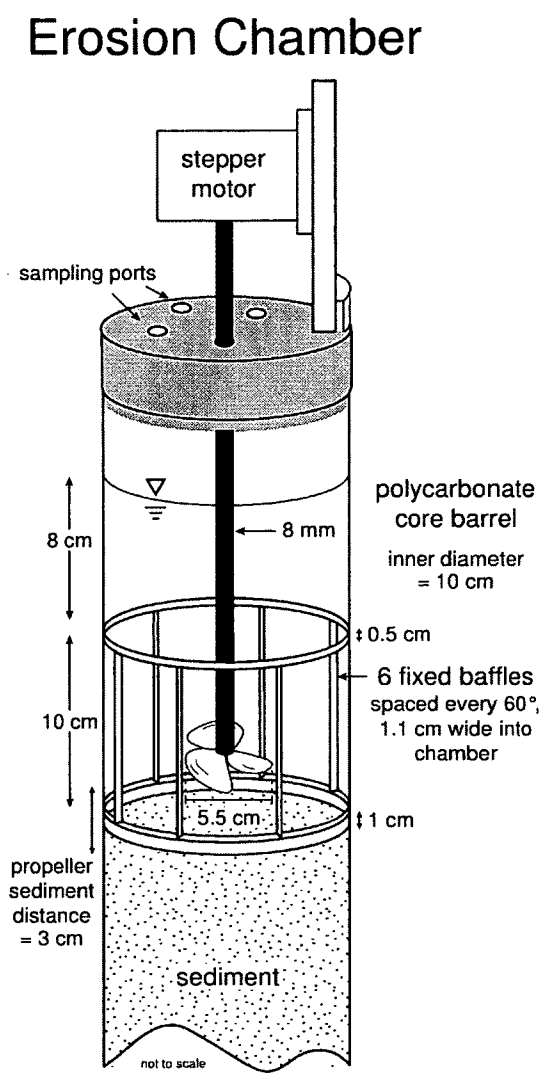

Figure 2-1: Erosion chamber used for all eight erosion experiments. In the three experiments involving the turbidity chamber tubing was inserted through the top sampling ports and water was continuously recycled over the course of the experiment. Figure from (Kalnejais et al., 2010).

A polycarbonate piston was inserted through the base of the erosion chamber and the sediment column was raised, so the sediment-water interface was approximately 1 cm from the chamber baffles. The chamber was then filled to a fixed level of water, and maintained at a constant volume during the course of each experiment.

The impeller rotation rate was previously calibrated for shear stress using a Shield's curve for resuspended sand (Kalnejais et al., 2007). The shear stress along the interface was increased in steps within a range of shear stresses typical of coastal regions (Mehta and Parchure, 2000). The time allowed for the system to reach steady-state after altering the shear stress varied between experiments, but usually ranged 10-20 minutes. For a few of the higher shear stresses, the sampling time was lengthened so that multiple samples could be taken. Syringes were used to remove approximately 50-100 mls samples (determined by weight) of overlying water at each shear stress step, or several samples at individual stresses. Samples were then filtered through either acid-cleaned 0.45 μm Nuclepore filter membranes (metal/nutrient analyses), or pre-combusted Whatman GF-F (nutrients, CHN analysis), and refrigerated at 4°C during or immediately after each experiment.

For the August sampling at JEL and SQM, a turbidity chamber was constructed to allow continuous monitoring of temperature, dissolved oxygen (DO), salinity, pH, and turbidity of the overlying water in the erosion chamber. The turbidity chamber consisted of a 10 cm (internal diameter) polycarbonate cylinder open to the atmosphere, connected to the erosion chamber with 0.25" Tygon tubing. A peristaltic pump (at 700 mL/min) circulated the water between both chambers. Temperature, DO, salinity, pH, and turbidity were measured with a HydroLab Water quality Datasonde 5 in intervals of 15 seconds. The sediment in the turbidity chamber was kept suspended using a magnetic stirrer.

Several complications arose from the turbidity chamber apparatus. The magnetic stirrer seemed to transfer heat to the overlying water, raising the temperature sig-

nificantly (Fig 2-8). In addition, leaks from the water ports occurred several times during sampling at JEL during August, and the volume of water added back to the chamber was not recorded making accurate estimates of the chamber water volume difficult.

2.2.2 Analysis

Nutrients were analyzed with standard spectrophotometric methods as outlined in Chapter 1 Section 1.2.3. Trace metals were analyzed with ICP-MS as outlined in Chapter 1 Section 1.2.4. Suspended particulate matter (SPM) was measured by mass difference after accounting for salt deposited on the filters from evaporated seawater.

The Hydrolab Datasonde was calibrated for dissolved oxygen, pH, turbidity and conductance before each experiment. Experiments were conducted with the Hydro-Lab datasonde monitoring characteristics of the overlying water for Fall JEL Core 2 and both SQM cores. Data from Fall JEL Core 2 was disregarded due to leakage and other complications with the apparatus during sampling times. The process was more streamlined for the SQM Cores and is more representative of actual erosion phenomena. Turbidity output (NTU) was converted to SPM by linear regression of turbidity with SPM gathered from water filtration from each experiment. The calibration for both cores is shown in Fig. 2-2. There is a significant linear relationship for both cores but with the slopes differing by a factor of 2. The difference in slope of calibration curves is unexpected, however it may be due different distribution of particle sizes in the overlying water and captured in filter papers. More turbidity experiments using mud samples may help to determine what causes the difference between cores.

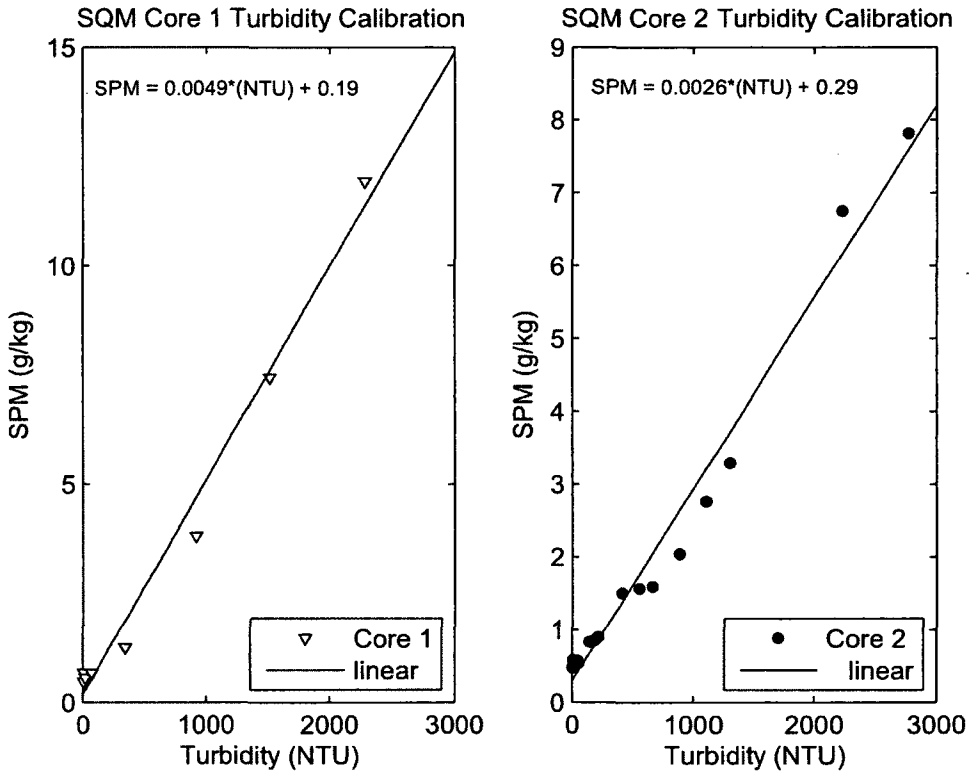

Figure 2-2: Calibration curves for SQM Erosion Cores 1 and 2 using SPM gathered during experiment and turbidity output (NTU) from the HydroLab Datasonde

2.3 Results

2.3.1 Erosion and Sediment Resuspension

Figure 2-3 displays suspended partculate matter (SPM) at each shear stress increment. A critical shear stress (τ_c) range of 0.14-0.27 N/m^2 was ubiquitous in all erosion experiments. The data falls within the range for surficial estuarine cohesive sediments, which exhibit a shear strength of 0-0.80 N/m^2 (Mehta and Parchure, 2000). Before τ_c there were no observable changes in SPM of the overlying water. After τ_c, the amount of sediment eroded depended upon the time between stress steps but more so on the magnitude of the shear stress increment. It was not until a stresses above 0.27 N/m^2 that the step time of 10 minutes became inadequate for the erosion to reach steady-state.

The SPM measurements were converted to an erosion depth by assuming erosion occured equally over the sediment-water interface. Except in TMP Core 1, at higher than τ_c the depth of erosion increased exponentially (Fig. 2-4). Erosion thresholds usually increase with lower water content and higher bulk sediment density (Mitchener and O'Brien, 2000), however there was no change between Spring and Fall JEL even though porosity at the sediment-water interface increased from 0.68 to 0.85 (Fig. 1-4). Furthermore, disregarding Fall JEL Core 2 because of the longer time allowed between stepping times (due to the turbidity chamber experiment), the depth of erosion as a function of shear stress at this was only slightly higher in the fall, likely due to the increase in porosity. For shear stresses up 0.40 N/m^2 erosion occurs on the scale of millimeters to a few centimeters.

The importance of knowing erosion depths is that it enables one to compare releases of dissolved solutes to what is actually in the pore water at different erosion horizons. As seen in Chapter 1, early diagenetic reactions dominate different depth zones. For Fe and Mn expecially, the peak in pore water concentrations occurs in

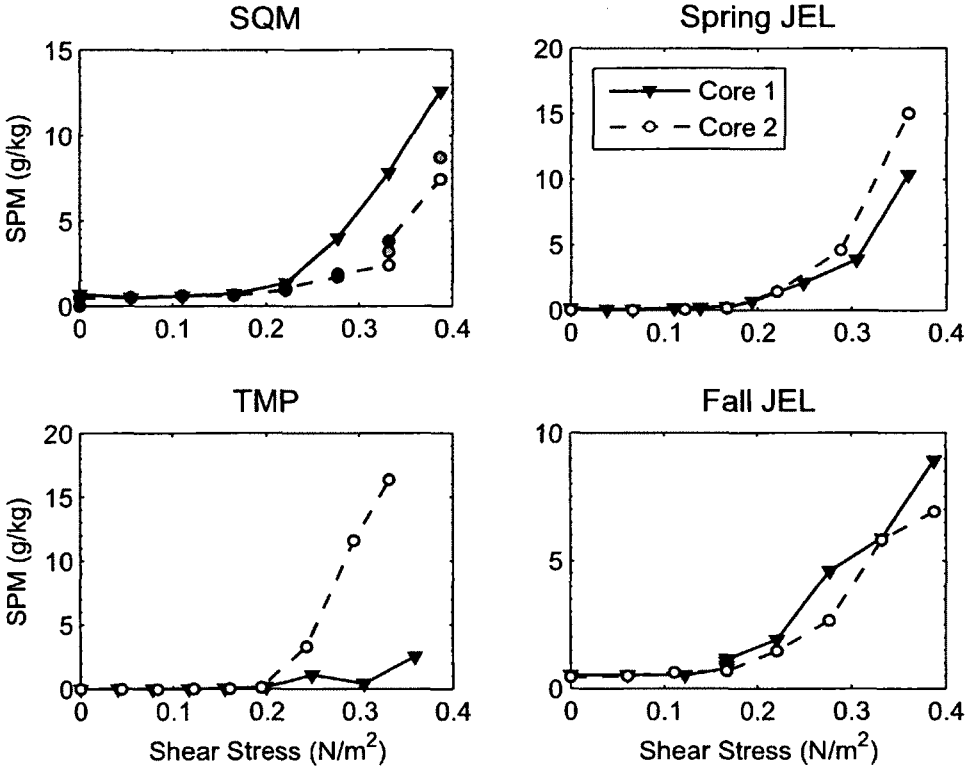

Figure 2-3: Suspended particulate matter (SPM) as a function of shear stress for all eight erosion experiments. SPM was corrected for the mass removed from sampling. Samples from SQM Core 2 are colored from lighter to darker shade based on the order the sample was taken at the particular shear stress.(Note: The overlying water in both SQM cores and Fall JEL Core 2 was approximately doubled due to incorporation of the turbidity chamber apparatus.)

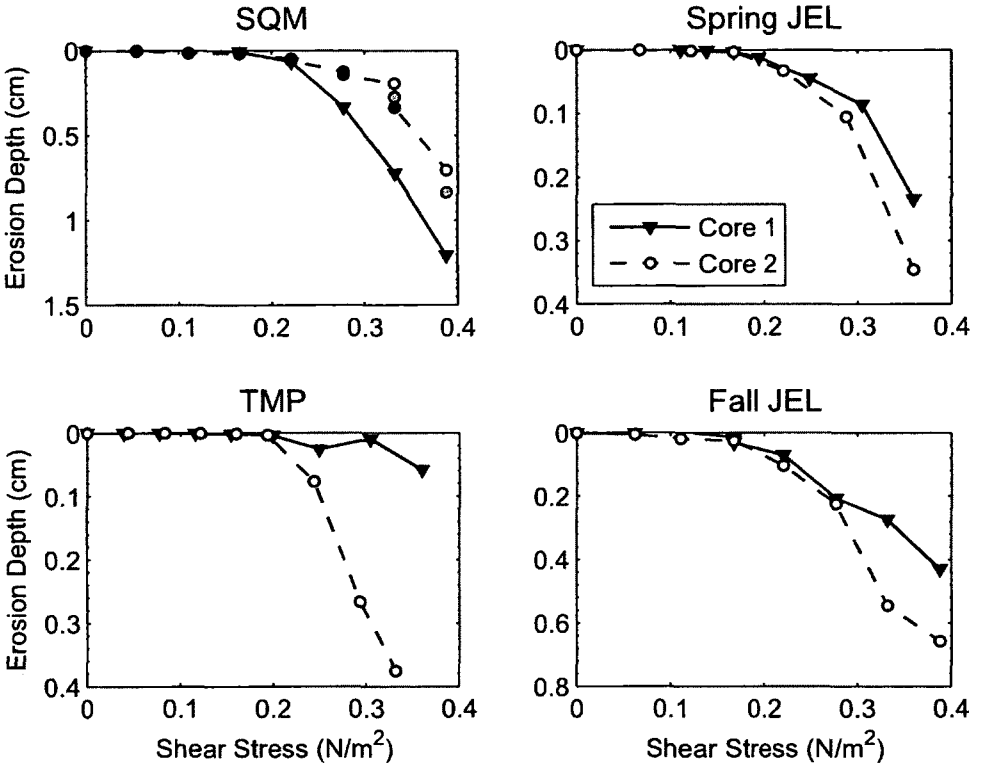

Figure 2-4: Depth of erosion for all eight erosion cores at each shear stress, calculated from SPM concentrations assuming equal erosion across the sediment water interface.

the upper 1 cm of the bed, and it can be expected that release will occur during resuspension. For NO_3^- and PO_4^{3-} however, pore water concentrations were generally minimal in the top 1-2 cm of sediment which suggests that there would be no appreciable release of these two solutes during sediment resuspension.

Suspended particulate matter and shear stress steps are displayed in Fig. 2-5 over the duration of the experiment. High resolution suspended sediment concentrations allows insight into both the total erosion of sediment and the rate of sediment erosion. As expected, at lower shear stresses there was no erosion, and SPM remained relatively constant. Even after τ_c the amount eroded was minimal, and the rate of erosion quickly decreased after 5-10 minutes. At higher shear stresses (above 0.27 N/m^2) the rate of erosion exponentially decreased with time as the sediment-water interface eroded to deeper sediment. The exponential decrease has been observed by other

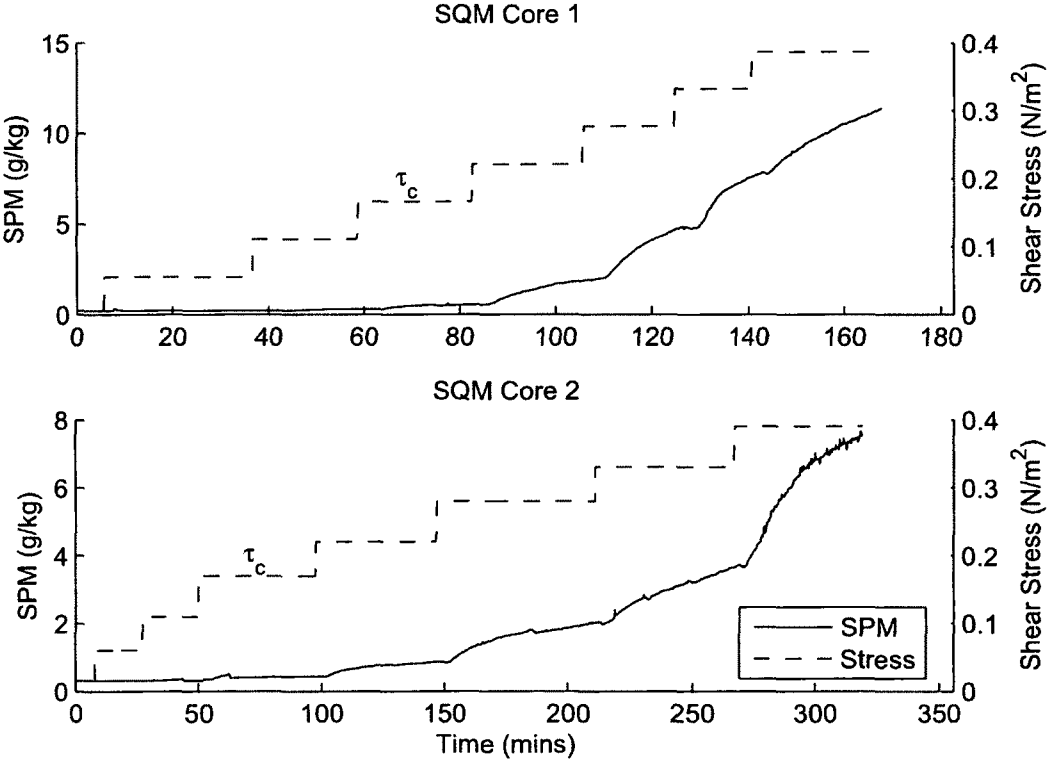

Figure 2-5: Plots of SPM, shear stress, and time in the overlying water of both SQM erosion cores

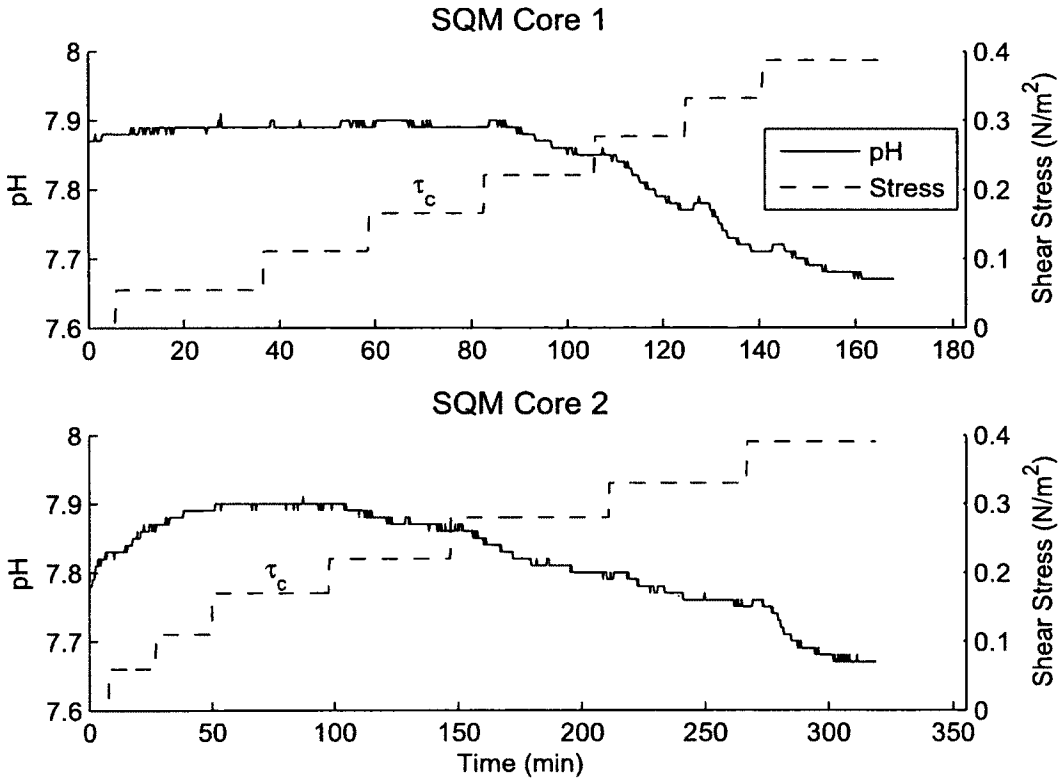

Figure 2-6: pH of the overlying water in the turbidity chamber measured by the Hydrolab Datasonde

authors (Mehta and Parchure, 2000) and can mainly be attributed to the difference between sediment shear strength and the stress applied to the bed.

This resuspension caused fluxes of nutrients and metals into the overlying water by means other than simple molecular diffusion. In addition, resupension led to a lowering of the pH (Fig. 2-6) and dissolved oxygen (DO, Fig. 2-7) of the overlying water in the SQM erosion experiments. In both experiments the initial pH was close to 7.9 and decreased to 7.7 by the end of both experiments. The pH reduction was most likely due to advection of more acidic pore water into the overlying water as well as acid-producing diagenetic reactions such as aerobic remineralization. The timescale of the erosion for SQM Core 2 was almost twice as long than for Core 1, yet the pH reduction was the same. More dissolved oxygen was removed in SQM Core 1 than in Core 2 (Fig. 2-7) which could be in part due to the increase in temperature

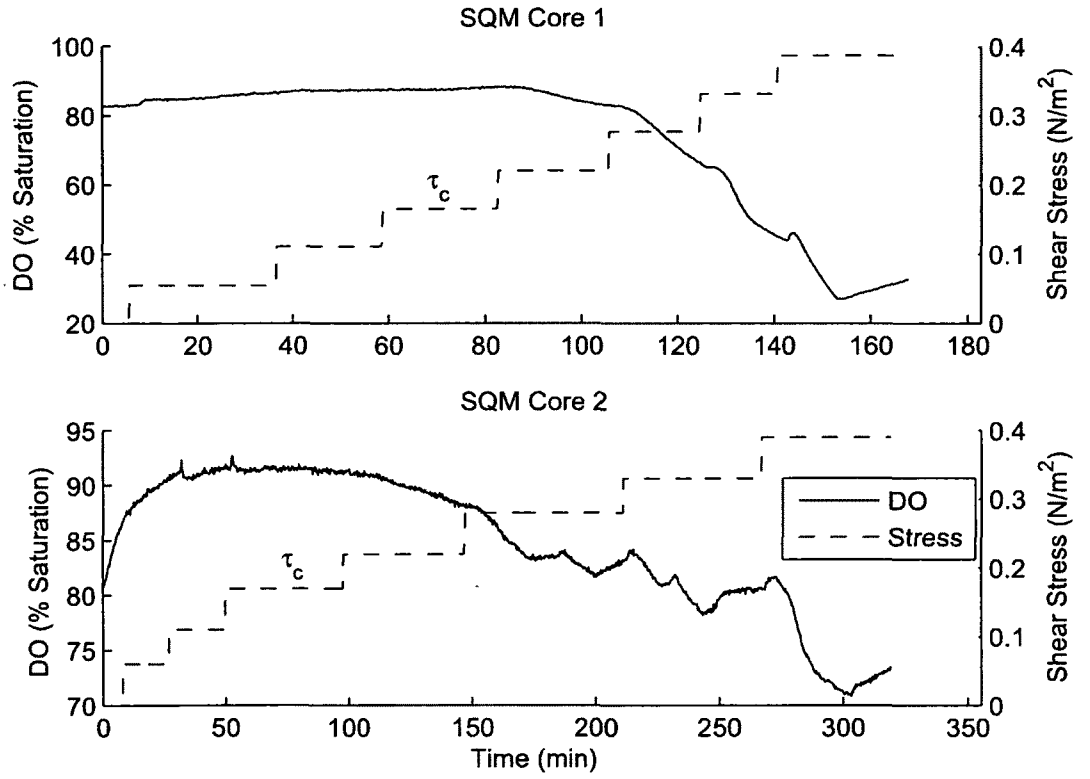

Figure 2-7: Changing saturation of dissolved oyxgen measured by the Hydrolab datasonde in both SQM erosion cores. The segments of each curve where DO sharply increases was due to the fresh water used to replace the extracted water samples. SQM Core 2 was run on the following day of field collection and stored at 4°C overnight.

(Fig. 2-8). However the 5°C temperature increase in SQM Core 1 did not cause a noticible change in DO saturation over the first 120 minutes. DO was not removed in Core 1 until several steps after the critical shear stress, whereas DO removal started to occur at τ_c in Core 2. Further analyses of pH and DO results are provided in sections 2.3.3, 2.3.5, and 2.3.7.

2.3.2 Nutrient Release

Dissolved nutrient releases as a function of shear stress for all experiments are shown in Figs. 2-9-2-13. Corrected overlying water concentrations (μmol L^{-1}) are shown in Figs. B-1-B-4. The amount released was calculated by the following equa-

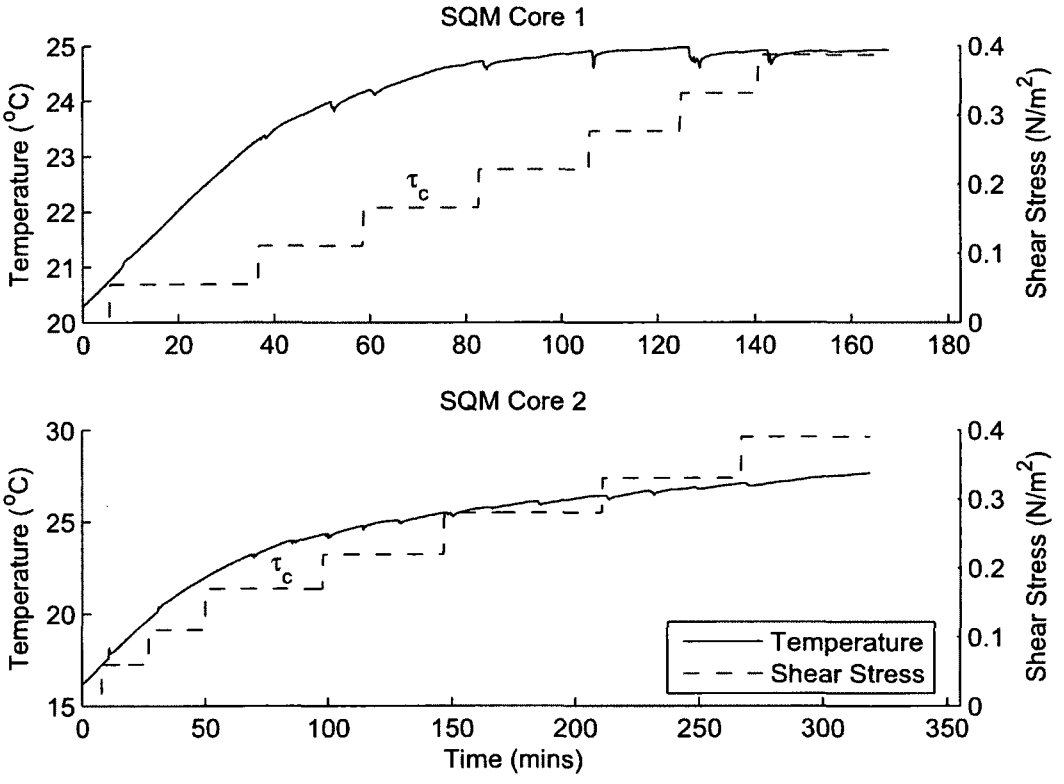

Figure 2-8: Changing water temperature (°C) measured by the Hydrolab datasonde in both SQM erosion cores. The segments of each curve where temperature dips was due to the fresh water used to replace the extracted water samples. SQM Core 2 was run on the following day of field collection and stored at 4°C overnight, causing a change in the intitial temperature.

tion:

$$R_N = \frac{V(C_N - C_o)}{A} \tag{2.1}$$

where R_N is the release (mmol m^{-2}) at any shear stress, C_N is the concentration (mmol L^{-1}) at the shear stress, C_o is the intitial concentration of the overlying water (mmol L^{-1}), V is overhead volume (L) and A is the cross-sectional area of the core barrel (m^2). Each measured concentration was corrected for the mass of nutrient pipetted out from previous water samples. The contribution of dissolved nutrients from pore water was calculated by determining the quantity of pore water eroded at each shear stress step. This was accomplished by multiplying the mean concentration of the first pore water sample (Chapter 1) from each sectioned core by pore water eroded and follows Eqn. 2.2

$$R_{pw} = \frac{C_{pw}[SPM]\rho_w V\phi}{A(1-\phi)} \tag{2.2}$$

where R_{pw} is the areal release of nutrient from pore water (mmol m^{-2}), C_{pw} is the average pore water concentration (mmol L^{-1}), ρ_w is the density of the overlying water (kg L^{-1}), V is the overhead volume (L), and A is the cross-sectional area of the core barrel (m^2).

For nitrate, silica and NH_4^+, the release of dissolved solute was greater that what was modeled from pore water. Kalnejais et al. (2010) found that dissolved concentrations of solutes increased in the overlying water more than what was expected from simple pore water inclusion. They determined that pore water advection by flushing was insignificant over the course of the experiment by comparing silicic acid pore water profiles before and after erosion. In this experiment similar observations were made, however pore water profiles were not measured post-erosion. Futhermore, erosion cores were discarded immediately afterwards and not analyzed for the pres-

ence of meiofauna. An additional source may be from ion exchange or desorption reactions (Kalnejais et al., 2010) as well as flushing of interstital water from worm burrows from the stirring of the overhead or bio-irrigation (Kristensen, 2000) during the experiments.

2.3.3 Ammonium Release

NH_4^+ sources to the overlying water include the amount mixed in from pore water, contribution from desorption reactions and aerobic remineralization. NH_4^+ release did not occur until after the critical shear stress (Fig. 2-9), except in Spring JEL Core 1. The maximum amount released was greatest in the SQM cores, reflecting the greater concentrations in the sediments at this site (Figs. 1-5). At JEL however, there was a greater release in spring than in the fall even though the depth eroded was similar, and both porosity and pore water concentrations were greater in the fall. Leakage from Fall JEL Core 2 may explain why the NH_4^+ trend does not follow the monotonically increasing trend exhibited by the other cores, as lost water was replaced, but the relatively lower NH_4^+ release from Fall JEL Core 1 compared to the spring is puzzling given that NH_4^+ release should have been higher based on the higher concentrations in the sediment. An alternative solution may be that NH_4^+ was oxidized to NO_3^- over the course of the experiment. Looking at NO_3^- release (Fig. 2-12), it can be seen that release was significantly greater than contributions from pore water, suggesting that NH_4^+ was converted to NO_3^-. Furthermore, the slight reduction in pH (Fig. 2-6) indicates that acid-producing reactions occured over the time scale of these experiments.

In these experiments NH_4^+ releases were about an order of magnitude greater than from pore water. In some cases NH_4^+ desorption can contribute up to two-thirds of total release from resuspended sediments (Morin and Morse, 1999). Previous work has shown that NH_4^+ partition to sediment follows a linear isotherm when dissolved

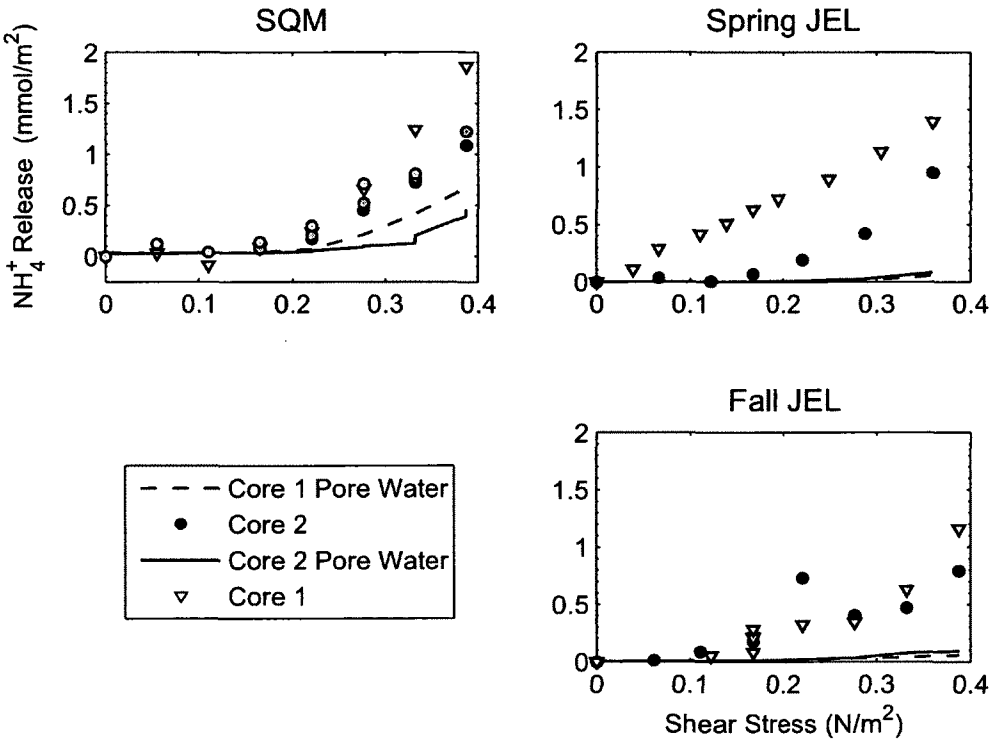

Figure 2-9: NH_4^+ released into the dissolved phase from each shear stress. Multiple water samples were taken at individual shear stresses in SQM Core 2. Data points are plotted from darker to lighter shade based on the order the samples were taken.

NH_4^+ is at relatively high concentrations ($\geq$40 μM) (Rosenfeld, 1979; Raaphorst and Malschaert, 1995). However, at low concentrations adsorption properties may change due to selective partioning between different sediment repositories. Raaphorst and Malschaert (1995) observed the ratio of adsorbed to dissolved NH_4^+ increased at concentrations lower than 40 μM, possibly due to organic matter dominating the sorbent phase.

To determine if desorption occured after the critical shear stress, changes in residual NH_4^+ were normalized to changes in SPM between individual samples (Fig. 2-10) after subtracting the contribution from pore water. Kinetically, NH_4^+ desorption is separated into a period of quick release (minutes) immediately following resuspension by a period of slow release (hours) (Morin and Morse, 1999). In both this study and Morin and Morse (1999) there was greater NH_4^+ per gram SPM at lower suspended sediment concentrations, and there was relatively less release of NH_4^+ per g sediment at higher SPM concentrations. This is surprising because this sediment found deeper should have been at equilibrium with higher pore water concentrations. Furthermore, the change from anoxic or suboxic conditions (which occurs in the first couple millimeters) to oxic conditions in the overlying water should release more NH_4^+ simply because sediment in oxic conditions has lower K than anoxic conditions (Morin and Morse, 2005).

One possible explanation of the higher NH_4^+ to SPM ratios at lower SPM concentrations is that aerobic remineralization (Eqn. 2.3, (Froelich et al., 1979)) released NH_4^+ and that small SPM changes enlarged the ratio.

$$(CH_2O)_x(NH_3)_y(H_3PO_4) + xO_2 + yH^+ \rightarrow xCO_2 + yNH_4^+ + HPO_4^{2-} + 2H^+ + xH_2O \quad (2.3)$$

For example, looking at the Δ NH_4^+/ Δ SPM in SQM Core 2 over the time period

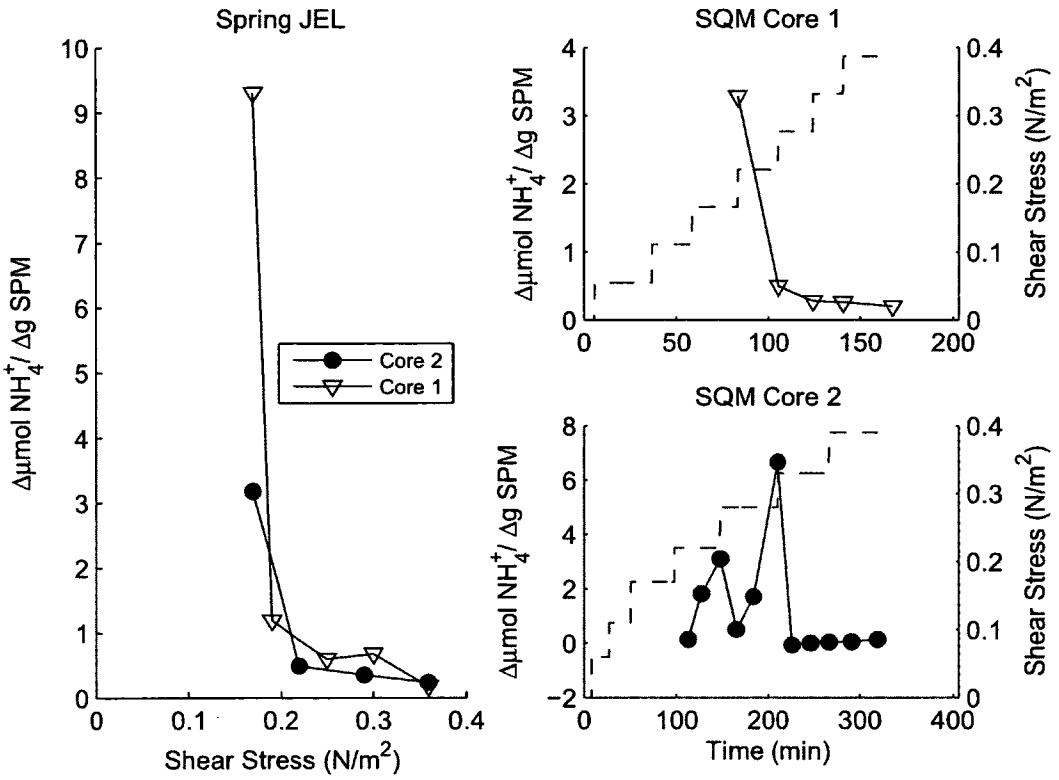

Figure 2-10: NH_4^+ changes normalized to changes in SPM between individual shear stresses for the Spring JEL and SQM Cores. Shear stresses '–' are plotted on the right-axis of SQM Core 1, and SQM Core 2 graphs.

of the critical shear stress (0.22 N/m^2) and the stress immediately afterwards the ratios increased over the time of constant stress. Initially, there was was a release of NH_4^+ coinciding with erosion. Unlike the points at higher shear stresses, erosion rates quickly decreased after the intital application of shear stress (Fig. 2-5), but not the rate of NH_4^+release. NH_4^+ increase in the absence of significant erosion indicates pore water is not that cause of the release. The reduction in ratio between 0.22 and 0.28 N/m^2 was due to the pulse of sediment that occured once higher stress was applied, likewise with the subsequent stresses. NH_4^+ release occured more rapidly than what can be explained by molecular diffusion. DO measurements over the course of the experiments indicated oxygen consumption occured (Fig. 2-7). By the stoichiometry of the reaction (Eqn. 2.3), oxygen consumption to NH_4^+ release is the same as the C:N ratio of the decaying organic material. The Δ O_2/Δ NH_4^+ from before erosion to the last sample for SQM Cores 1 and 2 were 19 and 16 respectively. Compared to the C:N molar ratio of 10.2 from CHN analysis (Sec. 1.2.5), it is apparent that there was enough oxygen consumed to account for NH_4^+ release. Furthermore, the larger DO consumption indicates that there were more oxidation processes occuring in the overlying water.

2.3.4 Phosphate Release

Phosphate (PO_4^{3-}) release fluctuated greatly between cores and with generally small concentration changes in the overlying water (Fig. 2-11). At SQM after τ_c, 0.6 mmol m^{-2} of phosphate was removed in Core 1 whereas there was a release of approximately 0.3 mmol m^{-2} in Core 2. At Spring JEL there was removal after τ_c but by the end of the experiment there was not significant release or removal. TMP was opposite in that there was a release after τ_c but removal afterwords, resulting in no net release. At Fall JEL, phosphate release occured after the τ_c and increased for higher shear stresses.

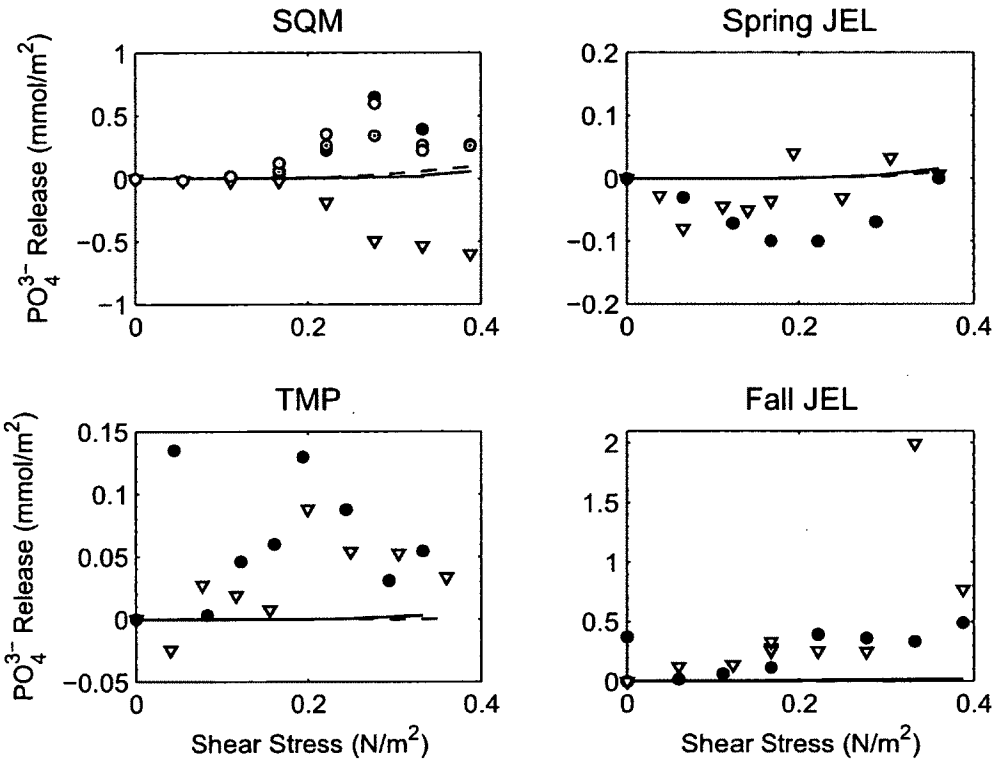

Figure 2-11: Release (mmol m^{-2}) of dissolved phosphate in all eight erosion experiments. Multiple water samples were taken at individual shear stresses in SQM Core 2. Data points are plotted from darker to lighter shade based on the order the samples were taken.

The lack of PO_4^{3-} (P) release from simulated erosion may be due to several reasons. First, low pore water concentrations of phosphate would not provide P as a source into the overlying water. This is likely given the relatively low concentrations of P in the oxic zone of the sediments (especially at Thomas Point) and the good comparison between calculated P profiles from pore water advection into the overlying water with actual P release. However, in several instances P fluctuated significantly between individual shear stress steps, indicating other mechanisms act to provide or sequester P. There was one instance of a large pulse of P in the erosion experiments at 0.33 N/m^2 in Fall JEL Core 1. This P increase may be the result of fecal material or injection of interstitial water from a sediment burrow capped prior to erosion.

One commonality between P profiles was that there was removal at some point

during each experiment, even though P release was small and variable between duplicate cores and between individual sites. This generally occured at higher shear stress when the erosion depth was greater. P removal after the critical stress may be due to adsorption to amorphous iron oxyhydroxides (Lehtoranta et al., 2009). Previous work has shown that the sediments near the Squamscott River have relatively low bioturbation compared to those at JEL (Hines and Jones, 1985), resulting in a shallow oxic layer. The reducing quality of these sediments causes the oxygen penetration and dissolved iron in porewater to exhibit maxima closer to the sediment-water interface. As a result, more dissolved iron may be incorporated into the overlying water during erosion may oxidize and adsorb P. Comparing the P and Fe release from SQM cores (Fig. 2-15) it is apparent that P removal occurs immediately after the pulse of Fe into the overlying water. This supports the claim that P associates with iron hyroxides.

2.3.5 Nitrate Release

There was generally a release of nitrate, the exception to this was TMP Core 2 (Fig. 2-12). Like NH_4^+ the amount of nitrate release exceeded the expectation based on pore water concentrations. Of the four nutrients tested, the observed nitrate release in comparison to the amount predicted to have advected from pore water was the most extreme. Nitrate release only occured after the critical shear stress the exception being Fall JEL Core 2. Oxidation of NH_4^+ to NO_3^- may have taken place, but it is undeterminable based on the data here. All that can be said is that nitrate increases coincided with NH_4^+ increases (Fig. 2-9) and DO drawdown (Fig. 2-7). NO_3^- release was lesser than NH_4^+ release by 50% at SQM whereas releases were similar between the two solutes at Spring and Fall JEL. NH_4^+ will be nitrified in the overlying water and so NO_3^- release may ultimately increase over time.

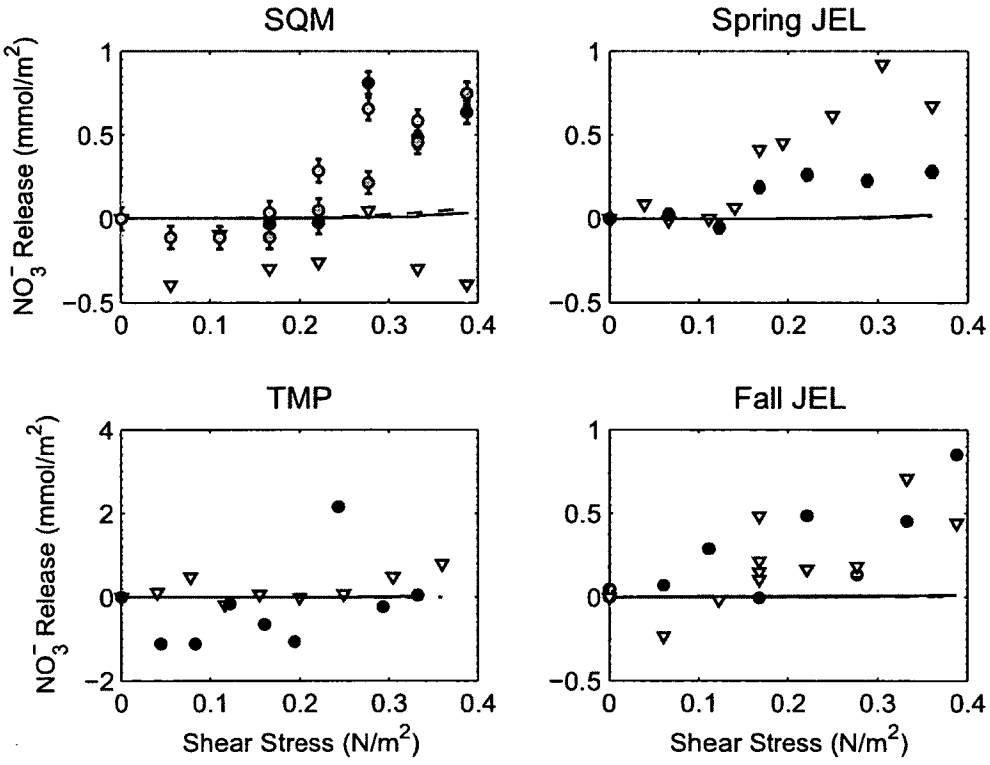

Figure 2-12: NO_3^- released into the dissolved phase from each shear stress. Multiple water samples were taken at individual shear stresses in SQM Core 2. Data points are plotted from darker to lighter shade based on the order the samples were taken. Error bars are the average standard error (Appendix A)

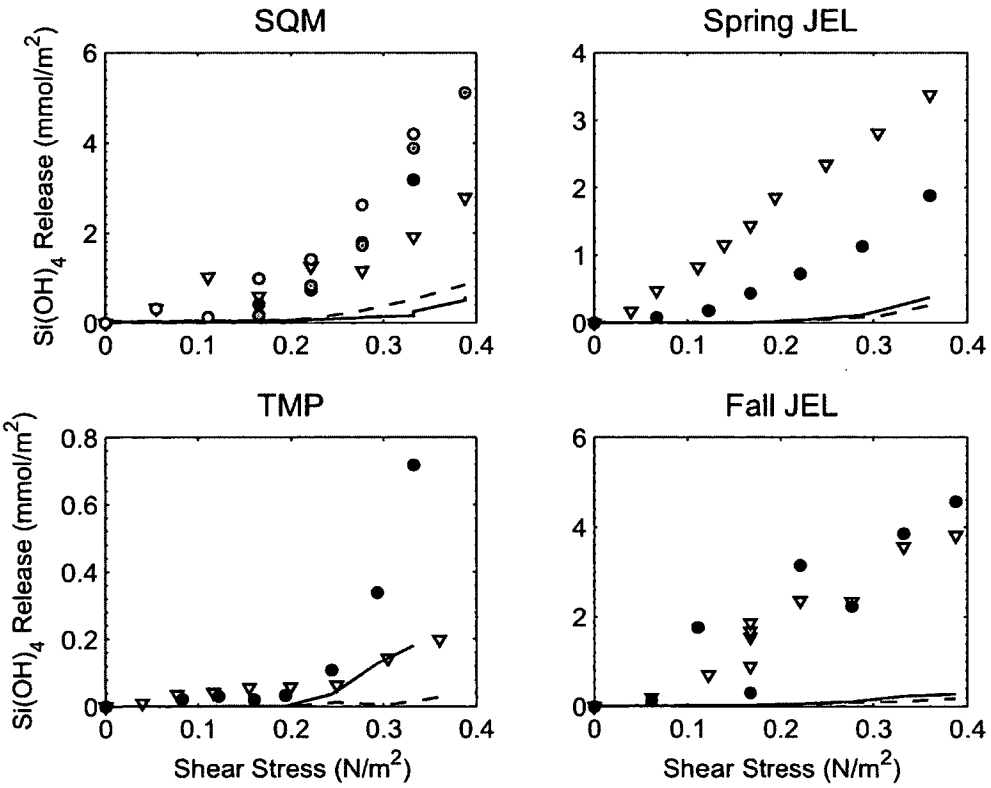

Figure 2-13: Silica released into the dissolved phase at each shear stress. Multiple water samples were taken at individual shear stresses in SQM Core 2. Data points are plotted from darker to lighter shade based on the order the samples were taken.

2.3.6 Silica Release

Silica release either monotonically increased or remained constant at each shear stress step. Silica was not removed from solution during any experiment. Similar to the NH_4^+ and NO_3^- behavior, silica added to the overlying water greatly exceed contribution from pore water. An extra source may have been dissolution of biogenic opal from SPM but over the time scale of these experiments appreciable dissolution is unlikely. Desorption reactions of silicic acid may have occured due to the changing redox and pH of the pore water environment to the overlying water.

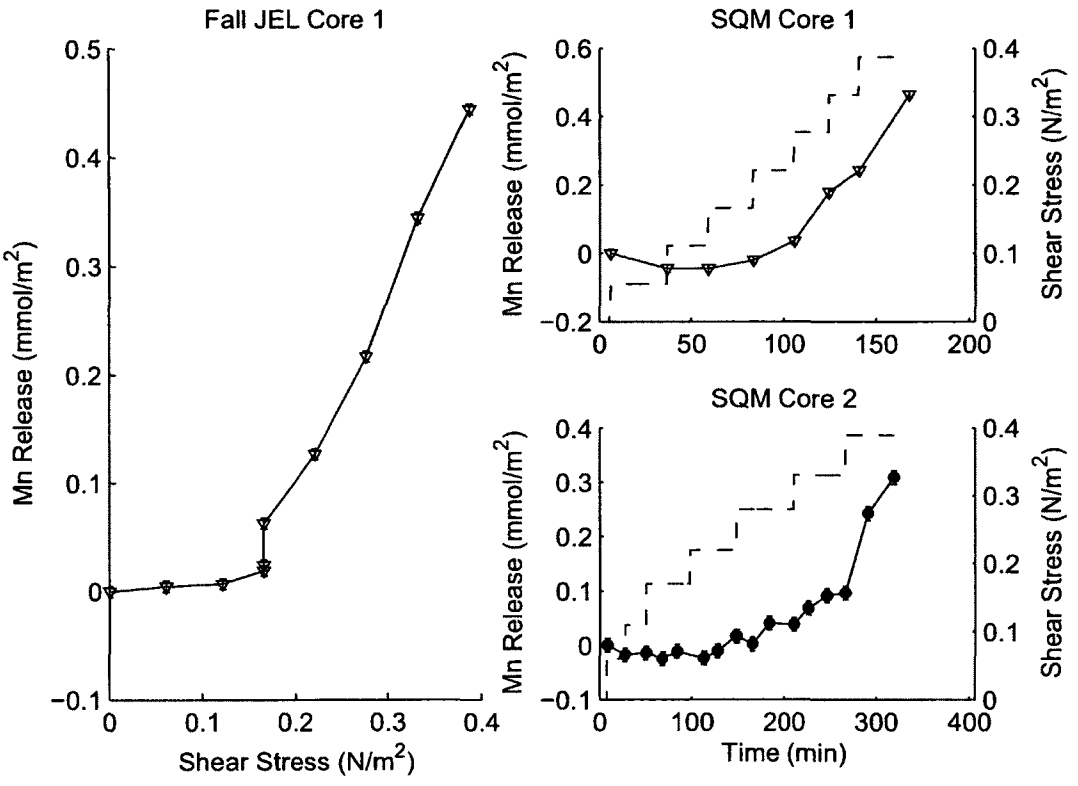

Figure 2-14: Release mmol m^{-2} of Mn in the dissolved phase in three erosion core experiments.

2.3.7 Dissolved Metal Release

Water samples from three erosion experiments were analyzed for Mn and Fe, and dissolved releases are shown in Figures 2-14 and 2-15. In each case Mn concentrations increased after the critical shear stress was attained and continued to increase at higher shear stresses. At JEL during the fall Mn concentrations continued to increase in the erosion core even though the sediment-water interface was eroded past the peak in pore water concentration (at 3 mm, Fig 1-8). Using a particle entrainment simulator (PES), Cantwell et al. (2002) demonstrated that scavenging of Mn by suspended particles was minimal, and that most Mn released from resuspended sediment was in the dissolved phase, increasing in concentration over the course of a 12 hour experiment. Similar results are observed here.

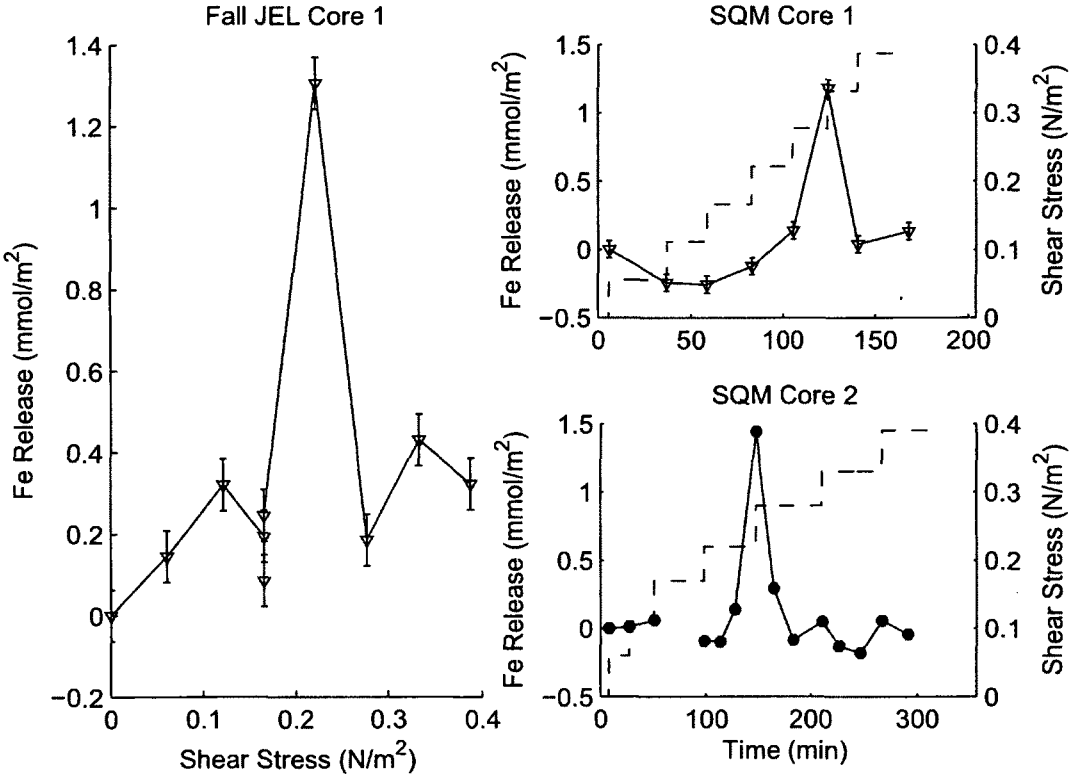

Figure 2-15: Release mmol m^{-2} of Fe to the dissolved phase in three erosion core experiments. Discontinuities are due to data that was dropped due to large RSE from ICP-MS analysis

Iron profiles were significantly different between experiments. There was a single shear stress in each core when dissolved Fe release increased dramatically, and then a subsequent drawdown in the following sample. The peak in Fe is most likely due to erosion to the depth of maximum Fe concentrations (0.5 cm at JEL). The quick removal of iron was likely due to adsorption or precipitation. In contrast to Mn, iron was not released in any appreciable amount.

One interesting observation was that the percent saturation of dissolved oxygen started to decrease at the shear stress at which iron release occured. DO from the Hydrolab datasonde is shown in Figure 2-7 for the two SQM cores. Although the erosion core and turbidity chamber were open to the atmosphere and exchange of atmospheric oxygen surely took place, DO reduction was still apparent. The plausibilty of DO oxidation of Fe is supported by the fact that DO reduction occured after the peak in Fe and was not significant just after τ_c had been attained. Although small in concentration, SPM content increased at 0.17 N/m^2 in SQM core 1, though DO concentration remained relatively constant. As previously stated, other oxidation reactions may have also occured, such as oxidation of NH_4^+ to NO_3^- but it appears that Fe oxidation is a sink for dissolved oxygen.

2.3.8 Particulate Metal Release

Suspended particulate matter collected on filter papers was digested to determine potential release of particulate phase metals during sediment erosion. Concentrations of six trace metals are plotted in Figure 2-16 in similar fashion to Figure 2-15. At shear stresses below τ_c, metal concentrations were generally less than the concentration of surficial particles measured in bulk sediment (Table 1.11). At the critical shear stress (0.17 N/m^2) metal concentrations started to approach the sediment bulk concentration due to inclusion of surficial sediment into the overlying water. At the next stress step (0.22 N/m^2) after τ_c, metals increased by 200-500% compared to the bulk,

after which SPM metal concentrations approached the bulk sediment composition due to resuspension of more sediment.

Peaks in both particulate metals (Fig. 2-16) and dissolved iron (Fig. 2-15) occured after τ_c but over the same shear stress step change (0.22 N/m^2), with the peak in particulate metals (t = 110) occuring before the peak in dissolved iron (t = 150 min). It is possible that particles enriched in these trace metals reside as a concentrated layer between the sediment-water interface and the dissolved pore water Fe maximum. This depth range occured in the top 5 mm at SQM (Fig. 2-15), yet the depth of erosion at the applied shear stress of 0.22 N/m^2 was even less (approximately 1.5 mm, Fig. 2-4). Between 0 and 5 mm depth dissolved Fe concentrations decreased significantly (Fig. 1-8), due in part to the diffusive flux, but moreso to oxidation of Fe and ensuring adsorption/precipitation reactions (as dissolved Fe is not released into the overlying water (Fig. 2-15)). Several of these trace metals (Cr (Richard and Bourg, 1991), Cu, Zn, Pb (Burdige, 1993)) are known to coprecipitate with Fe oxyhydroxides. The fact that all of these trace metals peaked alongside Fe supports the possibility of a sediment layer concentrated in trace metals.

The concentrated SPM may also have been due to winnowing of smaller grain sizes. Clay and silt particles tend to be more enriched in trace metals due to the large surface area available for metal adsorption (Cantwell et al., 2002). At shear stresses near τ_c, applied forces are nearly enough to disturb the sediment-water interface and suspend smaller particles. The energy applied to the bed however may not be enough to resuspend larger grain sizes, causing an apparent enrichment in SPM over bulk material. On the other hand, if winnowing was the cause SPM enrichment, then particles suspended at the critical shear stress would have been enriched, yet this was not the case in SQM Core 2 (Fig. 2-16). Although for the other erosion experiments SPM enrichment occured at τ_c. An experiment measuring changing grain sizes of in situ SPM as a function of applied shear stress could illuminate these results further.

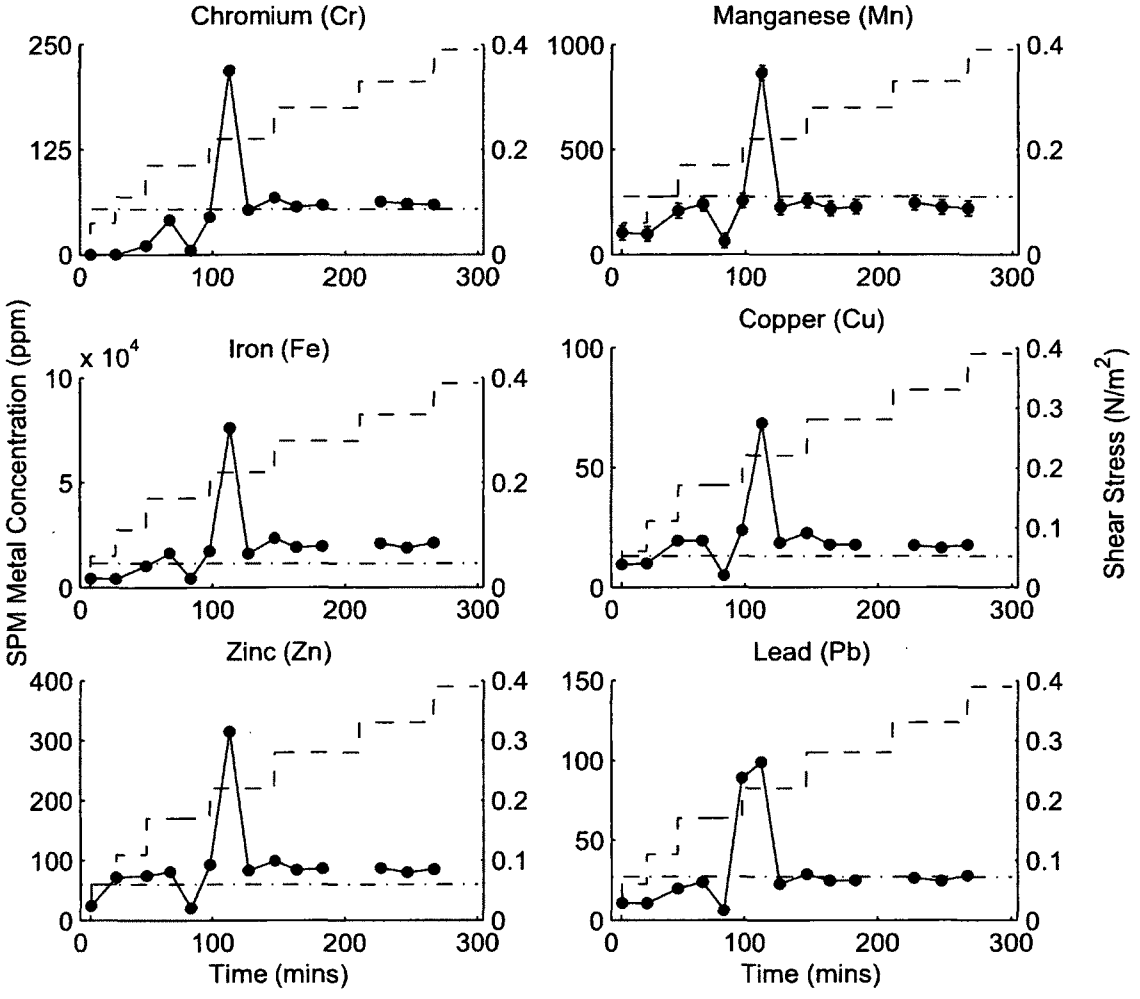

Figure 2-16: Particulate metal concentrations (ppm, μg/g dry weight) of SPM from SQM Core 2 erosion experiment. The critical shear stress was in this experiment was 0.17 N/m^2. Solid circles are metal concentrations, dashed lines are shear stress, and dashed-dot lines are metal concentrations in the surficial bulk sediment. The points at t = 80 minutes had significantly lower SPM captured on the filter paper.

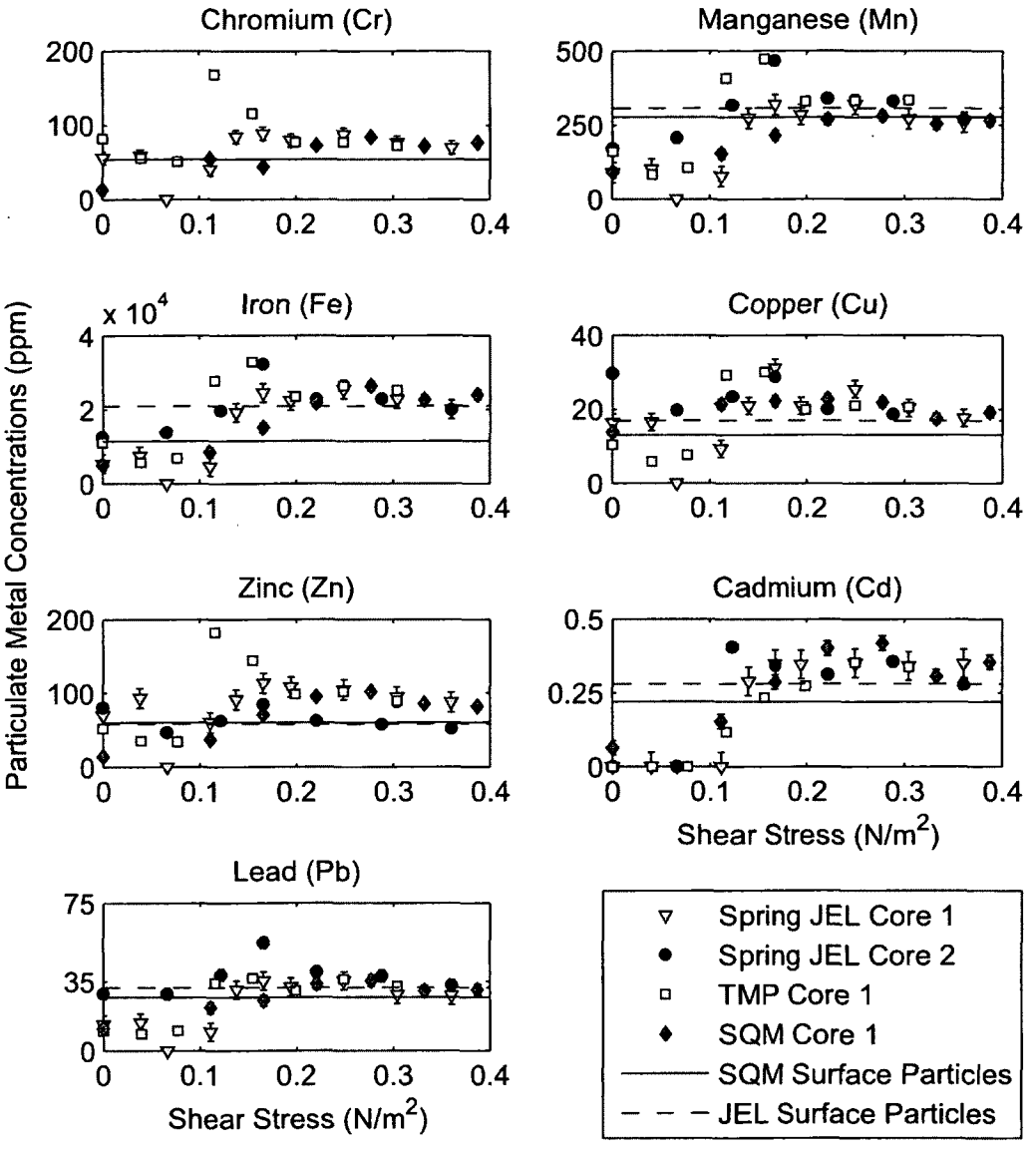

Figure 2-17: Particulate metal concentrations (ppm, μg/g dry weight) of SPM from 4 erosion core experiments. Samples beneath the LOD are plotted as zero. The range of critical shear stresses was from 0.14 to 0.20 N/m^2. Solid and dashed lines are metal concentrations in surficial particles at the JEL and SQM sites. There was no data for Cr at JEL, and Zn concentrations were the same at both JEL and SQM.

Similar results are shown in Figure 2-17 for four erosion experiments. In general, SPM metals increased in concentration as sediment was eroded. Once the critical shear stress was attained there was enrichment of several trace metals (Cr, Cu, Zn, and Pb) in Spring JEL Core 2 and TMP Core 1 whereas there was little to no enrichment in SQM Core 1 and Spring JEL Core 1. In all cases however, the enrichment in trace metals occured in the presence of Fe and Mn enrichment. An enrichment factor (EF) may be used to determine the magnitude of SPM metal enrichment in comparison to the bulk sediment (Cantwell et al., 2002). This is defined below:

$$EF = \frac{Me_{SPM}}{Me_{bulk}} - 1 \tag{2.4}$$

Metal enrichment factors (EF) are shown in Figure 2-18. The EF's of these particles were Fe > Cu > Zn > Cr > Pb > Mn at SQM and Cu,Pb > Fe > Mn > Zn at JEL. There was insignificant enrichment of Cd in all experiments. In several erosion experiments by Cantwell et al. (2002) where material was kept in suspension over the course of 12 hours, metal enrichment generally followed Cu > Zn,Pb > Fe > Mn > Cd. In similar experiments to the present study, Kalnejais et al. (2007) found that metal enrichment in SPM was Cu > Pb > Mn, Fe. Cantwell et al. (2002) explained the order of metal enrichment was due to the relative stability of each metal as an organo-metallic complex. Upon resuspension, collision between particles, the higher pH and the presence of oxygen lead to reactions in the overlying water. The relatively larger enrichment of Fe at SQM indicates that further reactions may occur over time, which exchange Fe with other trace metals to form more stable organo-metallic compounds.

The metal enrichment causes these trace metals to surpass the lower treshold of sediment quality criteria by up 200% for Cu, Zn, and Pb and 260% for Cr (from SQM Core 2) even when the bulk sediment is at natural levels (Table 1.11). This means that benthic (and marine) organisms may be exposed to high metal concentrations

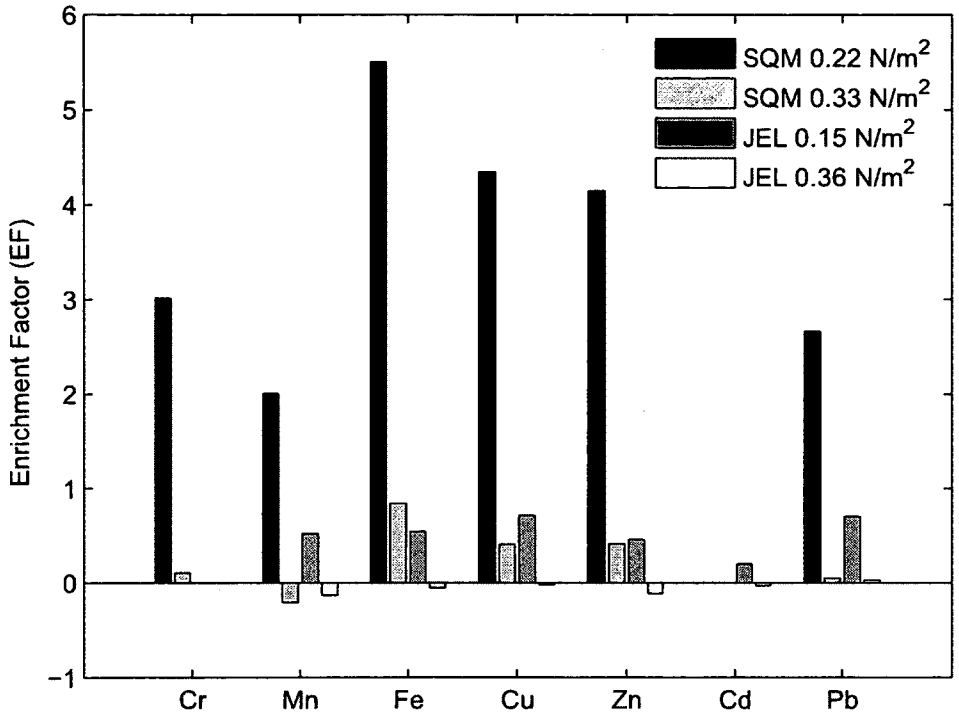

Figure 2-18: Enrichment factors (Eqn. 2.4) of several trace metals in suspended particulate matter from Spring JEL Core 2 and SQM Core 2 erosion experiments. At SQM the shear stress of 0.22 N/m^2 occured after the critical shear stress step, whereas at JEL 0.15 N/m^2 was the critical shear stress. Particles from higher stress steps approached the bulk concentrations of the surficial particles at both sites.

in seemingly unpolluted sediment. The effect may be compounded in contaminated sediment.

2.3.9 Case Study: Tropical Storm Irene

A case study of a severe episodic weather event was performed to put metal and nutrient data into the context of the environmental conditions of the Great Bay which might lead to contaminant release. Tropical Storm Irene swept through the Great Bay during August 28th and 29th, 2011. Water samples were gathered periodically over the course of the storm and following days from the dock at JEL using a Niskin bottle. Likewise the Hydrolab Datasonde was used to measure water characteristics

during sampling times. Suspended particulate matter and turbidity measurments revealed that SPM increased over the duration of the storm (On day 8/28, Fig. 2-19). It is mostly likely the peak in SPM is from sediment resuspension instead of runoff, as there was no lag between the passing storm and SPM concentrations, and SPM concentrations decreased significantly after the storm had subsided (after 8/29). Using a Nortek Vectrino II Acoustic Doppler Profiling Velocimeter and Nortek Vector Acoustic Doppler Velocimeter, Wengrove (2012) measured profiles of water velocities and calculated shear stresses exhibited on the seafloor at JEL over the duration of the storm. Incipient motion of sediment particles was found to begin at 0.10 N/m^2– comparable to the τ_c observed in this study (Fig 2-3). Furthermore, bed stresses exceeded 0.30 N/m^2 in several instances during the event. Table 2.1 lists hourly-averaged bed stresses observed by Wengrove (2012) over the two flood tides that occured on August 28th during Tropical Storm Irene. Regular tidal cycle bed stresses at JEL are below τ_c and are on the order of 0.003 - 0.07 N/m^2 (slack to mid-tide) (Wengrove, 2012).

Table 2.1: Hourly-averaged bed stresses exerted on sediment at JEL uring of Tropical Storm Irene from Wengrove (2012). Stresses are during the two flood tides on August 28th. Low tide during the peak storm began at 7:15 am, whereas low tide during the waning storm began at 7:45 pm. All units in N/m^2.

Phase of Tide		Peak Storm	Waning Storm
Low Tide	hour 1	0.005	0.005
	hour 2	0.19	0.30
	hour 3	0.21	0.31
	hour 4	0.27	0.35
	hour 5	0.20	0.26
High Tide	hour 6	0.10	0.13

Releases of NH_4^+, NO_3^-, PO_4^{3-}, $Si(OH)_4$, and Mn^{2+} during Tropical Storm Irene were estimated for the JEL site using data from the Fall JEL erosion experiments.

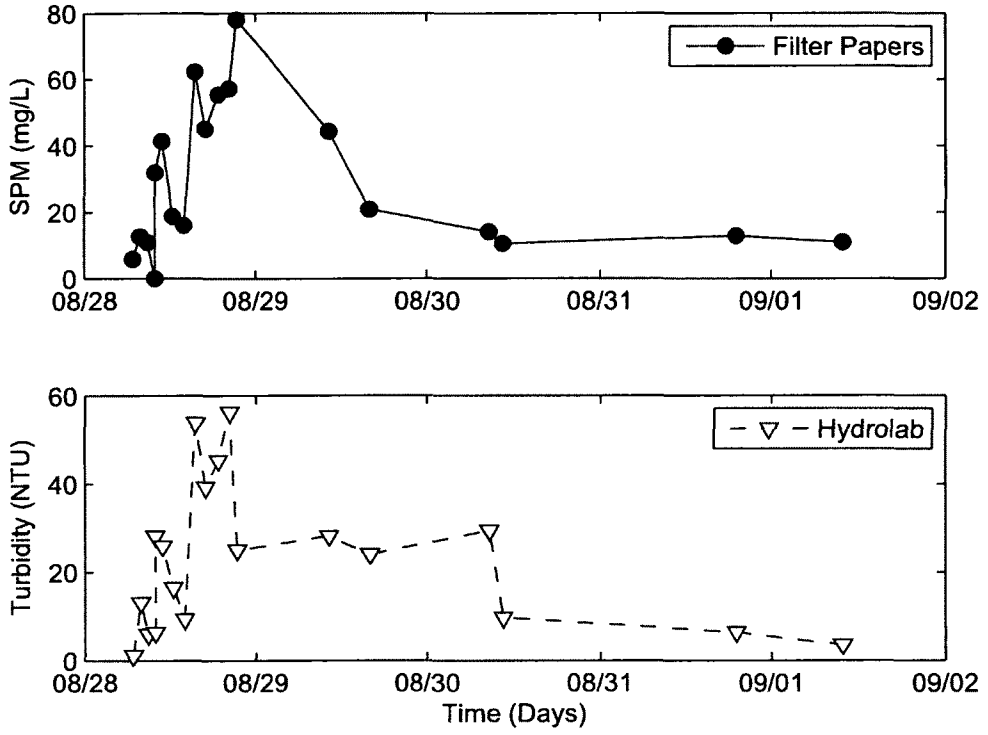

Figure 2-19: Suspended particulate matter (SPM) analyzed from water samples and turbidity measured with the Hydrolab Datasonde during Tropical Storm Irene. SPM was determined my mass difference on filter paper.

Nutrient release at shear stresses between τ_c (0.14 - 0.16 N/m^2) and 0.25 N/m^2 (Fig. 2-5) can be considered as a pulse into the overlying water because net erosion ceases within minutes. At bed stresses above 0.25 N/m^2, erosion is more severe and occurs over a longer period, so a time-dependent nutrient release must be incorporated to improve the flux calculations. Fluxes were determined however by assuming contaminants were input as a pulse and using the average values of contaminant input at 0.38 N/m^2 from Figures 2-9, 2-11, 2-12, 2-13, and 2-14 for NH_4^+, NO_3^-, PO_4^{3-}, $Si(OH)_4$, and Mn^{2+} respectively. This was the maximum stress imposed during the Fall JEL erosion experiments and was only slightly higher than in situ stresses measured by Wengrove (2012) (Table 2.1). Input from resuspension is shown in Figure 2-20, daily diffusion release under quiescient water conditions is also included for comparison.

Nutrients released as a function of shear stress according to Section 2.3.2 were only determined over short time scales (<1 hr), and most likely understimate fluxes that occured during Irene. It is evident that desorption from SPM (as well as aerobic remineralization) occurs over time in the overlying water, which ultimately makes nutrient release a function of both time and shear stress. Furthermore, nutrient fluxes calculated in Chapter 1 are potential fluxes under laminar flow conditions in which nutrient transport is explained through simple molecular diffusion. Increasing water turbulence causes mixing of 'stratified' water layers, potentially increasing nutrient transport through turbulent eddy diffusion (Boudreau, 1997). It is assumed that hydrodynamic flow conditions in the Great Bay during Tropical Storm Irene are similar to those in the erosion chamber, and thus the effect of turbulent diffusion is incorporated into nutrient releases from simulated erosion. However, over the short timescales of sediment erosion the contribution from turbulent diffusion is probably negligible.

The diffusive flux may also be higher due to erosion to deeper sediment layers where dissolved solutes are more concentrated (thereby increasing the concentration

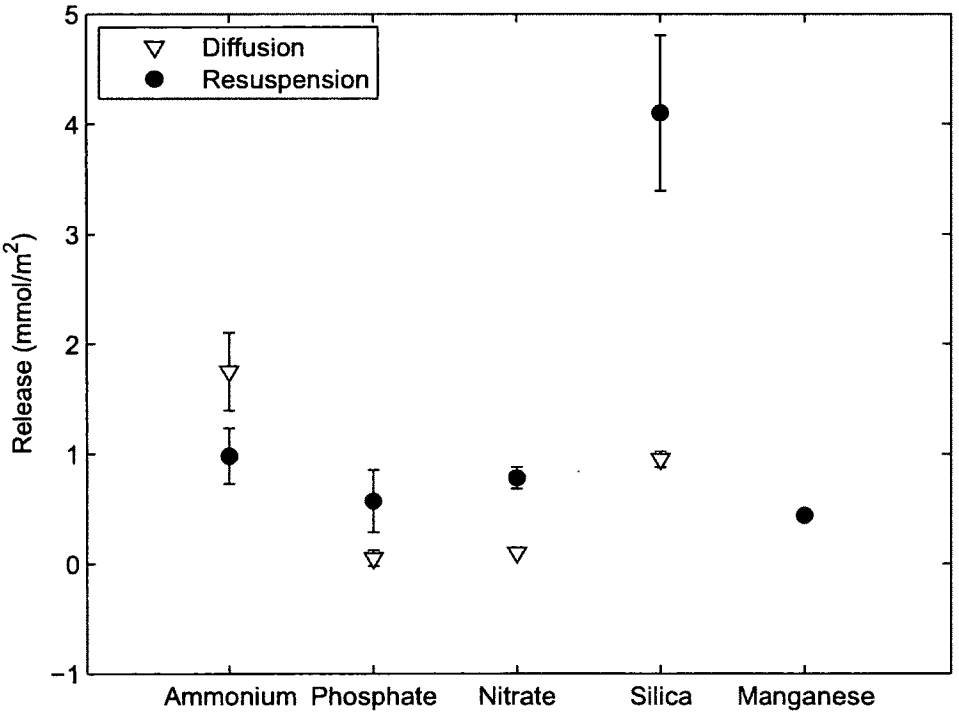

Figure 2-20: Potential contaminant fluxes from sediment to the overlying water due to sediment resuspension during Tropical Storm Irene. Diffusive fluxes are included for comparison. Values for molecular diffusion are average fluxes from both cores in Table 1.16 over the course of one day. Fluxes from sediment resuspension are average contaminant releases from erosion the experiment at Fall JEL at the shear stress of 0.38 N/m^2. Errors are the standard deviations from the average of both cores.

gradient and thus the flux rate). Fluxes from both diffusion and resuspension were within one order of magnitude with the greatest difference exhibited by $Si(OH)_4$ (400% increase from resuspension). It is important to note that while diffusion occurs continuously over the course of a day, sediment resuspension can be episodic in nature, meaning that the same fluxes due to resuspension in Fig. 2-20 can occur over the course of minutes (as made apparent from the erosion experiments). So though the total fluxes from resuspension and diffusive in Figure 2-20 may be comparable, kinetically resuspension is much quicker.

To predict contaminant releases on a estuarine wide scale future work will be needed to address the distribution of fine-grained sediments as well as areas where these sediments are subjected to high shear stress (during the tidal cycle and during extreme weather events). A spatial study searching for in situ sediment shear strength below 0.14 N/m^2 would quickly divulge areas more susceptible to erosion. Predicting the contaminant flux from these areas however will require a rigorous modeling approach that takes into account the distribution of contaminants with depth in the sediment, the rate of erosion as function of time and shear stress, and time-dependent desorption processes in the overlying water.

2.4 Conclusion

The results obtained in this experiment revealed that resuspension of sediment can lead to fluxes of dissolved nutrients and metals orders of magnitude greater than contributions from molecular diffusion and over shorter timescales. For ammonium and silica, the amount released is up to an order of magnitude greater than what can be predicted by advection of pore water during erosion. In contrast, the behaviours of nitrate and phosphate are variable between different sediment. Phosphate is usually removed upon inclusion of dissolved iron into the overlying water, likely due to adsorp-

tion and/or precipitation reactions. Nitrate release is likely dominated by oxidation of ammonium in the overlying water, as higher nitrate release coincided with greater ammonium release. Dissolved iron release occurs once sediment has been eroded down to the pore water iron maximum (which occurs in the top 5 mm of sediment), but is removed from solution within minutes. Conversely manganese is released continually over the entire shear stress range, and there is no manganese removal from solution over the timescales of these experiments (minutes to a few hours).

The critical erosion threshold of Great Bay sediment occurs between 0.14-0.27 N/m^2. At shear stresses near the critical shear stress, net erosion starts and stops rapidly (<5 mins) as the stress applied quickly approaches the cohesive strength of the sediment. At higher shear stresses (> 0.28 N/m^2), more sediment is eroded and the time required for erosion to reach steady state is much longer ($\geq$ 1 hr). The erosion rate however exponentially decreases with time. Chemical characteristics of the overlying water such as pH and dissolved oxygen change due to reactions in the overlying water, such as sediment oxidation and aerobic remineralization. The timescales over which sediment is resuspended will determine the severity of an event to dissolved oxygen removal.

The topmost sediment layers (top 1-2 mms) are the most enriched in particulate trace metals due to adsorption and/or coprecipitation with iron and manganese oxy-hydroxides. As a result, resuspended particulates can be enriched in copper, zinc, chromium and lead by 300-500% over bulk sediment concentrations. This sediment represents a small portion of what can be eroded however, so during events with large bed-applied shear stresses exhibited over relatively longer time scales (10-30 minutes) or during sediment dredging, bulk sediment concentration may be more applicable to predicting metal concentrations in suspended particulates. Over less severe events however, resuspension of concentrated particulate matter may be common. Further work is needed to determine if lower intensity yet more regular-occuring resuspension

events lead to continual releases of concentrated particulate-phase trace metals.

Based on the results of the this study, knowledge of the dynamics of sediment resuspension and underlying chemistry is essential in order to maintain accurate budgets of contaminants entering the waters of the Great Bay Estuary. The fact that pore water solutes can be released in such large quantities is concerning, and should be observed in the long term. Futhermore, future work will be required to improve in situ estimates of contaminant fluxes during resuspension events.

APPENDIX A

Chemical Analysis and Error Calculations

All of the below equations were either programmed into Matlab m-files or used internally in Microsoft Excel 2010. They were applicable in numerous aspects of this study and are referenced throughout this document. For each chemical analysis a linear calibration curve was used to relate machine output units (absorbance or counts per second) to known concentrations of standards. For spectrophotometric methods, the slope and intercept of calibration curves remained fairly consistent with differing batches of standards but differed significantly between machines due to absorbance cell pathlengths. The squared Pearson product moment correlation coefficient (r^2) relates variance of a dependent variable to the variance of an independent variable and was used to determine the correlation between concentration and absorbance units.

$$r^2 = \left[\frac{\sum (x - x_i)(y - y_i)}{\sqrt{\sum (x - x_i)^2 \sum (y - y_i)^2}} \right]^2 \tag{A.1}$$

where x, y are sample averages, and x_i, y_i are individual sample measurements. The spread of data from a mean was calculated using the following equation for standard deviation (σ_D):

$$\sigma_D = \sqrt{\frac{\sum (x - x_i)^2}{n - 1}} \tag{A.2}$$

where n is the sample size. Although analytical blanks should give outputs of zero (absorbance units or cps), machine error and contamination reduces sensitivity, and puts a limit on the lower end of detection. The limit of detection (LOD) is the lowest

concentration that is interpreted as being statistically different from the blank, shown below.

$$LOD = Blank\ Average + 5\sigma_D \tag{A.3}$$

Machine error, analytical method error, and human error all contribute to variations between samples. Standard errors (σ_E) were used to quantify the error associated from sampling to analysis by determining concentrations in duplicate samples.

$$\sigma_E = \frac{\sigma_D}{\sqrt{n}} \tag{A.4}$$

It was not feasible run replicates and therefore calculate σ_E for each sample, so the average of the σ_E was attributed to the sample population and propagated in further calculations. Finally, the following three equations for slope (m), intercept (b), and slope uncertainty (σ_M) were used in performing linear least squares regressions on concentrations profiles for determination of dissolved fluxes (Cantrell, 2008).

$$m = \frac{n\sum x_i y_i - \sum x_i \sum y_i}{n\sum x_i^2 - (\sum x_i)^2} \tag{A.5}$$

$$b = \frac{\sum x_i^2 \sum y_i - \sum x_i \sum x_i y_i}{n\sum x_i^2 - (\sum x_i)^2} \tag{A.6}$$

$$\sigma_m = \frac{\sqrt{\frac{\sum y_i^2 - b\sum y_i - m\sum x_i y_i}{n-2}}}{\sqrt{n\sum x_i^2 - (\sum x_i)^2}} \tag{A.7}$$

APPENDIX B

Supplemental Figures

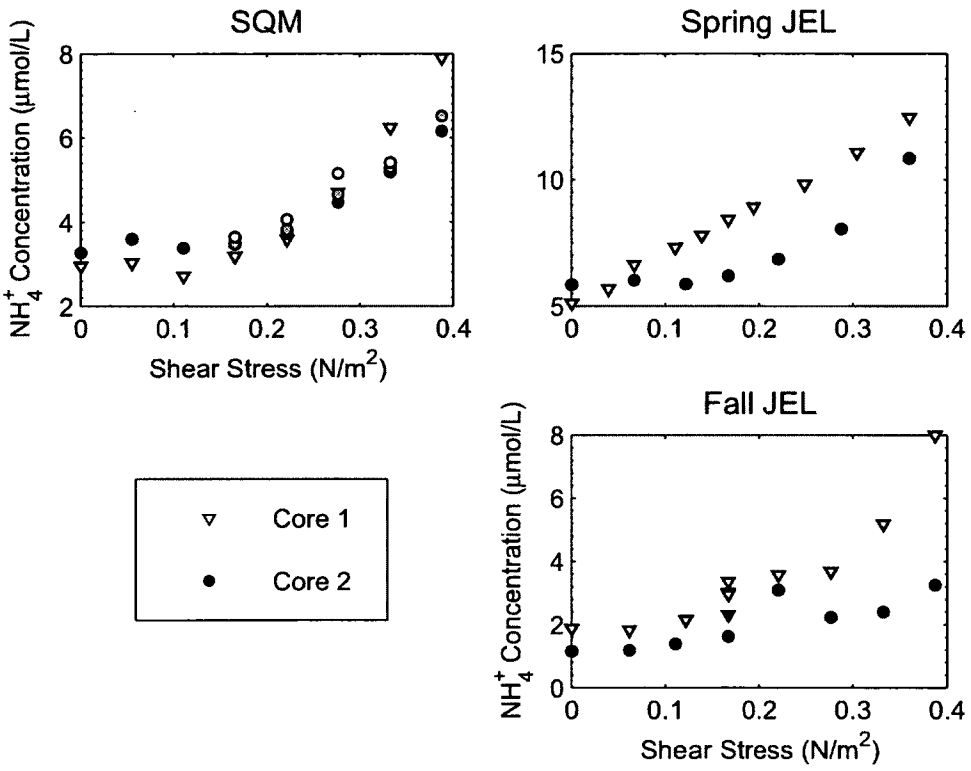

Figure B-1: Overlying water concentrations of NH_4^+ in the erosion chamber as a function of shear stress. Multiple data points (2-3 samples) at constant shear stress (SQM Core 2 and Fall JEL Core 1 at $\tau = 0.17$ N/m^2) are shaded from dark to light based on the order they were taken. Error bars are the average standard error

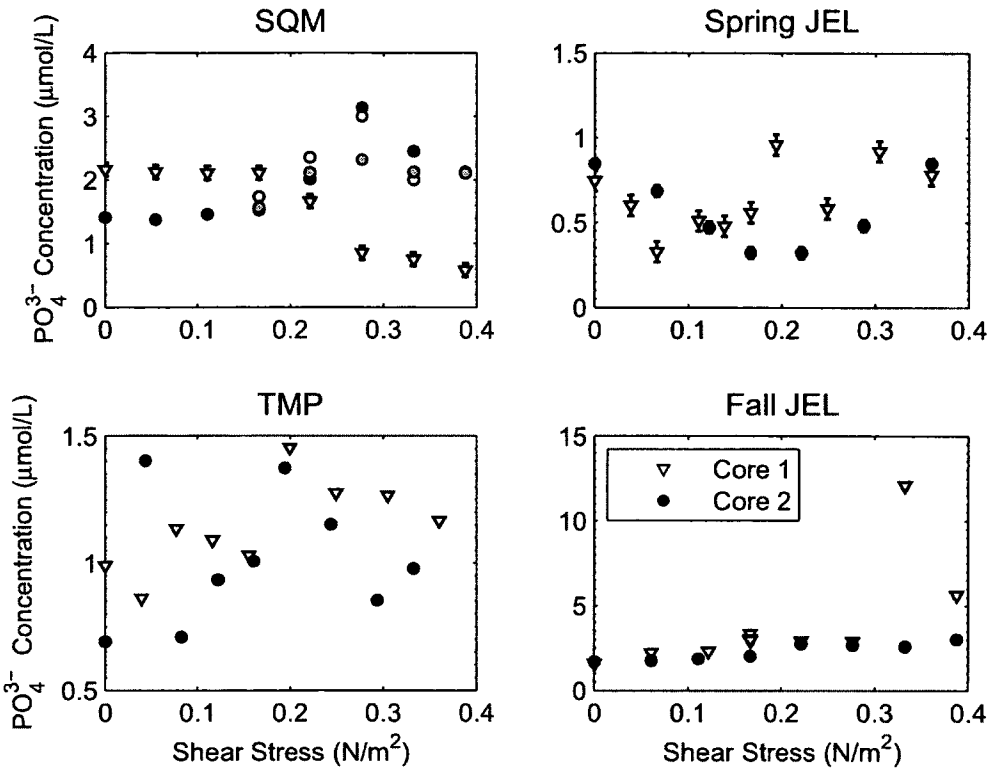

Figure B-2: Overlying water concentrations of $PO_4{}^{3-}$ in the erosion chamber as a function of shear stress. Multiple data points (2-3 samples) at constant shear stress (SQM Core 2 and Fall JEL Core 1 at $\tau = 0.17$ N/m^2) are shaded from dark to light based on the order they were taken. Error bars are the average standard error

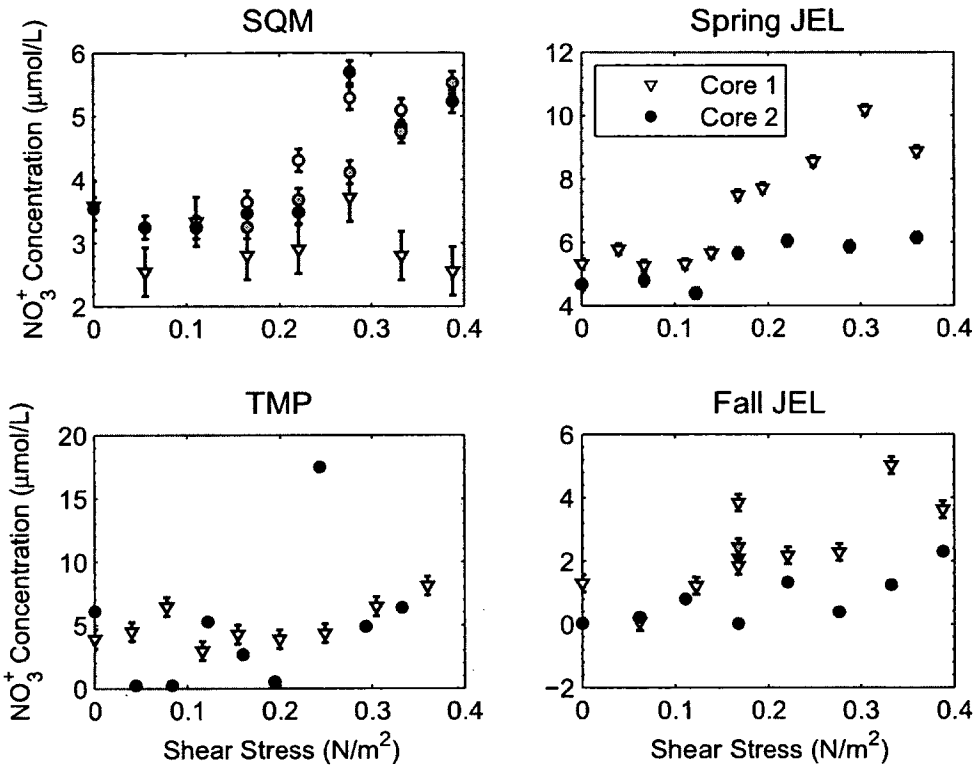

Figure B-3: Overlying water concentrations of NO_3^- in the erosion chamber as a function of shear stress. Multiple data points (2-3 samples) at constant shear stress (SQM Core 2 and Fall JEL Core 1 at $\tau = 0.17$ N/m^2) are shaded from dark to light based on the order they were taken. Error bars are the average standard error

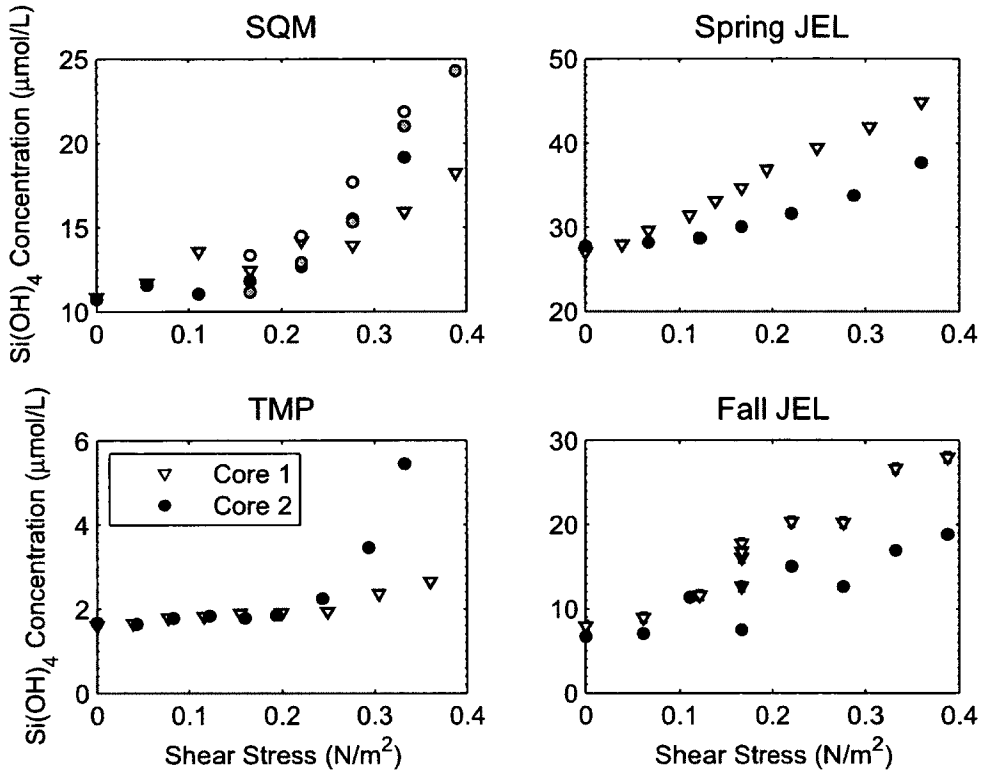

Figure B-4: Overlying water concentrations of silica in the erosion chamber as a function of shear stress. Multiple data points (2-3 samples) at constant shear stress (SQM Core 2 and Fall JEL Core 1 at $\tau = 0.17$ N/m^2) are shaded from dark to light based on the order they were taken. Error bars are the average standard error

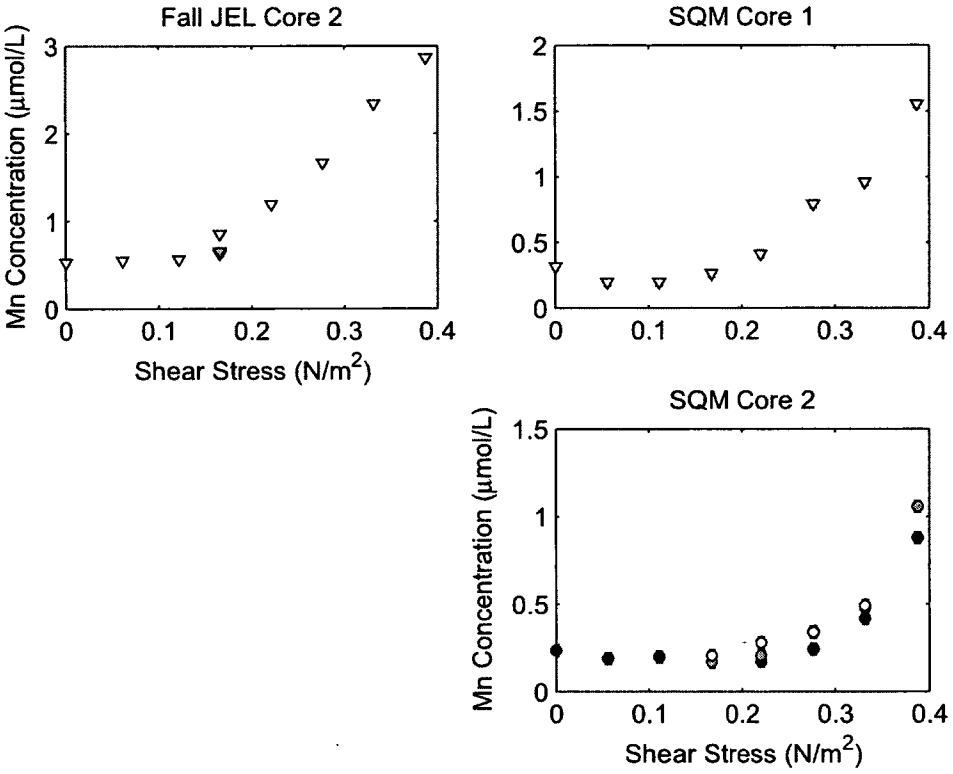

Figure B-5: Overlying water concentrations of Mn in the erosion chamber as a function of shear stress. Multiple data points (2-3 samples) at constant shear stress (SQM Core 2 and Fall JEL Core 1 at $\tau = 0.17$ N/m^2) are shaded from dark to light based on the order they were taken. Error bars are approximately the size of the data markers.

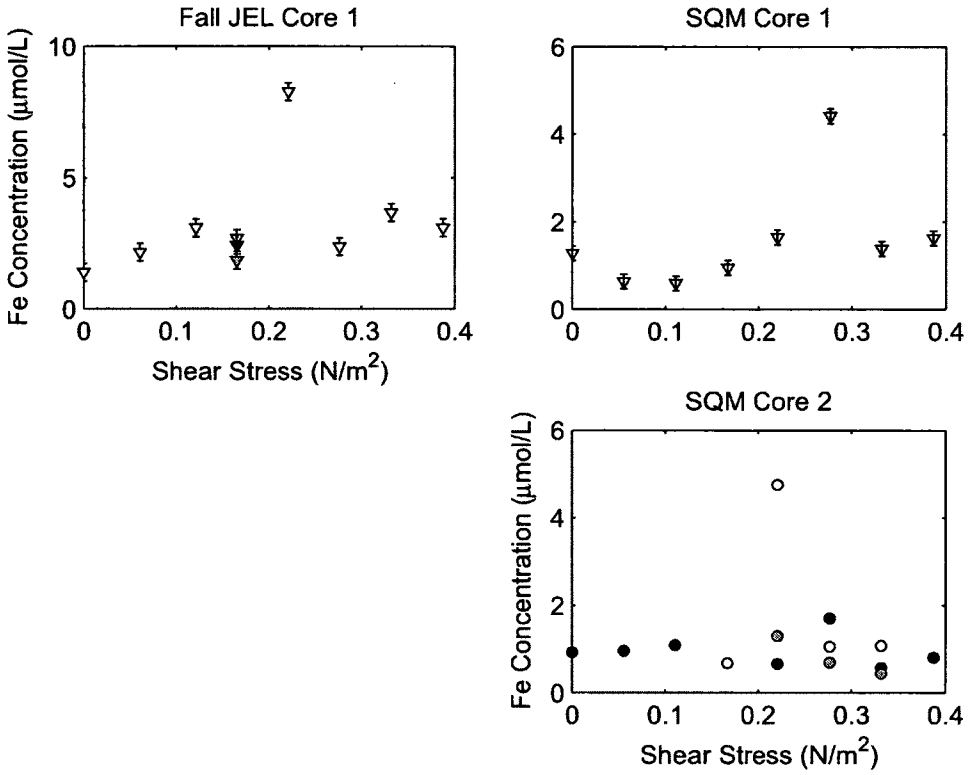

Figure B-6: Overlying water concentrations of Fe in the erosion chamber as a function of shear stress. Multiple data points (2-3 samples) at constant shear stress (SQM Core 2 and Fall JEL Core 1 at $\tau = 0.17$ N/m^2) are shaded from dark to light based on the order they were taken. Error bars are approximately the size of the data markers.

REFERENCES

3050B, 1996. Acid Digestion of Sediments, Sludges, and Soils. Environmental Protection Agency.

Aller, R. C., Mackin, J. E., Ullman, W. J., Chen-Hou, W., Shing-Min, T., Jian-Cai, J., Yong-Nian, S., Jia-Zhen, H., 1985. Early chemical diagenesis, sediment-water solute exchange, and storage of reactive organic matter near the mouth of the Changjiang, East China Sea. Continental Shelf Research 4, 227–251.

Armstrong, P., Hanson, G., Gaudette, H., 1976. Minor elements in sediment of the Great Bay Estuary, New Hampshire. Environmental Geology 1, 207–214.

Arrigo, K., 2005. Marine microorganisms and global nutrient cycles. Nature 437, 349–355.

ATSDR, 2012. Agency for Toxic Substances and Disease Registry (atsdr). URL `www.atsdr.cdc.gov`

Babatope, B., Williams, P., Williams, D., 2006. In situ rheometry of cohesive sediments under water wave pressure. Continental Shelf Research 26, 488498.

Banta, G., Giblin, A., Hobbie, J., Tucker, J., 1995. Benthic respiration and nitrogen release in Buzzards Bay, Massachusetts. Journal of Marine Research 53, 107–135.

Bartlett, R., Mortimer, R., Morris, K., 2008. Anoxic nitrification: Evidence from Humber Estuary sediments (UK). Chemical Geology 250, 29–39.

Berner, R., 1977. Stoichiometric models for nutrient regeneration in anoxic sediments. Limnology and Oceanography 22, 781–786.

Berner, R., 1979. Kinetics of nutrient regeneration in anoxic marine sediments. Physics and Chemistry of the Earth 11, 279–292.

Berner, R., 1980. Early Diagenesis. Princeton University Press.

Bilgili, A., Proehl, J., Lynch, D., Smith, K., Swift, M., 2005. Estuary/ocean exchange and tidal mixing in a Gulf of Maine Estuary: A Lagrangian modeling study. Estuarine, Coastal and Shelf Science 65, 607–624.

Boudreau, B., 1997. Diagenetic Models and Their Implementation. Springer, p. 414.

Briggs, P., Meier, A., 1999. The determination of forty-two elements in geological materials by inductively couple plasma-mass spectroscopy. Tech. Rep. 99-166, U.S. Geological Survey.

Burdige, D., 1993. The biogeochemistry of manganese and iron reduction in marine sediments. Earth-Science Reviews 35, 249–284.

Calender, E., Metre, P., 1997. Environmental policy analysis, peer reviewed: Reservoir sediment cores show U.S. lead declines. Enviromental Science and Technology 31, 424–428.

Cantrell, C., 2008. Technical note: Review of methods for linear least-squares fitting of data and application to atmospheric chemistry problems. Atmospheric Chemistry and Physics Discussions 8, 6409–6436.

Cantwell, M., Burgess, R., Kester, D., 2002. Release and phase partitioning of metals from anoxic estuarine sediments during periods of simulated resupension. Environmental Science and Technology 36, 5328–5334.

Capuzzo, J. M., Anderson, F. E., 1973. The use of modern chromium accumulations to determine estuarine sedimentation rates. Marine Geology 14, 225–235.

Cline, J., 1969. Spectrophotometric determination of hydrogen sulfide in natural waters. Limnology and Oceanography 14, 454–458.

Couceiro, F., Rauen, W., Millward, G., 2009. Transport and reactivity of nickel in estuarine sediments: Results from a high capacity flume. Marine Chemistry 117, 71–76.

Eggleton, J., Thomas, K., 2004. A review of factors affecting the release and bioavailability of contaminants during sediment disturbance events. Environmental International 30, 973–980.

EPA, 2000. Northeast 2000-2006 summary data.
URL `http://www.epa.gov/emap/nca/html/regions/ne0006/index.html`

Forstner, U., 1980. Trace metal analysis on polluted sediments part i: Assessment of sources and intensities. Environmental Technology Letters 1, 494–505.

Froelich, P., Klinkhammer, G., Bender, M., Leudtke, N., Heath, G., Cullen, D., Dauphin, P., Hammond, D., Hartman, B., Maynard, V., 1979. Early oxidation of organic matter in pelagic sediments of the eastern equatorial Atlantic: suboxic diagenesis. Geochimica et Cosmochimica Acta 43, 1075–1090.

GBSC, 2010. Final report of the commission to study the causes, effects, and remediation of siltation in the Great Bay Estuary. Tech. rep., Great Bay Siltation Commission.

Gehlen, M., Malschaert, H., Raaphorst, W. R. V., 1995. Spatial and temporal variability of benthic silica fluxes in the southeastern North Sea. Continental Shelf Research 15, 1675–1696.

Gieskes, J., Gamo, T., Brumsack, H., 1991. Chemical methods for interstitial water analysis aboard JOIDES resolution. ODP Technical Note 15, 1–60.

Hines, M., 1981. Seasonal biogeochemistry in the sediments of the Great Bay estuarine complex, New Hampshire. Ph.D. thesis, University of New Hampshire.

Hines, M., Jones, G., 1985. Microbial biogeochemistry and bioturbation in the sediments of Great Bay, New Hampshire. Estuarine, Coastal and Shelf Science 20, 729–742.

Hines, M., Lyons, W., Armstrong, P., Orem, W., Spencer, M., Gaudette, H., Jones, G., 1984. Seasonal metal remobilization in the sediments of Great Bay, New Hampshire. Marine Chemistry 15, 173–187.

Kalnejais, L. H., Martin, W. R., Bothner, M. H., 2010. The release of dissolved nutrients and metals from coastal sediments due to resuspension. Marine Chemistry 121, 224–235.

Kalnejais, L. H., Martin, W. R., Signell, R. P., Bothner, M. H., 2007. Role of sediment resuspension in the remobilization of particulate-phase metals from coastal sediments. Environmental Science and Technology 41, 2282–2288.

Klump, J., Martens, C., 1989. The seasonality of nutrient regeneration in an organic-rich coast sediment: Kinetic modeling of changing pore-water nutrient and sulfate distributions. Limnology and Oceanography 34, 559–577.

Kristensen, E., 2000. Organic matter diagenesis at the oxic/anoxic interface in coastal marine sediments, with emphasis on the role of burrowing animals. Hydrobiologia 426, 1–24.

Krom, M., Berner, R., 1980. Adsorption of phosphate in anoxic marine sediments. Limnology and Oceanograpy 25, 797–806.

Lehtoranta, J., Ekholm, P., Pitknen, H., 2009. Coastal eutrophication thresholds: A matter of sediment microbial processes. Ambio 38, 303–308.

Lerat, Y., Lasserre, P., le Corre, P., 1985. Seasonal changes in pore water concentrations of nutrients and their diffusive fluxes at the sediment-water interface. Journal of Experimental Marine Biology and Ecology 135, 135160.

Long, E., Field, L., MacDonald, D., 1998. Predicting toxicity in marine sediments with numerical sediment quality guidelines. Environmental Toxicology and Chemistry 17, 714–727.

Lyons, W. B., Loder, T. C., Murray, S. M., 1982. Nutrient pore water chemistry, Great Bay, New Hampshire: Benthic fluxes. Estuaries 5, 230–233.

Malecki, L., White, J., Reddy, K., 2004. Nitrogen and phosphorus flux rates from sediment in the Lower St. Johns River Estuary. Journal of Environmental Quality 33, 1545–1555.

Martens, C., Berner, R., Rosenfeld, J., 1978. Interstitial water chemistry of anoxic Long Island Sound sediments. 2. Nutrient regeneration and phosphate removal. Limnology and Oceanograpy 23, 605–617.

Mehta, A., Parchure, T., 2000. Surface erosion of fine-grained sediment revisited. Vol. 3. pp. 55–74.

Meyers, P., 1994. Preservation of elemental and isotopic source identification of sedimentary organic matter. Chemical Geology 114, 289–302.

Mitchener, H., O'Brien, D., 2000. Seasonal variability of sediment erodibility and properties on a macrotidal mudflat, Peterstone Wentlooge, Severn Estuary, UK. Vol. 3. pp. 301–321.

Morin, J., Morse, J., 1999. Ammonium release from resuspended sediments in the Laguna Madre Estuary. Marine Chemistry 65, 97–110.

Morin, J., Morse, J., 2005. Ammonium interaction with coastal marine sediments: Influence of redox conditions on K*. Marine Chemistry 95, 107–112.

Mulsow, S., Boudreau, B., Smith, J., 1998. Bioturbation and porosity gradients. Limnology and Oceanography 43, 1–9.

Nixon, S., 1995. Coastal marine eutrophication: A definition, social causes and future. Ophelia 41, 199–219.

NOAA, 2012. Great bay national estuarine research reserve.
URL `http://nerrs.noaa.gov/Reserve.aspx?ResID=GRB`

Oczkowski, A., 2002. Riverine inputs of nutrients to the Great Bay, NH (USA). Master's thesis, University of New Hampshire.

Officer, L., 2012. Seasonal variation of benthic nutrient fluxes in the Great Bay Estuary, NH.

Orem, W., 1982. Organic matter in anoxic pore water from the Great Bay, New Hampshire. Ph.D. thesis, University of New Hampshire.

Phillips, S., Johnson, J., Miranda, E., Disenhof, C., 2011. Improving CHN measurements in carbonate-rich marine sediments. Limnology and Oceanography: Methods 9, 194–203.

PREP, 2009. State of the estuaries 2009. Tech. rep., Piscataqua Region Estuaries Partnership and University of New Hampshire.

Raaphorst, W. V., Malschaert, J. F. P., 1995. Ammonium adsorption in superficial North Sea sediments. Continental Shelf Research 16 (11), 1415–1435.

Redfield, A., 1958. The biological control of chemical factors in the environment. American Scientist 46, 230A–221.

Richard, F., Bourg, A., 1991. Aqueous geochemistry of chromium: A review. Water Research 25, 807–816.

Rosenfeld, J., 1979. Ammonium adsorption in nearshore anoxic sediment. Limnology and Oceanography 24, 356–364.

Ruttenberg, K., 1992. Development of a sequential extraction method for different forms of phosphorus in marine sediments. Limnology and Oceanography 37, 1460–1482.

Santschi, P., Hhener, P., Benoit, G., ten Brink, M. B., 1990. Chemical processes at the sediment-water interface. Marine Chemistry 30, 269–315.

Sarmiento, J., Gruber, N., 2006. Ocean Biogeochemical Dynamics. Princeton University Press, Ch. 7, pp. 271–317.

Schrum, H., Spivak, A., Kastner, M., D'Hondt, S., 2009. Sulfate-reducing ammonium oxidation: A thermodynamically feasible metabolic pathway in subseafloor sediment. Geology 37, 939–942.

Smith, V., Tilman, G., Nekola, J., 1999. Eutrophication: Impacts of excess nutrient inputs on freshwater, marine, and terrestrial ecosystems. Environmental Pollution 100, 179–196.

Strickland, J., Parsons, T., 1968. A manual for seawater analysis. Fisheries Research Board of Canada, pp. 1–185.

Taki, K., 2001. Critical shear stress for cohesive sediment transport. Vol. 3. pp. 53–61.

ten Brink, M. B., Manheim, F., Mecray, E., Hastings, M., Currence, J., Farrington, J., Fredette, T., Jones, S., Liebman, M., Larsen, P., Leo, W. S., Tripp, B., Jr, G. W., Ward, L., 2002. Contaminated sediments database for the Gulf of Maine, U.S. geological survey open-file report No. 02-403. Tech. rep., USGS.
URL pubs.usgs.gov/of/2002/of02-403/

Townsend, A., Palmer, A., Stark, S., Samson, C., Scouller, R., Snape, I., 2007. Trace metal characterisation of marine sediment reference materials MESS-3 and PACS-2 in dilute HCl extracts. Marine Pollution Bulletin 54, 236–239.

Trowbridge, P., Jones, S., 2009. Summary report National Coastal Assessment Monitoring Program 2000-2001. Tech. rep., NH Department of Environmental Sciences.

Tyrrell, T., 1999. The relative influences of nitrogen and phosphorus on oceanic primary production. Nature 400, 525–531.

Vanderborght, J.-P., Wollast, R., Billen, G., 1977. Kinetic models of diagenesis in disturbed sediments. Part 1. mass transfer properties and silica diagenesis. Limnology and Oceanograpy 22, 787–793.

Wengrove, M., 2012. Observations of a developing boundary layer in a tidally forced estuary. Master's thesis, University of New Hampshire.

Westrich, J., Berner, R., 1984. The role of sedimentary organic matter in bacterial sulfate reduction: The G model tested. Limnology and Oceanography 29, 236–249.

Wijsman, J., Herman, P., Middelburg, J., Soetaert, K., 2002. A model for early diagenetic processes in sediments of the continental shelf of the Black Sea. Estuarine, Coastal and Shelf Science 54, 403421.

Winston, J., Anderson, F., 1971. Bioturbation of sediments in a northern temperate estuary. Marine Geology 10, 39–49.

Wollast, R., 1974. The silica problem. In: Goldberg, E. (Ed.), Marine Chemistry. Harvard University Press, Ch. 11, pp. 359–392.

Wollast, R., Garrels, R., 1971. Diffusivity coefficient of silica in seawater. Nature Physical Science 229, 94.

Wood, M., Trowbridge, P., 2012. Nitrogen, phosphorus, and suspended solids concentrations in tributaries to the great bay estuary watershed in 2011: A final report to the piscataqua region estuaries partnership. Tech. rep., N.H. Department of Environmental Services.

Zhang, J.-Z., Fischer, C., 2006. A simplified resorcinol method for direct spectrophotometric determination of nitrate in seawater. Marine Chemistry 99, 220–226.

Zoumis, T., Schmidt, A., Grigorova, L., Calmano, W., 2001. Contaminants in sediments: Remobilisation and demobilisation. Science of The Total Environment 266, 195–202.